Chinese Journal of Physics 88 (2024) 212–269

Contents lists available at ScienceDirect

Chinese Journal of Physics

journal homepage: www.sciencedirect.com/journal/chinese-journal-of-physics

# Intelligent computing paradigm for unsteady magneto nano-polymeric Casson nanofluid with Ohmic dissipation and thermal radiation

Zeeshan Ikram Butt [a], Iftikhar Ahmad [a], Syed Ibrar Hussain [b,c,*], Muhammad Asif Zahoor Raja [d], Muhammad Shoaib [e], Hira Ilyas [f]

[a] Department of Mathematics, University of Gujrat, Gujrat, 50700, Pakistan
[b] Dipartimento di Matematica e Informatica, Università degli Studi di Palermo, Via Archirafi 34, 90123, Palermo, Italy
[c] Department of Mathematics, University of Houston, Houston, TX, USA
[d] Future Technology Research Centre, National Yunlin University of Science and Technology, 123 University Road, Section 3, Douliou, Yunlin 64002, Taiwan, ROC
[e] Yuan Ze University, AI Center, Taoyuan 320, Taiwan, ROC
[f] Department of physical sciences, University of Chenab, Gujrat, 50700, Pakistan

ARTICLE INFO

*Keywords:*
Magneto nano-polymeric Casson nanofluid (MNP-CNF)
intelligent computing paradigm
Stochastic numerical technique
Artificial intelligence

ABSTRACT

In this present investigative mode of study, a biological innovational approach is adopted in the form of an intelligent computing paradigm to investigate the properties of flow in the case of incompressible magneto nano-polymeric Casson nanofluid using a stochastic numerical technique named artificial neural networks based on the hybridization of genetic algorithms with highly efficient local search solvers which is sequential quadratic programming. The governing PDEs of the suggested fluid model are first converted into a system of ODEs using appropriate similarity transformations and then solved for sundry scenarios generated based on physical parameters existing in the ODEs to examine the velocity profile, thermal profile and nanofluid concentration. Furthermore, by uplifting the value of Casson parameter, the temperature of the nanofluid hikes however this effect is reversed in case of radiation parameter. The strong motivation behind this study is to obtain the numerical solution of a system of nonlinear differential equations involving fifth-order derivatives with strong accuracy. A comprehensive error analysis based on tables and graphs is presented to further enhance the scientific significance of this research in the results and discussion section.

## 1. Introduction

Nanofluid (NF) is a structural combination of tiny particles each of size less than $10^{-6}$mm in a base fluid. These tinny particles are called nanoparticles and can be made from substances like semi-conductors (SiC), metals (Ag, Cu, Au), carbide ceramics (TiC, SiC), oxide ceramics (CuO), compounds like pump oil, engine oil, ethylene glycol, water and $Al_{70}Cu_{30}$. NF theory was given in 1995 and Choi with Eastman [1] are its pioneers. NFs have been used in numerous technologies along with porous media, turbulent flows, solar collectors, chemical energy coating processes and geothermic. Moreover, some recent applications are automotive engine cooling,

* Corresponding authors.
*E-mail addresses:* syedibrar.hussain@unipa.it, syed.ibraras@gmail.com (S.I. Hussain).

https://doi.org/10.1016/j.cjph.2024.01.009
Received 8 August 2023; Received in revised form 17 November 2023; Accepted 3 January 2024
Available online 7 January 2024

**Nomenclature**

| | |
|---|---|
| ANN | Artificial Neural Networks |
| $x, y$ | Plane coordinates |
| $u, v$ | Velocity components |
| $\mu$ | Apparent viscosity |
| $c_p$ | Specific heat capacity of fluid |
| $\mathrm{T_m}$ | Fluid temperature |
| $V_w(x,y)$ | Free stream velocity |
| $G$ | Gravity acceleration |
| $Tm_\infty$ | Ambient fluid temperature |
| B | Constant of expansion |
| $\theta$ | Dimensionless temperature |
| $g^{'}$ | Dimensionless velocity |
| $\phi$ | Dimensionless nanofluid |
| $\mu_B$ | Dynamic viscosity |
| $k_s$ | Nanoparticle conductivity |
| $k_g$ | Base fluid conductivity |
| $m$ | Nanoparticle shape |
| $\varphi$ | Volume fraction |
| $A = \frac{c}{a}$ | Unsteadiness parameter |
| $\mathrm{Pr} = \frac{\nu}{\alpha_f}$ | Prandtl number |
| $e_{il}$ $(i,l)$th | component of deformation rate |
| $Sc = \frac{\nu}{D_B}$ | Schmidt parameter |
| $Q = \frac{xQ_0}{(\rho c_f)V_w(Tm_w - Tm_\infty)^2}$ | Heat generation/absorption Coefficient |
| $R = \frac{16\overset{*}{\sigma} Tm_\infty^3}{3k\overset{*}{k}}$ | Radiation parameter |
| $Nt = \frac{(\rho c)_p D_T(Tm_f - Tm_\infty)}{\nu(\rho c)_f Tm_\infty}$ | Thermophoresis parameter |
| $Nb = \frac{(\rho c)_p D_B(C_w - C_\infty)}{\nu(\rho c)_f}$ | Brownian motion |
| $P_y$ | Yield stress of the fluid |
| $\pi$ | Product of the deformation |
| $\pi_c$ | Critical value of $\pi$ |
| $\mathrm{Re} = \frac{V_w x}{\nu}$ | local Reynolds number |
| $Gr = \frac{(g(\beta_T)_f(Tm_w - Tm_\infty)x^3}{\nu^2}$ | Grashof number |
| $\lambda = \frac{Gr}{\mathrm{Re}^2}$ | Buoyancy parameter |
| $Ec = \frac{(V_w^2)}{(C_p)_f(Tm_w - Tm_\infty)}$ | Eckert number |
| $M = \frac{(\sigma_f B_0^2(1-ct))}{(a\rho_f)}$ | Magnetic parameter |

polymeric materials, food biophysics, drag delivery, crystal growth and rocket propellant combustion [2–9]. Masuda et al [10] explained a boost in thermal conductivity as the key feature of NF by applying the RK-Fehlberg method. Butt et al. [11] investigated Prandtl-Eyring NF flow across a stretching sheet (SS) using feed-forward neural networks and concluded that the concentration of NF diminishes by uplifting the temperature difference parameter as well as the Schmidt number. Taseer et al. [12] discussed Maxwell NF flow along the boundary layer (BL) through a liner SS. The authors concluded that for large value of magnetic field parameter, temperature and NF concentration increase. Mandal et al. [13] comprehensively discussed convective heat transfer along a rotating SS during flow of a NF and revealed that entropy production quantifies through Bejan number. Makinde along with Aziz [14] numerically examined the BL flow of NF along a linearly SS and observed a minimal effect of Lewis number on thermal distribution. Khan with Pop [15] investigated the BL flow of NF past a flat SS and concluded that a higher value of Prandtl number reduces the value of Sherwood number. NF along SS is also discussed in [16,17].

Fluids are mainly categorized as Newtonian and non-Newtonian fluids. The field of non-Newtonian fluids is eye-catching for researchers due to its result-oriented use in commerce and industrial levels. The Casson fluid (CF) model's strong thinning characteristics distinguish it from other non-Newtonian fluids. Crude oil, fruit juices, molten chocolate, blood, and tomato puree are some of the existing examples of CF. The study of CNF is the hot favorite area amongst the researchers of the 21$^{st}$ century. Malik et al [18] explained the BL flow of CNF along a stretching cylinder. Nadeem et al [19] examined CNF flow with boundary conditions along the boundary layer. Ibrahim along with Makinde [20] studied the heat transfer of CNF as stagnation-point flow past SS.

Magneto fluid dynamic or MHD is the analysis of electrically supervised fluids under the effect of the magnetic field. MHD is a rich

field with several applications. Raju along with Sandeep [21] examined MHD in CF over permeable SS. Babu and Sandeep [22] analyzed Brownian motion effects due to MHD slip flow of NFs over SS. Ghadikolaei et al [23] investigated MHD stagnation-point flow in TiO2-Cu/water hybrid NF. Hsiao [24] examined the MHD effect on NF flow towards SS along multimedia features. Significant work related to NF is presented in [25–45].

Khalid et al [46] investigated the unsteady MHD flow of CF through a vertical plate sunk in a porous medium. Nadeem et al [47] studied MHD 3-dimensional CF flow through a porous and linear SS. Haq et al [48] investigate the effects of MHD on CNF flow through a contracting sheet.

There are several techniques used to investigate the solution of many flow problems, but stochastic numerical techniques (SNTs) are rapidly used due to their reliability and effectiveness. SNTs are used by different researchers to solve many problems [49–53]. Artificial intelligence-based SNTs are used in COVID-19 epidemic model [54], Thomas-Fermi system [55], model of mosquito dispersal [56], flow model of the electrohydrodynamic pump [57], the system of dusty plasma [58], Painlevé nonlinear (NL) models [59], Falkner scan NL models [60], model of fuel ignition [61], Troesch's problem [62], functional NL systems [63], NL singular systems [64, 65], Van der Pol NL system [66], system of NL equations [67], power [68], energy [69], MHD [70], system of fractional order equations [71–72], bioinformatics [73], signal processing [74], atomic physics [75], NFs [76], controls [77], nanotechnology [78] and in the models of motor induction [79].

All these applications motivate the authors to investigate and explore the properties of CNF flow through spiking neural networks (SNNT) based on a hybrid process involving GAs and SQP i.e. SNNT-GA-SQP in the presence of nano-particles cu and $Al_2O_3$. The major contribution of this SNNT-GA-SQP-based investigative study is summarized as follows:

- An Intelligent computing paradigm (ICP) is constructed and SNNT-GA-SQP solver is applied efficiently and effectively to investigate the properties of MNP-CNF flow.
- The velocity, temperature and concentration profile of the suggested fluid model in mathematical form is analyzed using sundry scenarios which are constructed based on various physical parameters involved in MNP-CNF problem.
- The continuously overlapped outcomes with exact form reference solution showed the accuracy and reliability of the used SNNT-GA-SQP.
- The validity of the suggested SNNT-GA-SQP is statistically verified using a large independent trials-based dataset.
- Stability, applicability, smooth implementation, and coherent structure are other key features of this research.

The order of the remaining work in this paper is as follows: A mathematical description of the problem will be illustrated in Section 2; in Section 3, the proposed methodology and mathematical formulation will be described; in Section 4, the results and discussion will be included; in Section 5, statistical analysis is presented and in Section 6, conclusion and directions about future research is presented.

## 2. Mathematical formulation

In this study, two-dimensional laminar and unsteady flow of incompressible magnetic nano polymer CNF is discussed. Furthermore, the flow over SS, which is NL, involves thermal radiation and heat generation/absorption (see Fig. 1). For the SS velocity at t=0, the y-axis is the normal to plane surface and the x-axis is in the upward direction of the sheet. The magnetized NF has a free stream temperature. The presence of transverse magnetic fields includes both ohmic and viscous types of dissipation.

The equation for incompressible CF is expressed as,

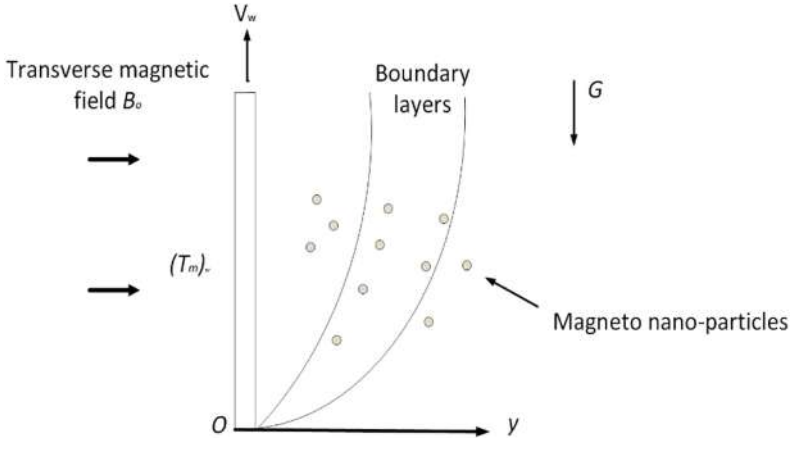


**Fig. 1.** Magnetized nano-polymeric stretching sheet outline.

$$\tau_{il} = \begin{cases} 2\left(\mu_B + \frac{P_y}{\sqrt{2\pi}}\right)e_{il},\ \pi > \pi_c \\ 2\left(\mu_B + \frac{P_y}{\sqrt{2\pi_c}}\right)e_{il},\ \pi_c > \pi \end{cases}, \tag{1}$$

Using these assumptions, the equations for the mass, momentum, energy, and nanoparticle concentration with the BL and Boussinesq approximations are given below (Table 1),

$$\frac{\partial u}{\partial x} + \frac{\partial v}{\partial y} = 0, \tag{2}$$

$$\rho_{ng}\left(\frac{\partial u}{\partial t} + u\frac{\partial u}{\partial x} + v\frac{\partial u}{\partial y}\right) = G(\rho\beta_{Tm})_{ng}(Tm - Tm_\infty) + \mu_{ng}\frac{\partial^2 u}{\partial y^2} - \eta_1\frac{\partial^4 u}{\partial y^4} - \sigma_{ng}B_0^2 u. \tag{3}$$

$$\begin{aligned}\frac{\partial Tm}{\partial t} + u\frac{\partial Tm}{\partial x} + v\frac{\partial Tm}{\partial y} = \frac{k_{ng}}{(\rho C_p)_{ng}}\frac{\partial^2 Tm}{\partial y^2} + \frac{(\rho c)_P}{(\rho C_p)_{ng}}\left(D_B\left(\frac{\partial C}{\partial y}\frac{\partial Tm}{\partial y}\right) + \left(\frac{D_{Tm}}{Tm_\infty}\right)\left(\frac{\partial Tm}{\partial y}\right)^2\right) + \\ \frac{v}{c_p}\left(1 + \frac{1}{\beta}\right)\left(\frac{\partial u}{\partial y}\right)^2 + \frac{k_{ng}}{(\rho C_p)_{ng}}\sigma_n B(x)^2 u^2 + \frac{1}{(\rho C_p)_{ng}}\frac{\partial q_r}{\partial y} + \frac{1}{(\rho C_p)_{ng}}\frac{Q_0}{(Tm - Tm_\infty)},\end{aligned} \tag{4}$$

$$\frac{\partial C}{\partial t} + u\frac{\partial C}{\partial x} + v\frac{\partial C}{\partial y} = D_B\frac{\partial^2 C}{\partial y^2} + \frac{D_{Tm}}{Tm_\infty}\frac{\partial^2 Tm}{\partial y^2} - K_0(C - C_\infty). \tag{5}$$

Boundary conditions under these substitutions are.

$$\begin{bmatrix} Tm = Tm_w, u = V_w,\ \ v = 0,\ \ Tm = Tm_w,\ \ C = C_w\ \ at\ y = 0 \\ Tm \to Tm_\infty, u = 0, C = C_\infty\ at\ y = 0, \\ u \to 0\ \ \frac{\partial u}{\partial y} \to 0\ as\ y \to \infty \end{bmatrix}. \tag{6}$$

Assuming

$$V_w(x,t) = \frac{a_1 x}{1 - ct}\ \ \text{and}\ \ Tm_w(x,t) = Tm_\infty + \frac{a_2 x}{(1 - ct)^2}. \tag{7}$$

These physical quantities under the application of Tiwari-Das nanoscale volume fraction model described as

$$\rho_{\eta g} = (1 - \phi)\rho_g + \phi\rho_s, \tag{8}$$

$$\mu_{\eta g} = \frac{\mu_g}{(1 - \phi)^{2.5}}, \tag{9}$$

$$\beta_{\eta g} = (1 - \phi)\beta_g + \phi\beta_s, \tag{10}$$

$$(\rho C_p)_{\eta g} = (1 - \phi)(\rho C_p)_g + \phi(\rho C_p)_s, \tag{11}$$

$$\sigma_{\eta g} = \sigma_g\left[1 + \frac{3\left\{\frac{\sigma_s}{\sigma_g} - 1\right\}\phi}{\left\{\frac{\sigma_s}{\sigma_g} + 2\right\} - \left\{\frac{\sigma_s}{\sigma_g} - 1\right\}\phi}\right]. \tag{12}$$

Also in this case formulation of the Hamilton-Crosser model for the thermal conductivity of the NF is

$$k_{\eta g} = k_g\left[\frac{k_s + (m-1)k_g - (m-1)(k_g - k_s)\phi}{k_s + (m-1)k_g + (k_g - k_s)\phi}\right]. \tag{13}$$

For dimensionless form, introduce.

**Table 1**
Thermo-physical properties of base fluids and nanoparticles.

| Materials | $\beta(K^{-1})$ | $k(Wm^{-1}K^{-1})$ | $C_p(Jkg^{-1}K^{-1})$ | $\sigma(\Omega m)^{-1}$ | $\rho(kg^{-3})$ |
|---|---|---|---|---|---|
| Water | $21 \times 10^6$ | 0.613 | 4179 | $5.5 \times 10^{-5}$ | 997 |
| Al2O3 | $0.85 \times 10^6$ | 40 | 765 | $35 \times 10^6$ | 3970 |
| Cu | $1.67 \times 10^6$ | 401 | 385 | $596 \times 10^6$ | 8933 |

$$\eta = \sqrt{\frac{a_1}{v(1-ct)}}y,\ \psi = \sqrt{\frac{a_1 v}{(1-ct)}}xg(\eta)$$
$$\theta(\eta) = \frac{Tm - Tm_\infty}{Tm_w - Tm_\infty}. \tag{14}$$

Substitute Eq. (14) in (1-6), we get ordinary differential equations system as follows:

$$(1-\varphi)^{2.5}\beta g^{v} - g^{''} + (1-\varphi)^{2.5}K_1\left[A\left(\frac{\eta}{2}g^{''} + g^{'}\right) + g^{'2} - gg^{''}\right] + (1-\varphi)^{2.5}MB_1 g^{'} - (1-\varphi)^{2.5}K_1K_2\lambda\theta = 0, \tag{15}$$

$$g^{'}\theta^{2} - g\theta\theta^{'} + A\left(\frac{\eta}{2}\theta\theta^{'} + 2\theta^{2}\right) - \frac{K_4}{\mathrm{Pr}K_3}\theta\theta^{''} - Nb\theta\theta^{'}\phi^{'} - Nt\theta\theta^{'2} - Ec\left(1+\frac{1}{\beta}\right)\theta g^{''2} - \frac{1}{K_3}Ec * M\theta g^{'2} + \frac{R}{\mathrm{Pr}K_3}\theta^{''} - \frac{Q}{K_3} = 0, \tag{16}$$

$$\phi^{''} + \frac{Nt}{Nb}\theta^{''} - A * Sc\left(\frac{\eta}{2}\right)\phi^{'} + Scg\phi^{'} = 0. \tag{17}$$

The performed values of $B_1, K_1, K_2, K_3$and $K_4$ in Eqs. (15 - 16) are defined as

$$B_1 = \left[\frac{(\sigma_s + 2\sigma_g) + 2(\sigma_s - \sigma_g)\phi}{(\sigma_s + 2\sigma_g) - 2(\sigma_s - \sigma_g)\phi}\right]$$
$$K_1 = (1-\phi) + \phi\frac{\rho_s}{\rho_g}, K_2 = (1-\phi) + \phi\frac{\beta_s}{\beta_g},$$
$$K_3 = (1-\phi) + \phi\frac{(\rho c_p)_s}{(\rho c_p)_g},$$
$$K_4 = \left[\frac{k_s + (m-1)k_g - (m-1)(k_g - k_s)\phi}{k_s + (m-1)k_g + (k_g - k_s)\phi}\right]. \tag{18}$$

The transformation of boundary conditions is as follows:

$$\left[\begin{matrix} g(0) = 0, & g^{'}(0) = 1, & g^{''}(0) = 0, & \theta(0) = 1, & \phi(0) = 1 \ at\ \eta = 0 \\ g^{'}(\eta)\to 0, & g^{''}(\eta)\to 0, \theta(\eta)\to 0, \phi(\eta)\to 0 as\ \eta\to\infty \end{matrix}\right]. \tag{19}$$

## 3. Proposed methodology

ICPs based on artificial neural networks (ANNs) have been used by researchers in solving different linear/nonlinear models [80–82]. The feed-forward multiple layers (input, hidden, output) ANNs structure produces models based on continuous mapping and provides quite valuable approximate solutions and their $j^{th}$ order derivatives as follows [83]:

$$[\widehat{g}(\eta), \widehat{\theta}(\eta), \widehat{\phi}(\eta)] = \left[\sum_{l=1}^{n} a_{g,l}F(b_{g,l}\eta + c_{g,l}), \sum_{l=1}^{n} a_{\theta,l}F(b_{\theta,l}\eta + c_{\theta,l}), \sum_{l=1}^{n} a_{\phi,l}F(b_{\phi,l}\eta + c_{\phi,l})\right], \tag{20}$$

$$\left[\widehat{g}^{(j)}(\eta), \widehat{\theta}^{(j)}(\eta), \widehat{\phi}^{(j)}(\eta)\right] = \left[\sum_{l=1}^{n} a_{g,l}F^{(j)}(b_{g,l}\eta + c_{g,l}), \sum_{l=1}^{n} a_{\theta,l}F^{(j)}(b_{\theta,l}\eta + c_{\theta,l}), \sum_{l=1}^{n} a_{\phi,l}F^{(j)}(b_{\phi,l}\eta + c_{\phi,l})\right]. \tag{21}$$

Here $n$ represents the order of derivatives and $j$ represents the number of used neurons. The terms $a, b$ and $c$ are the unknown weights and can be defined in vector form $W$ as:

$W = [W_g, W_\theta, W_\phi]$, for $W_g = [a_g, b_g, c_g]$, $W_\theta = [a_\theta, b_\theta, c_\theta]$ and $W_\phi = [a_\phi, b_\phi, c_\phi]$. The components used in the above vectors are defined as:

$$a_g = [a_{g,1}, a_{g,2}, \ldots, a_{g,n}],\ a_\theta = [a_{\theta,1}, a_{\theta,2}, \ldots, a_{\theta,n}],\ a_\phi = [a_{\phi,1}, a_{\phi,2}, \ldots, a_{\phi,n}]$$

$$b_g = [b_{g,1}, b_{g,2}, \ldots, b_{g,n}],\ b_\theta = [b_{\theta,1}, b_{\theta,2}, \ldots, b_{\theta,n}],\ b_\phi = [b_{\phi,1}, b_{\phi,2}, \ldots, b_{\phi,n}]$$

$$c_g = [c_{g,1}, c_{g,2}, \ldots, c_{g,n}],\ c_\theta = [c_{\theta,1}, c_{\theta,2}, \ldots, c_{\theta,n}],\ c_\phi = [c_{\phi,1}, c_{\phi,2}, \ldots, c_{\phi,n}]$$

Here $F(\eta) = \frac{1}{(1+e^{-\eta})}$ i-e, log-sigmoid function is used as an activation function. The log-sigmoid function, also known as the "logistic function", can be useful in certain situations when used in ANNs. The logistic sigmoid function provides a probabilistic interpretation of the network output. The output of a sigmoid can be interpreted as the probability that a particular event will occur. The approximate

solution values i-e $[\widehat{g}^{(j)}(\eta), \widehat{\theta}^{(j)}(\eta), \widehat{\phi}^{(j)}(\eta)]$ along their highest order derivatives are respectively expressed as:

$$[\widehat{g}^{(j)}(\eta), \widehat{\theta}^{(j)}(\eta), \widehat{\phi}^{(j)}(\eta)] = \left[\sum_{l=1}^{n} \frac{a_{g,l}}{1+e^{-\left(b_{g,l}\eta+c_{g,l}\right)}}, \sum_{l=1}^{n} \frac{a_{\theta,l}}{1+e^{-\left(b_{\theta,l}\eta+c_{\theta,l}\right)}}, \sum_{l=1}^{n} \frac{a_{\phi,l}}{1+e^{-\left(b_{\phi,l}\eta+c_{\phi,l}\right)}}\right], \tag{22}$$

$$\widehat{g}^{(v)}(\eta) = \sum_{l=1}^{n} (a_{g,l} b^{5}{}_{g,l} [\frac{120e^{-5\left(b_{g,l}\eta+c_{g,l}\right)}}{\left(1+e^{-\left(b_{g,l}\eta+c_{g,l}\right)}\right)^{6}} - \frac{240e^{-4\left(b_{g,l}\eta+c_{g,l}\right)}}{\left(1+e^{-\left(b_{g,l}\eta+c_{g,l}\right)}\right)^{5}} + \ldots + \frac{240e^{-\left(b_{g,l}\eta+c_{g,l}\right)}}{\left(1+e^{-\left(b_{g,l}\eta+c_{g,l}\right)}\right)^{2}}]), \tag{23}$$

$$\widehat{\theta}^{'}(\eta) = \sum_{l=1}^{n} (a_{\theta,l} b^{2}{}_{\theta,l} [\frac{2e^{-2\left(b_{\theta,l}\eta+c_{\theta,l}\right)}}{\left(1+e^{-\left(b_{\theta,l}\eta+c_{\theta,l}\right)}\right)^{3}} - \frac{e^{-\left(b_{\theta,l}\eta+c_{\theta,l}\right)}}{\left(1+e^{-\left(b_{\theta,l}\eta+c_{\theta,l}\right)}\right)^{2}}]), \tag{24}$$

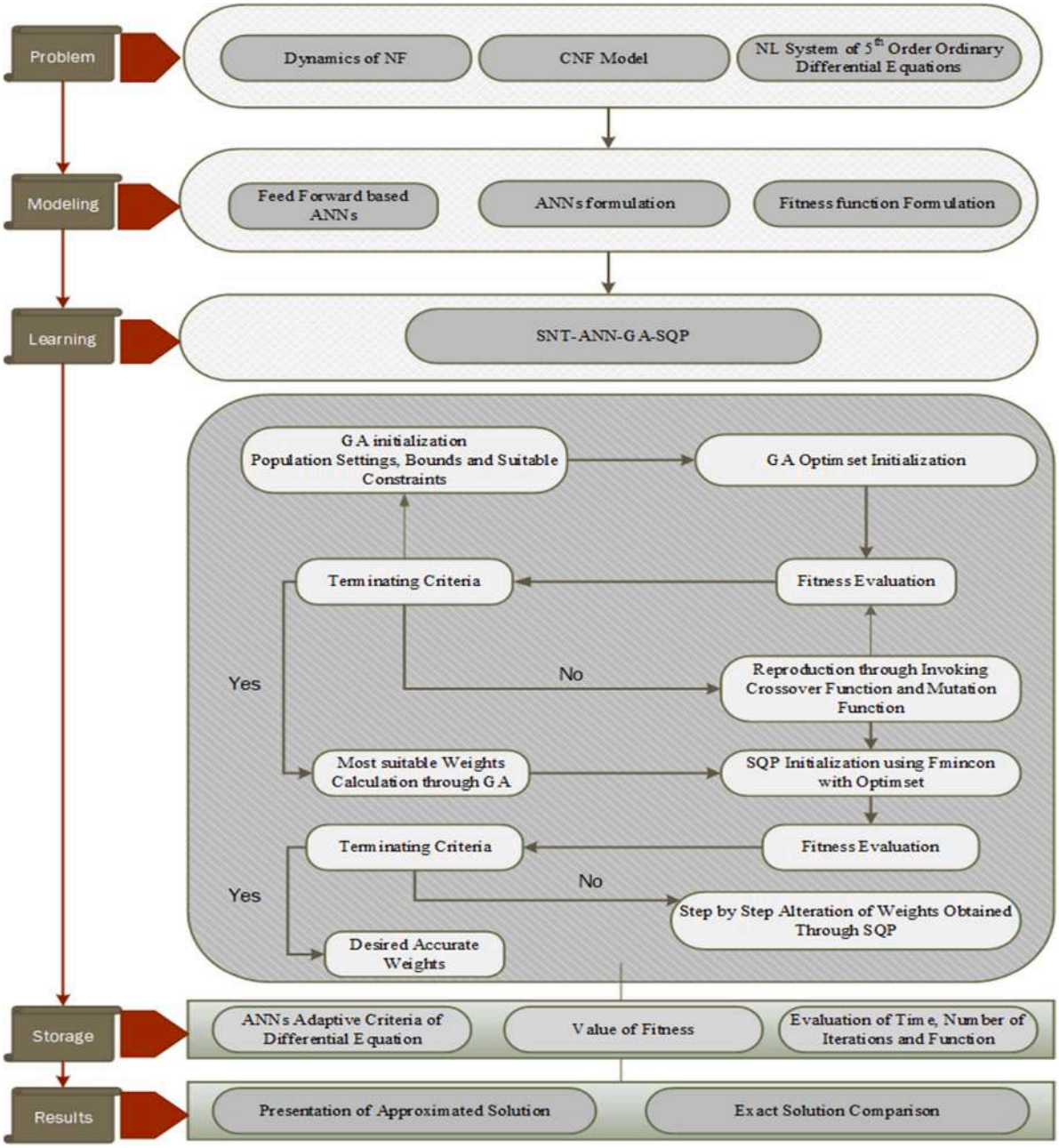


**Fig. 2.** Graphical abstract of SNNT-GA-SQP for solving MNP-CNF problem.

$$\widehat{\phi}^{''}(\eta)=\sum_{l=1}^{n}(a_{\phi,l}b^{2}{}_{\phi,l}[\frac{2e^{-2\left(b_{\phi,l}\eta+c_{\phi,l}\right)}}{(1+e^{-\left(b_{\phi,l}\eta+c_{\phi,l}\right)})^{3}}-\frac{e^{-\left(b_{g,l}\eta+c_{g,l}\right)}}{(1+e^{-\left(b_{g,l}\eta+c_{g,l}\right)})^{2}}]). \tag{25}$$

The formulation of fitness function is given as:

$$e_1=\frac{1}{n}\sum_{l=1}^{n}\left(\begin{array}{l}(1-\varphi)^{2.5}\beta g_l{}^{(v)}-g_l^{'''}+(1-\varphi)^{2.5}K_1\left[A\left(\frac{\eta}{2}g_l^{''}+g_l^{'}\right)+g_l{}^{'2}-g_lg_l^{''}\right]\\+(1-\varphi)^{2.5}MB_1g_l^{'}-(1-\varphi)^{2.5}K_1K_2\lambda\theta\end{array}\right)^{2}, \tag{26}$$

$$e_2=\frac{1}{n}\sum_{l=1}^{n}\left(\begin{array}{l}\left(g_l{}^{'}\theta_l{}^{2}-g_l\theta_l\theta_l^{'}+A\left(\frac{\eta}{2}\theta_l\theta_l^{'}+2\theta_l{}^{2}\right)-\frac{K_4}{\mathrm{Pr}K_3}\theta_l\theta_l^{''}-N_b\theta_l\theta_l^{'}\phi_l^{'}\right.\\\left.-N_t\theta_l\theta_l^{'2}-E_c\left(1+\frac{1}{\beta}\right)\theta_lg_l^{''2}-\frac{1}{K_3}E_cM\theta_lg_l^{'2}+\frac{R}{\mathrm{Pr}K_3}\theta_l^{''}-\frac{Q}{K_3})\right.\end{array}\right)^{2}, \tag{27}$$

$$e_3=\frac{1}{n}\sum_{l=1}^{n}\left(\phi_l^{''}+\frac{N_t}{N_b}\theta_l^{''}-ASc\left(\frac{\eta}{2}\right)\phi_l^{'}+Scg_l\phi_l^{'}\right)^{2}, \tag{28}$$

$$e_4=\frac{1}{9}\left[g_1{}^{2}+(g_1{}^{'}-1)^{2}+g_1{}^{''2}+(\theta_1-1)^{2}+(\phi_1-1)^{2}+g_n{}^{'2}+g_n{}^{''2}+\theta_n{}^{2}+\phi_n{}^{2}\right], \tag{29}$$

$$e=e_1+e_2+e_3+e_4, \tag{30}$$

Here $e1$,$e2$ and $e3$ represent error functions related to the system of Eqs. (15-17) and $e4$ represent the boundary conditions given in Eq. (19).

### 3.1. Optimization of networks

The detailed information regarding ANNs design for optimization based on genetic algorithms (GAs) and sequential quadratic programming (SQP) combination is given as:

**Genetic algorithm:** In case of an optimization problem, the population selected in case of GA for candidate solutions named as individuals progressing towards the improved or upgraded solutions. The evolutionary process in GA starts from a random selection of these individuals. This process is purely iterative and on each iteration, the fitness value of everyone selected in the population is calculated. Many applications of GA exist in the fields of applied sciences, engineering, and technology. GAs is used in the optimization problem of heterogeneous bin packing [84], optimization problem of cost [85], problems of residential building designs [86], system of wind power [87], system of intrusion detection [88] and in military networks designs [89]. GA becomes more effective when hybridized with some efficient local solver.

**Sequential quadratic programming:** It is one of the most efficient optimization techniques applied to sub-problems sequences. In this technique, linearization of constraints is involved to optimize an objective function. In case of unconstrained problems, this technique is restricted to the Newton method. Some applications related to SQP are economic load and dispatch problem [90], walking robot [91] and aircraft transportation [92].

In this present investigative research-based study an IQP is constructed through the hybridization of GA with SQP for the analysis of MNP-CNF. GA-SQP hybrid scheme based on some useful applications is presented in [93–96]. Fig. 2 represents the workflow diagram and Table A1 (in Appendix) represents Pseudo code based on SNNT-GA-SQP for system optimization.

### 3.2. Performance metric

The performance operators that are used to verify the reliability of the proposed methodology are TIC (Thieles in-equality coefficient), RMSE (root mean square error), $R^2$ (coefficient of determination), NSE (Nash-Sutcliffe efficiency) and VAF (various account for). The mathematical formulation of these five is given as:

$$\begin{bmatrix} TIC_{\hat{g}} \\ TIC_{\hat{\theta}} \\ TIC_{\hat{\phi}} \end{bmatrix} = \begin{bmatrix} \dfrac{\sqrt{\frac{1}{n}\sum_{l=1}^{n}\left(\widehat{g}_l - g_{ref:l}\right)^2}}{\sqrt{\frac{1}{n}\sum_{l=1}^{n}\widehat{g}_l^{\,2}} + \sqrt{\frac{1}{n}\sum_{l=1}^{n}g^2{}_{ref:l}}} \\ \dfrac{\sqrt{\frac{1}{n}\sum_{l=1}^{n}\left(\widehat{\theta}_l - \theta_{ref:l}\right)^2}}{\sqrt{\frac{1}{n}\sum_{l=1}^{n}\widehat{\theta}_l^{\,2}} + \sqrt{\frac{1}{n}\sum_{l=1}^{n}\theta^2{}_{ref:l}}} \\ \dfrac{\sqrt{\frac{1}{n}\sum_{l=1}^{n}\left(\widehat{\phi}_l - \phi_{ref:l}\right)^2}}{\sqrt{\frac{1}{n}\sum_{l=1}^{n}\widehat{\phi}_l^{\,2}} + \sqrt{\frac{1}{n}\sum_{l=1}^{n}\phi^2{}_{ref:l}}} \end{bmatrix}, \begin{bmatrix} RMSE_{\hat{g}} \\ RMSE_{\hat{\theta}} \\ RMSE_{\hat{\phi}} \end{bmatrix} = \begin{bmatrix} \sqrt{\frac{1}{n}\sum_{l=1}^{n}\left(\widehat{g}_l - g_{ref:l}\right)^2} \\ \sqrt{\frac{1}{n}\sum_{l=1}^{n}\left(\widehat{\theta}_l - \theta_{ref:l}\right)^2} \\ \sqrt{\frac{1}{n}\sum_{l=1}^{n}\left(\widehat{\phi}_l - \phi_{ref:l}\right)^2} \end{bmatrix}, \begin{bmatrix} R^2{}_{\hat{g}} \\ R^2{}_{\hat{\theta}} \\ R^2{}_{\hat{\phi}} \end{bmatrix} = \begin{bmatrix} \dfrac{SS_{reg:g}}{SS_{total:g}} \\ \dfrac{SS_{reg:\theta}}{SS_{total:\theta}} \\ \dfrac{SS_{reg:\phi}}{SS_{total:\phi}} \end{bmatrix},$$

$$\begin{bmatrix} VAF_{\hat{g}} \\ VAF_{\hat{\theta}} \\ VAF_{\hat{\phi}} \end{bmatrix} = \begin{bmatrix} \left(1 - \dfrac{\mathrm{var}\left(g_{ref:l} - \widehat{g}_l\right)}{\mathrm{var}(g_l)}\right) \times 100 \\ \left(1 - \dfrac{\mathrm{var}\left(\theta_{ref:l} - \widehat{\theta}_l\right)}{\mathrm{var}(\theta_l)}\right) \times 100 \\ \left(1 - \dfrac{\mathrm{var}\left(\phi_{ref:l} - \widehat{\phi}_l\right)}{\mathrm{var}(\phi_l)}\right) \times 100 \end{bmatrix},$$

$$\begin{bmatrix} NSE_{\hat{g}} \\ NSE_{\hat{\theta}} \\ NSE_{\hat{\phi}} \end{bmatrix} = \begin{bmatrix} 1 - \dfrac{\sum_{l=1}^{n}\left(\widehat{g}_l - g_{ref:l}\right)^2}{\sum_{l=1}^{n}\left(\widehat{g}_l - \overline{g_l}\right)^2} \\ 1 - \dfrac{\sum_{l=1}^{n}\left(\widehat{\theta}_l - \theta_{ref:l}\right)^2}{\sum_{l=1}^{n}\left(\widehat{\theta}_l - \overline{\theta_l}\right)^2} \\ 1 - \dfrac{\sum_{l=1}^{n}\left(\widehat{\phi}_l - \phi_{ref:l}\right)^2}{\sum_{l=1}^{n}\left(\widehat{\phi}_l - \overline{\phi_l}\right)^2} \end{bmatrix}, \begin{bmatrix} E - VAF_{\hat{g}} \\ E - VAF_{\hat{\theta}} \\ E - VAF_{\hat{\phi}} \end{bmatrix} = \begin{bmatrix} 100 - VAF_{\hat{g}} \\ 100 - VAF_{\hat{\theta}} \\ 100 - VAF_{\hat{\phi}} \end{bmatrix},$$

$$\begin{bmatrix} E - R^2{}_{\hat{g}} \\ E - R^2{}_{\hat{\theta}} \\ E - R^2{}_{\hat{\phi}} \end{bmatrix} = \begin{bmatrix} 1 - R^2{}_{\hat{g}} \\ 1 - R^2{}_{\hat{\theta}} \\ 1 - R^2{}_{\hat{\phi}} \end{bmatrix}, \begin{bmatrix} E - NSE_{\hat{g}} \\ E - NSE_{\hat{\theta}} \\ E - NSE_{\hat{\phi}} \end{bmatrix} = \begin{bmatrix} 1 - NSE_{\hat{g}} \\ 1 - NSE_{\hat{\theta}} \\ 1 - NSE_{\hat{\phi}} \end{bmatrix}.$$

Here $SS_{reg}$ and $SS_{total}$ represent squares-sum by regression and total squares-sum respectively. The criteria to check the reliability of

**Table 2**
Physical parameters variational values for MNP-CNF problem.

| Scenarios | Cases | | | |
|---|---|---|---|---|
| | **Case 1** | **Case 2** | **Case 3** | |
| **1** | β = 0.2 | β = 0.6 | β = 1.0 | **For Cu** |
| **2** | $\lambda$ =2 | $\lambda$ = 11 | $\lambda$ = 20 | |
| **3** | Q = 0.2 | Q = 0.6 | Q = 1.0 | |
| **4** | β = 0.4 | β = 0.8 | β = 1.2 | |
| **5** | Sc = 0.1 | Sc = 1.0 | Sc =2.0 | |
| **1** | β = 0.2 | β = 0.6 | β = 1.0 | **For $Al_2O_3$** |
| **2** | $\lambda$ = 0.1 | $\lambda$ = 2.0 | $\lambda$ = 4.0 | |
| **3** | R = 0.5 | R = 0.9 | R = 1.3 | |
| **4** | β = 0.1 | β = 0.3 | β = 0.7 | |

these performance operators is that the values obtained through these operators should be very close to zero.

## 4. Results and discussion

In the current investigative research, the effect of heat and ohmic dissipation during the unsteady flow of MNP-CNF model is observed through variation in parameters that influence the flow. The proposed problem is solved numerically in the form of a system of higher-order ordinary differential equations using the novel design SNNT-GA-SQP technique. The results obtained are illustrated numerically and graphically through figures. The variations in parameters are provided in the form of different scenarios of cu and $Al_2O_3$ in Table 2. The training of weights is performed using sigmoid function $(\eta) = \frac{1}{1+e^{-\eta}}$. Graphically, the trained weights in each case for all the scenarios of both cu and $Al_2O_3$ are presented for $\widehat{g}(\eta), \widehat{\theta}(\eta)$ and$\widehat{\phi}(\eta)$ through Figs. 3–11. Here $\widehat{g}(\eta), \widehat{\theta}(\eta)$ and$\widehat{\phi}(\eta)$ represent fluid flow, temperature, and concentration fields respectively. Substitution of these trained weights in Eq. 20 gives the required numerical results of MNP-CNF problem. Emerging parameters i-e Casson fluid parameter $\beta$, velocity slip parameter $\lambda$, radiation parameter R, heat generation/absorption coefficient Q and Schmidt number Sc for flow $\widehat{g}(\eta)$, velocity field $\widehat{g}'(\eta)$, temperature field $\widehat{\theta}(\eta)$and concentration of nano-particles $\widehat{\phi}(\eta)$are discussed in detail for different scenarios of cu and $Al_2O_3$. The effect of these parameters in case of cu is illustrated through Figs. 12–16 on the interval [0,1]. Fig. 12 explains that the velocity field $\widehat{g}'(\eta)$ and concentration $\widehat{\phi}(\eta)$of nano-particles decrease with the increase in the Casson fluid parameter $\beta$ while the temperature field $\widehat{\theta}(\eta)$has an inverse relation with $\beta$ as $\widehat{\theta}(\eta)$decreases with the increase in $\beta$. Fig. 15 shows that variation in graphical curves decreases with the increase in Casson fluid parameter β.

Fig. 13 shows that velocity $\widehat{g}'(\eta)$ and temperature $\widehat{\theta}(\eta)$both increase with the increase in velocity slip parameter λ. This increase in λ

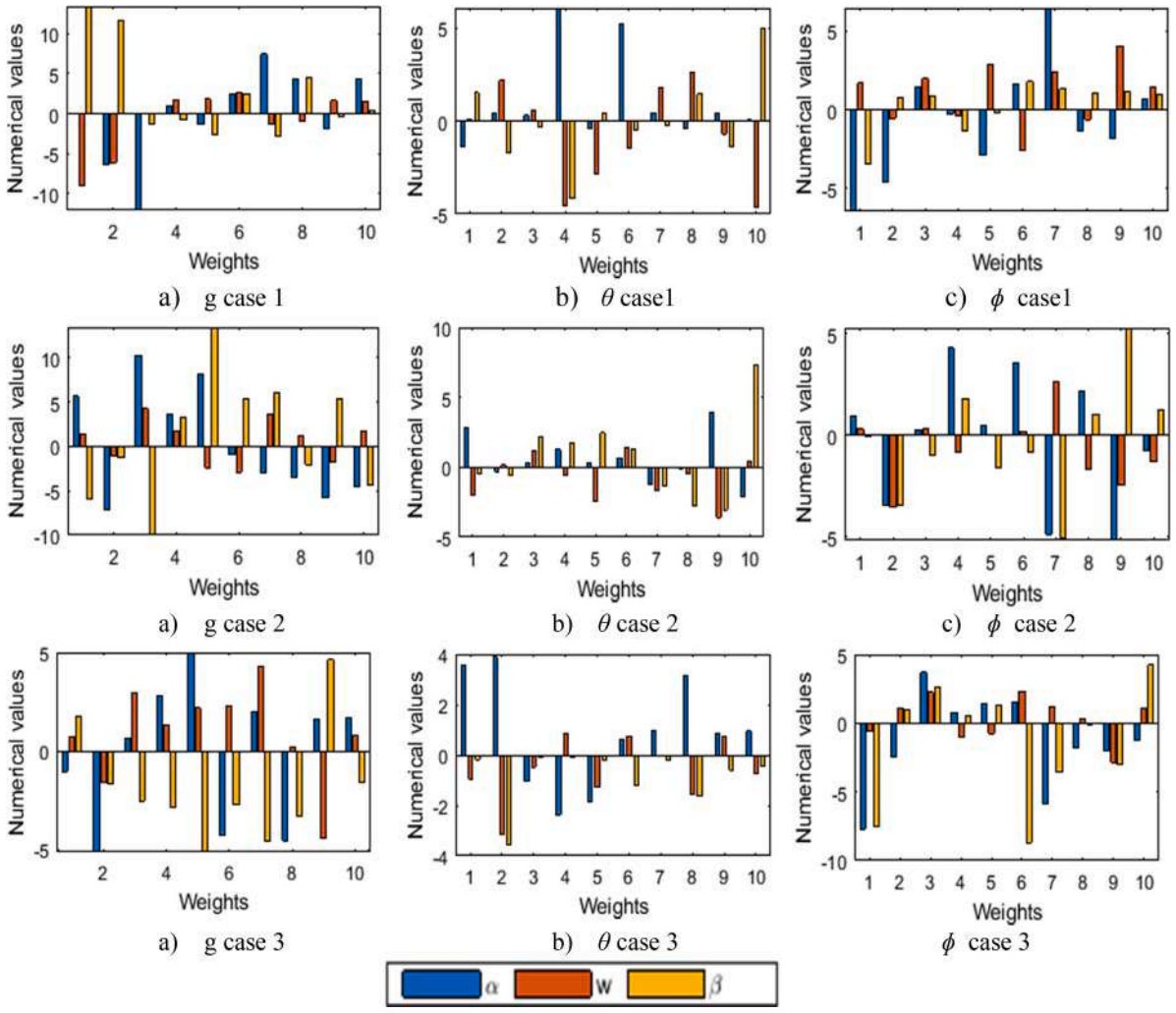


**Fig. 3.** Weights of $g$, $\theta$, and $\phi$ for scenario 1 of cu through SNNT-GA-SQP solver.

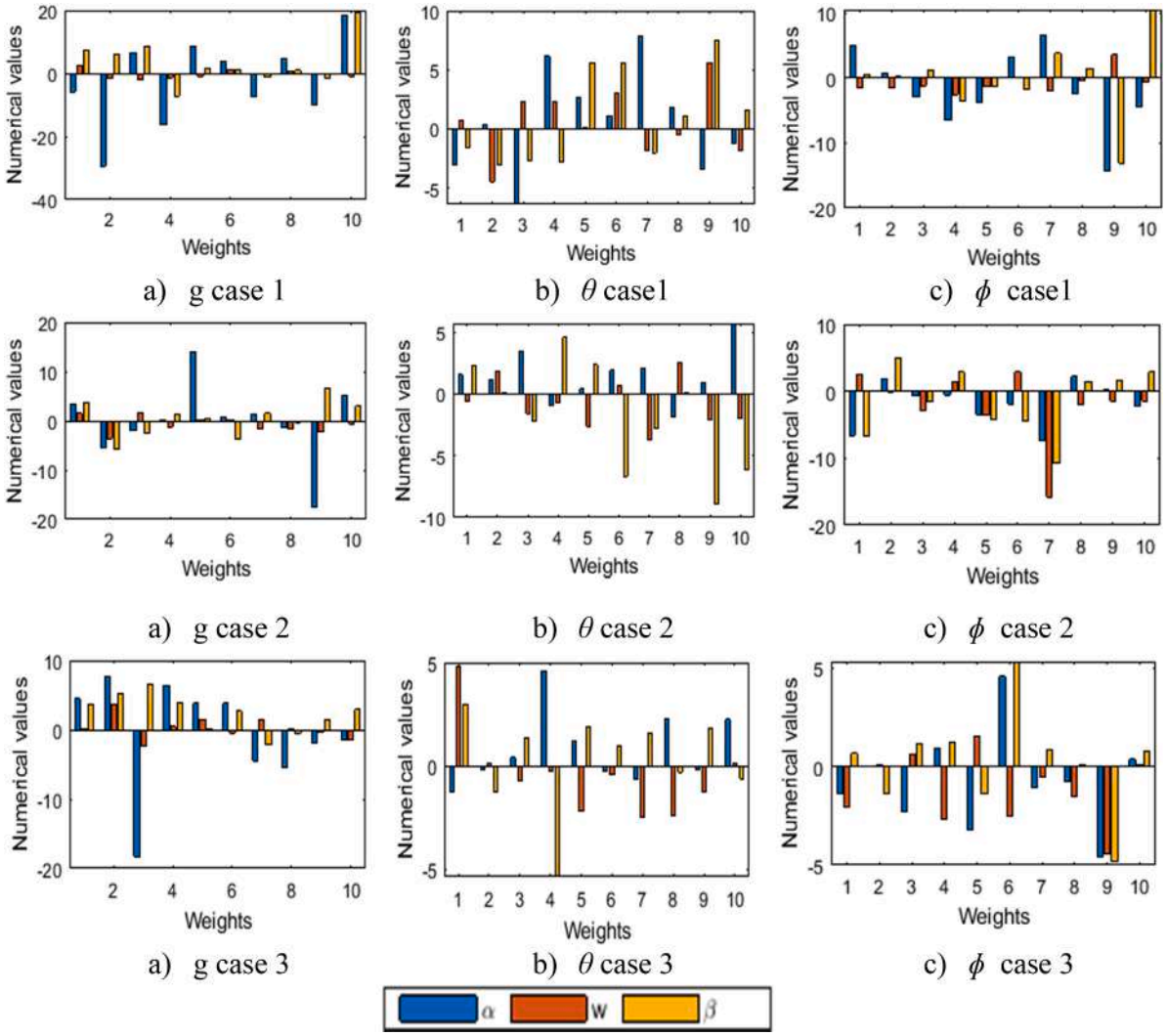


**Fig. 4.** Weights of $g$, $\theta$, and $\phi$ for scenario 2 of cu through SNNT-GA-SQP solver.

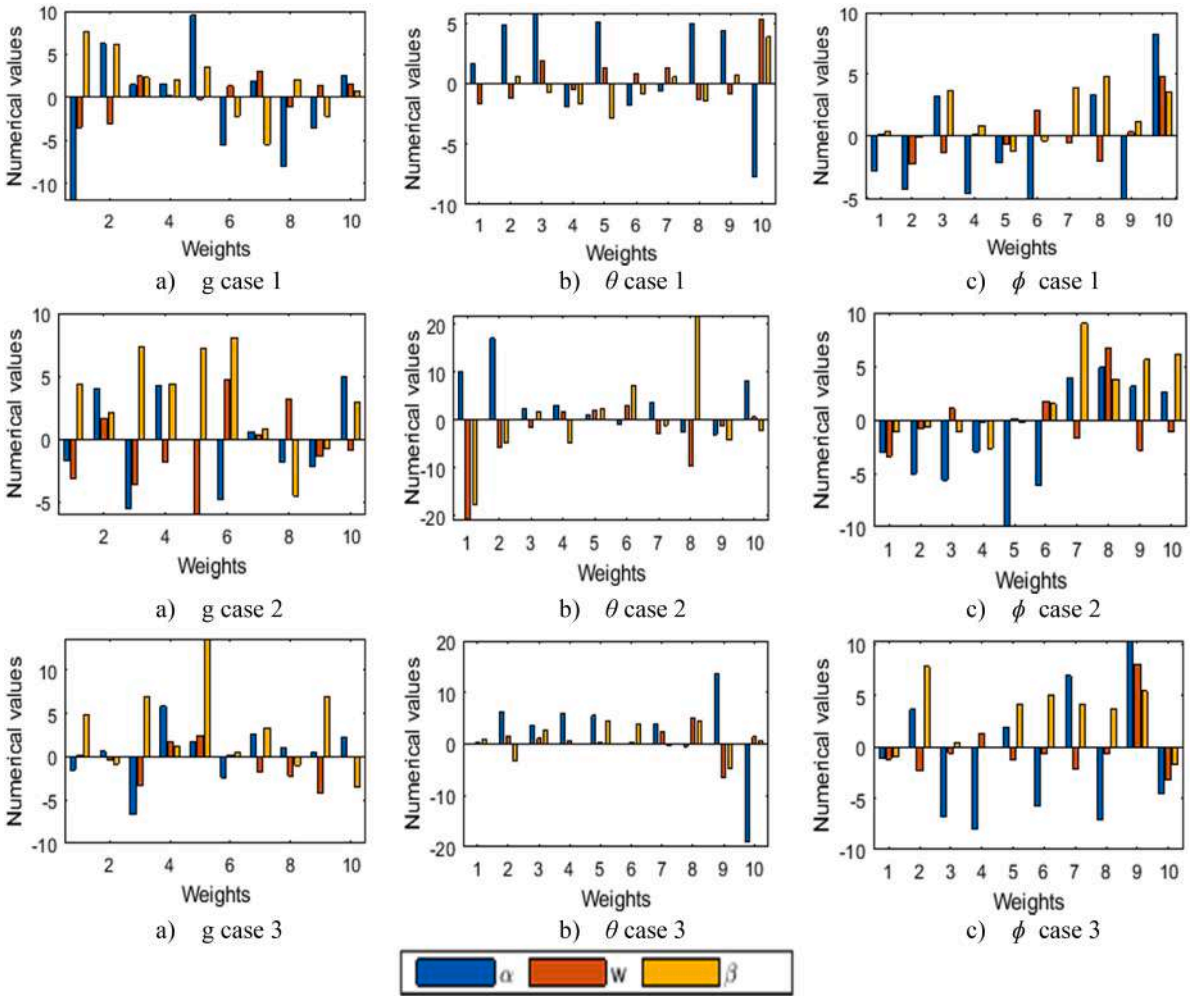


**Fig. 5.** Weights of *g*, *θ*, and *ϕ* for scenario 3 of cu through SNNT-GA-SQP solver.

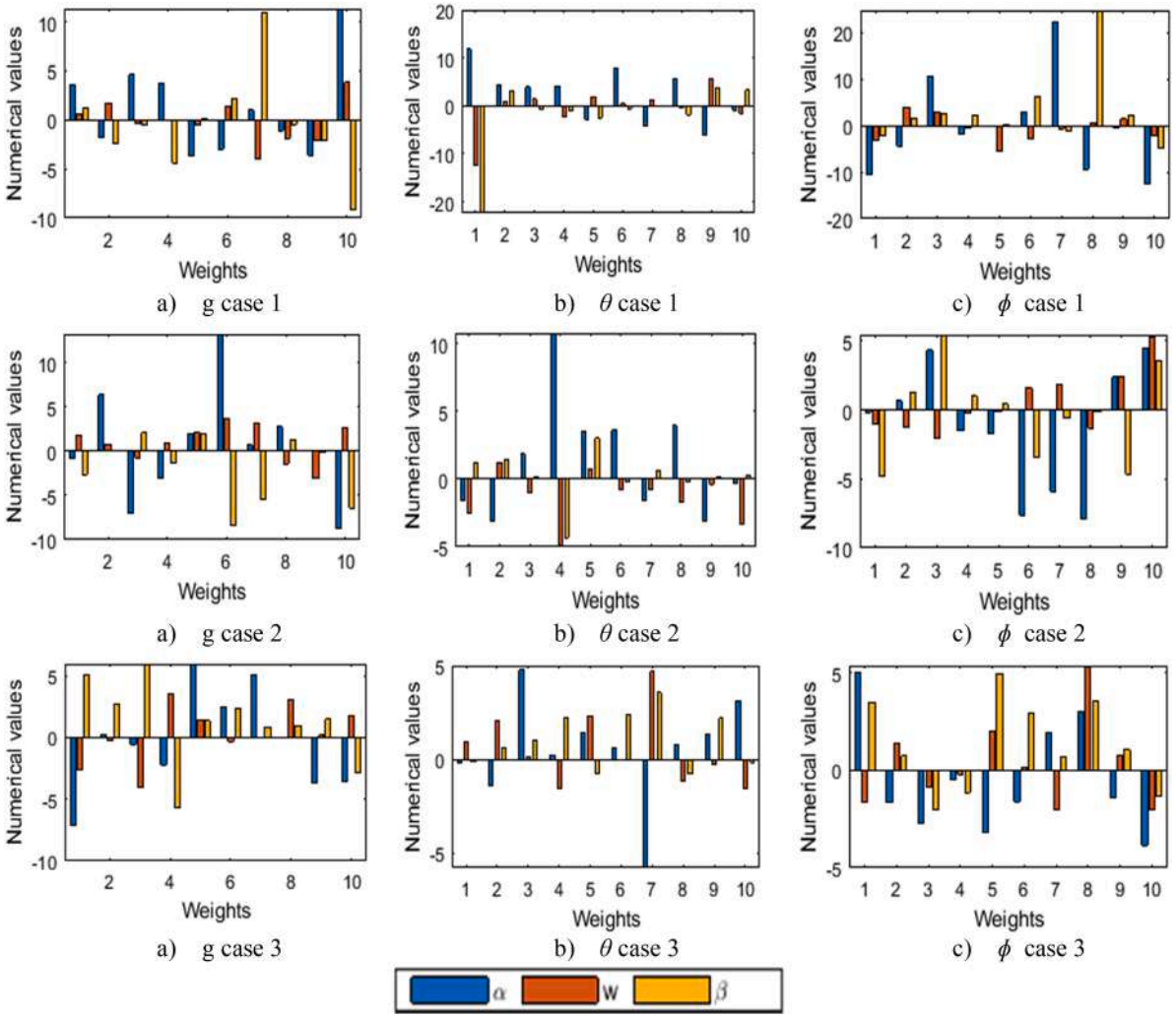


**Fig. 6.** Weights of *g*, $\theta$, and $\phi$ for scenario 4 of cu through SNNT-GA-SQP solver.

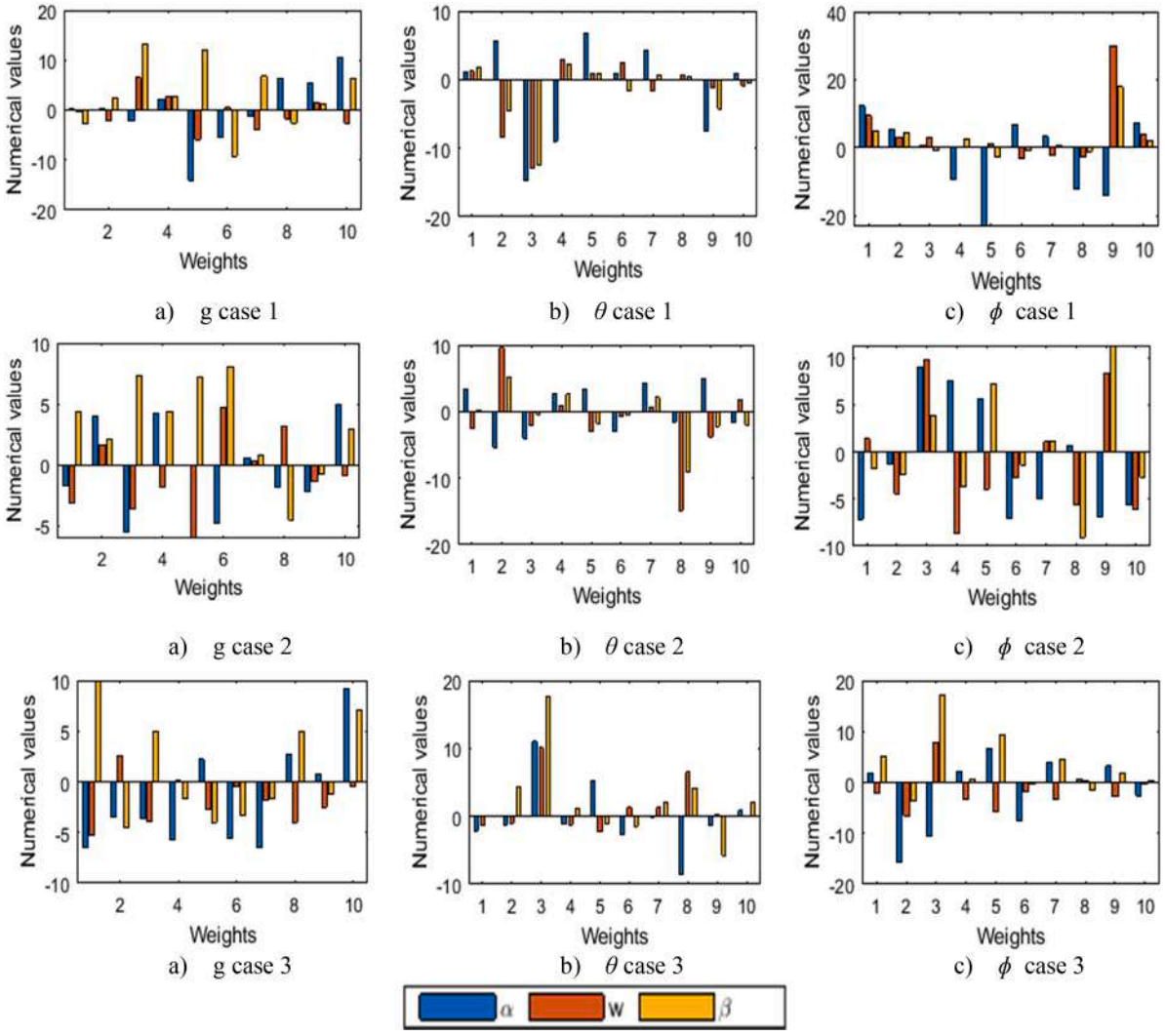


**Fig. 7.** Weights of *g*, *θ*, and *ϕ* for scenario 5 of cu through SNNT-GA-SQP solver.

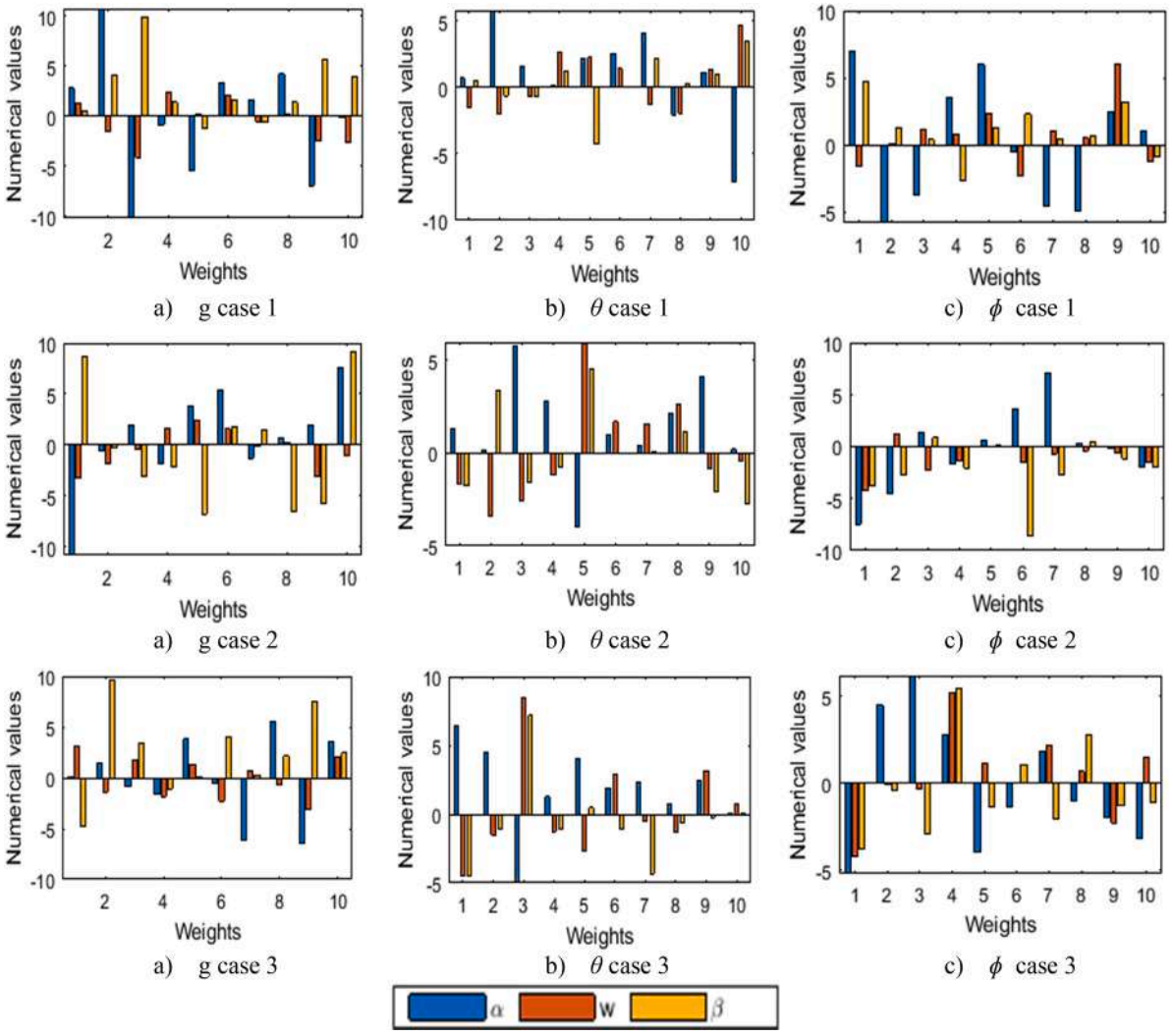


**Fig. 8.** Weights of $g$, $\theta$, and $\phi$ for scenario 1 of $Al_2O_3$ through SNNT-GA-SQP solver.

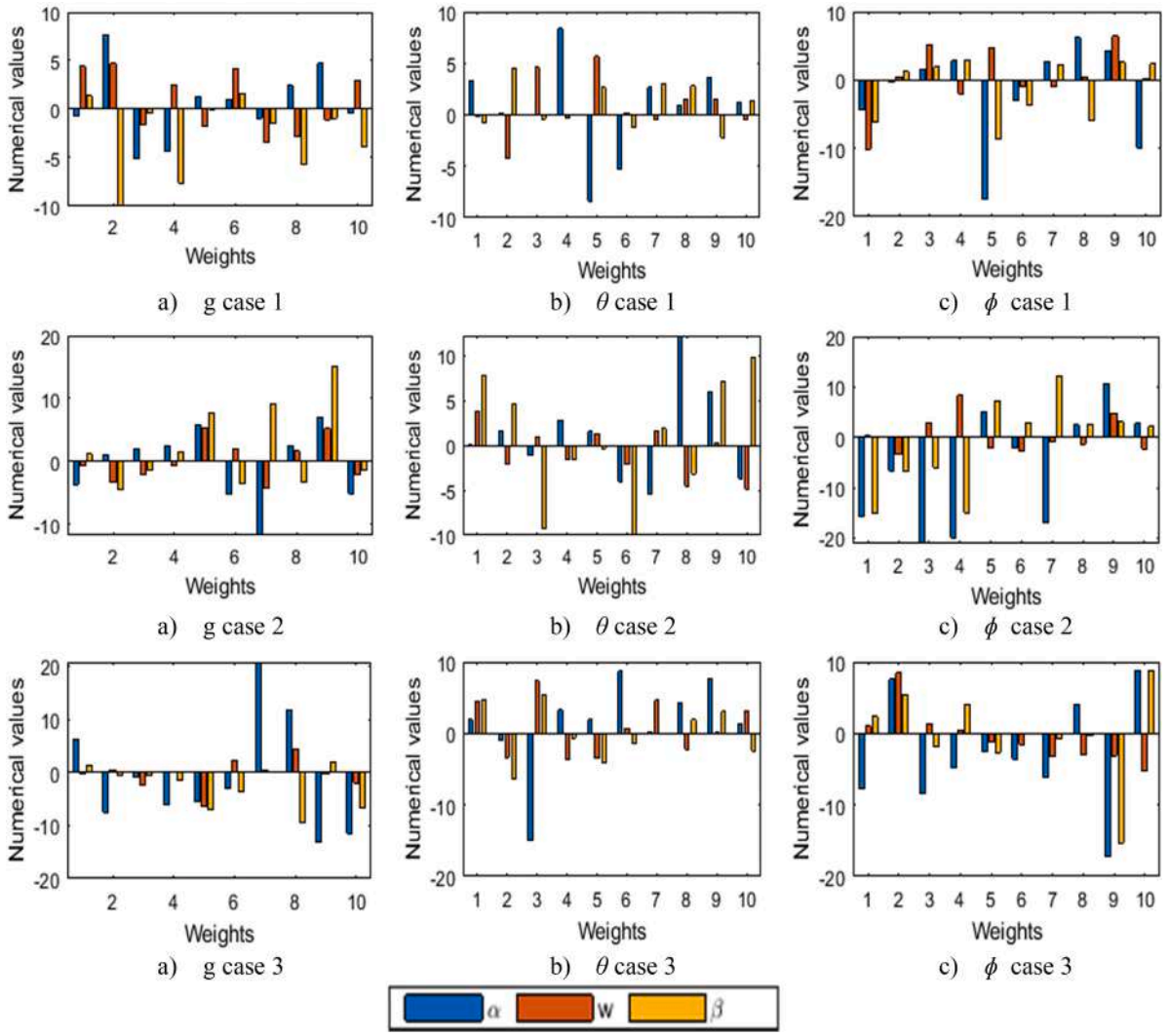


**Fig. 9.** Weights of $g$, $\theta$, and $\phi$ for scenario 2 of $Al_2O_3$ through SNNT-GA-SQP solver.

has an inverse relation with $\widehat{\phi}(\eta)$as concentration of nano-particles decreases with the increase in λ. Fig. 14 shows that heat generation/absorption coefficient Q has an inverse relation with velocity and temperature fields while the concentration of nano-particles increases with the increase in Q. Fig. 16 shows that Schmidt number Sc is the only emerging parameter that affects the concentration of nano-particles $\widehat{\phi}(\eta)$ directly The effect of the emerging parameters in case of $Al_2O_3$ is illustrated through Figs. 17-20. Fig. 17 explains that velocity field $\widehat{g}(\eta)$ and concentration $\widehat{\phi}(\eta)$of nano-particles decrease with the increase in Casson fluid parameter β while the temperature field $\widehat{\theta}(\eta)$has an inverse relation with $\beta$ as $\widehat{\theta}(\eta)$decreases with the increase in $\beta$.

Fig. 18 shows that temperature field $\widehat{\theta}(\eta)$ increases with the increase in velocity slip parameter $\lambda$ whereas this effect has an inverse relation with concentration of nano-particles $\widehat{\phi}(\eta)$. Fig. 19 shows that temperature field $\widehat{\theta}(\eta)$ decreases with the increase in radiation parameter R whereas the concentration of nanoparticles $\widehat{\phi}(\eta)$increases with the increase in R. Fig. 20 shows that variation in graphical curves increases with the decrease in Casson fluid parameter $\beta$. The numerical results obtained through SNNT-GA-SQP for each scenario of cu and $Al_2O_3$ overlap quite significantly with the reference solutions obtained through Mathematica on the interval [0,1]. Absolute errors (AEs) in $\widehat{g}(\eta)$, $\widehat{g}(\eta)$,$\widehat{\theta}(\eta)$ and $\widehat{\phi}(\eta)$ for all scenarios in the case of both cu and $Al_2O_3$ are also obtained and plotted.

Fig. 21 shows the accuracy of $g(\eta)$ and $g'(\eta)$ for all scenarios of cu. In case of $g(\eta)$ accuracy is from $10^{-2}$ to $10^{-7}$ while for $g'(\eta)$ the accuracy is from $10^{-2}$ to $10^{-6}$. Fig. 22 shows the accuracy of $\theta(\eta)$ and $\phi(\eta)$ for all scenarios of cu and it is from $10^{-3}$ to $10^{-7}$. Fig. 1 (in Appendix) shows the accuracy of $g(\eta)$ and $g'(\eta)$ for all scenarios of $Al_2O_3$.In case of $g(\eta)$ accuracy is from $10^{-2}$ to $10^{-6}$ while for $g'(\eta)$ the accuracy is from $10^{-1}$ to $10^{-6}$. Fig. 2 (in Appendix) shows the accuracy of $\theta(\eta)$ and $\phi(\eta)$ for all scenarios of $Al_2O_3$. In case of $\theta(\eta)$ accuracy is from $10^{-2}$ to $10^{-6}$ while for $\phi(\eta)$ the accuracy is from $10^{-2}$ to $10^{-7}$. Information regarding AE in tabulated form for all scenarios for cu are presented in Tables 8–12.

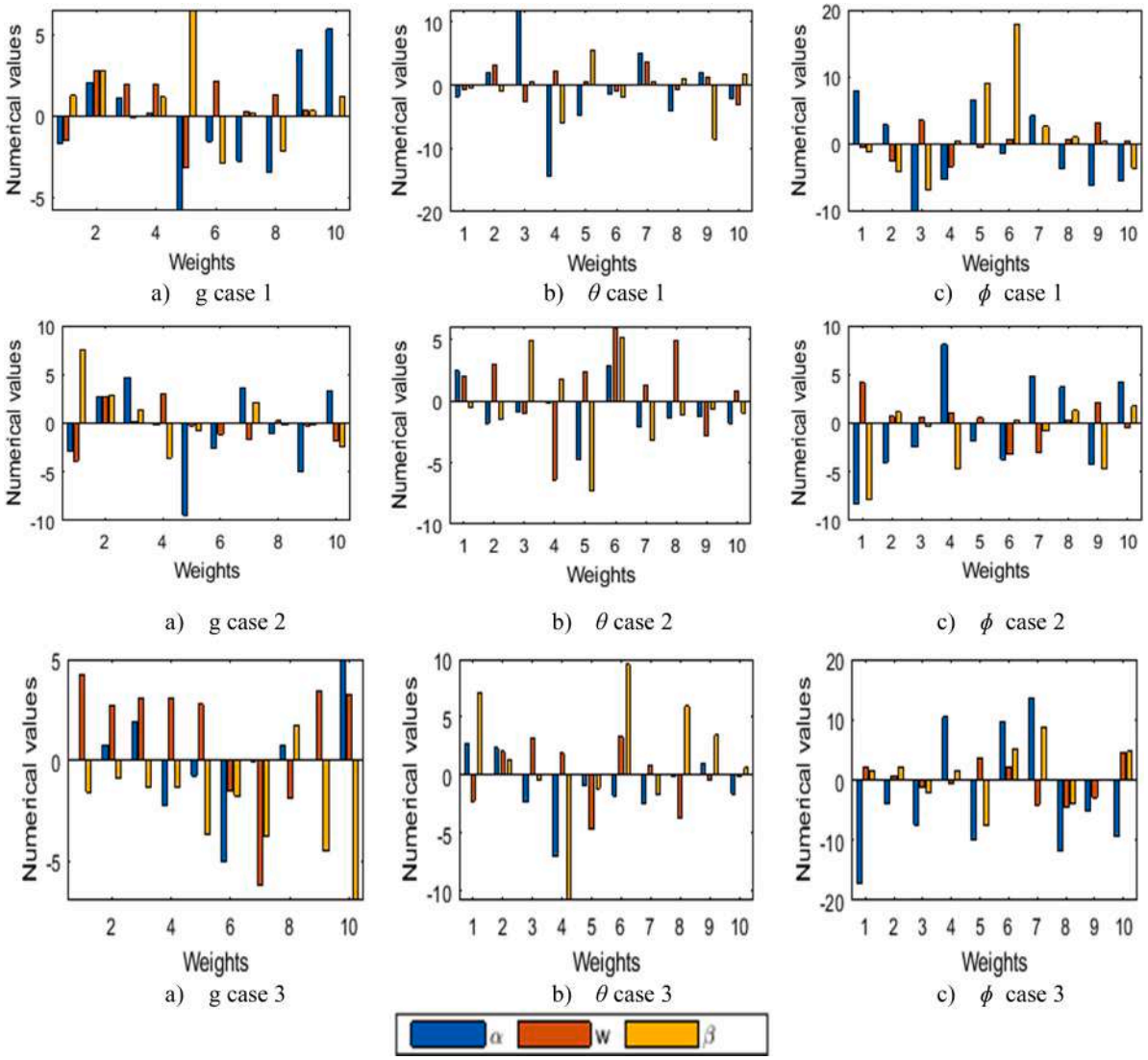


**Fig. 10.** Weights of $g$, $\theta$, and $\phi$ for scenario 3 of $Al_2O_3$ through SNNT-GA-SQP solver.

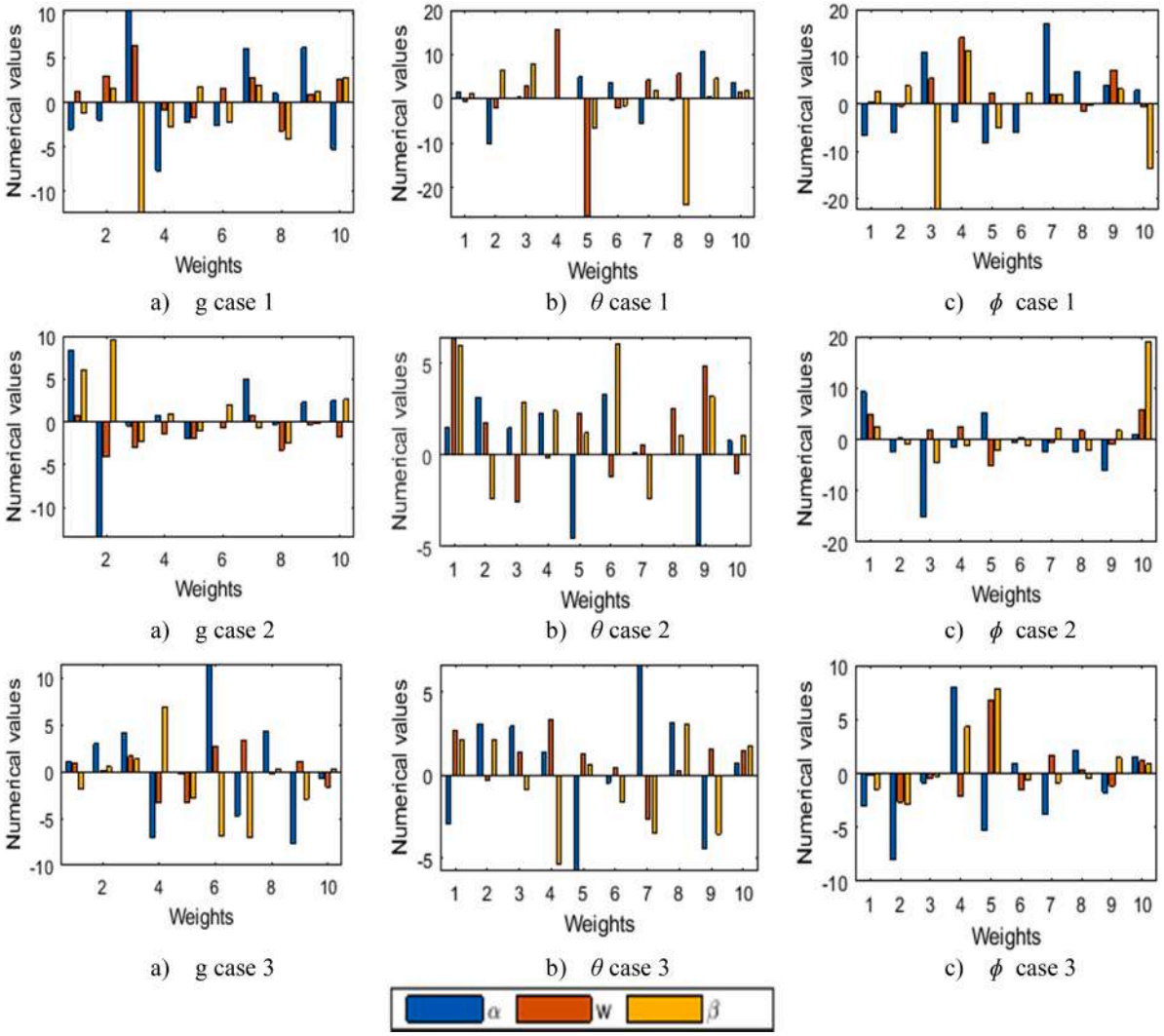


**Fig. 11.** Weights of $g$, $\theta$, and $\phi$ for scenario 4 of $Al_2O_3$ through SNNT-GA-SQP solver.

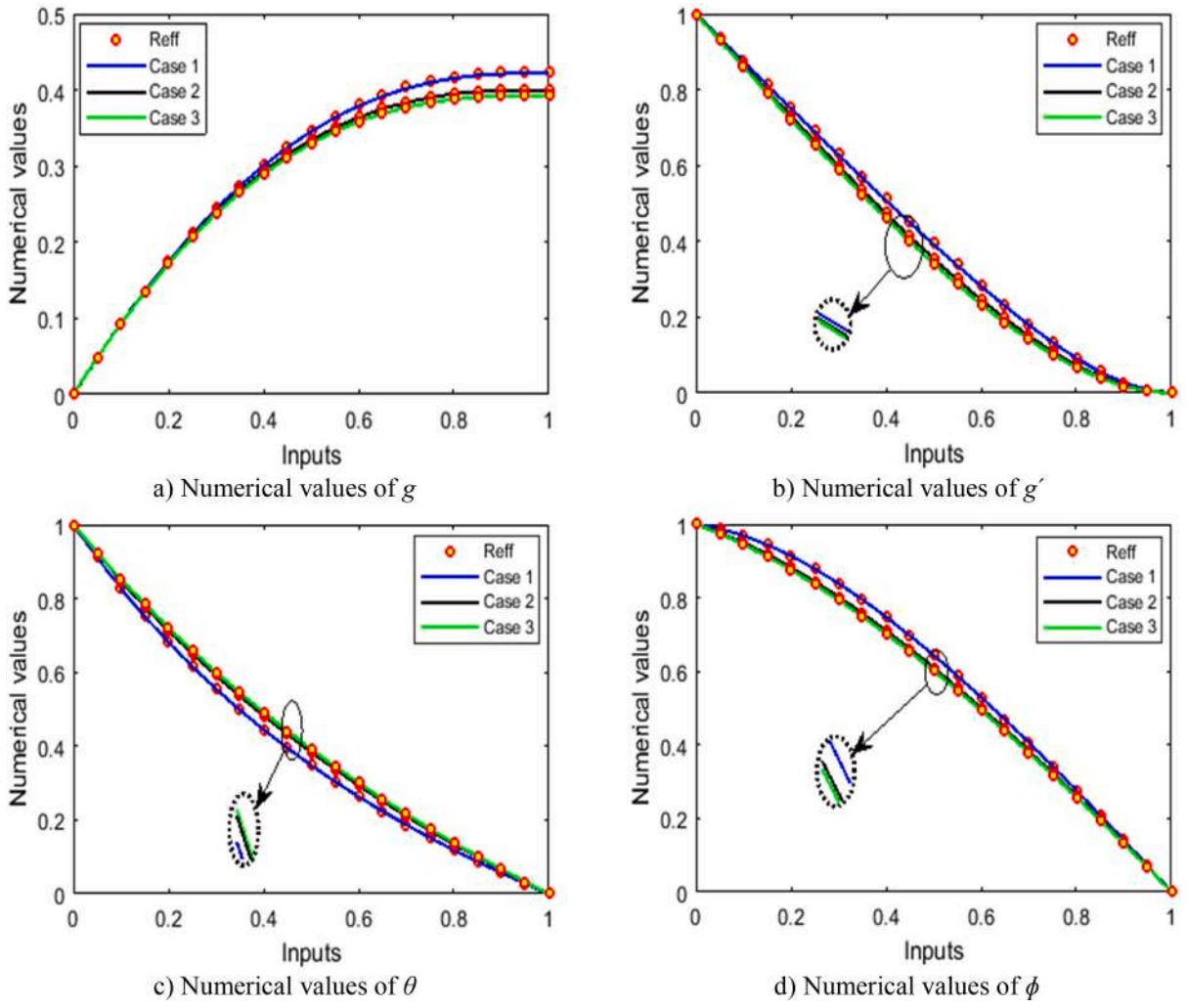


**Fig. 12.** Numerical values for scenario 1 of cu with all cases obtained through SNNT-GA-SQP.

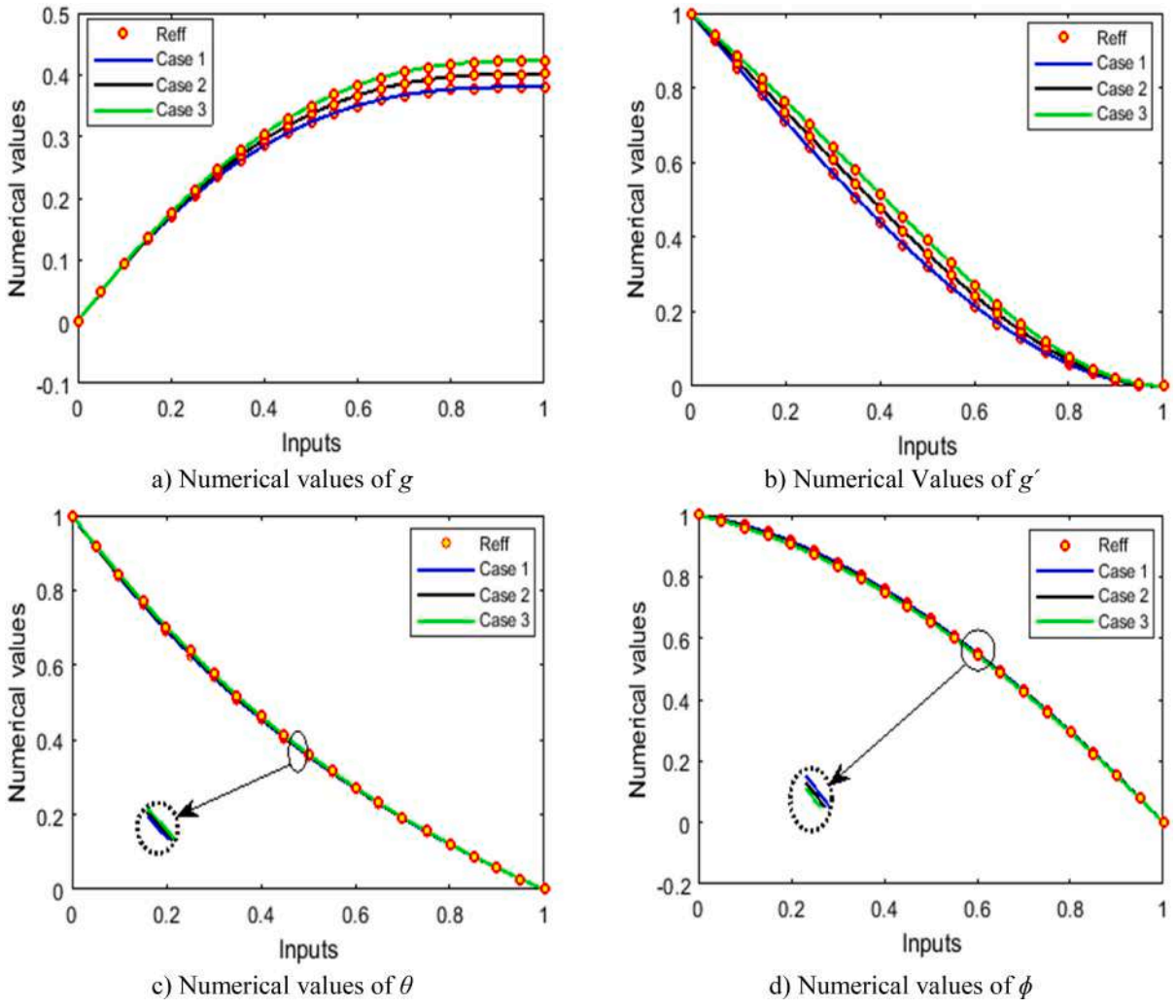


**Fig. 13.** Numerical values for scenario 2 of cu with all cases obtained through SNNT-GA-SQP.

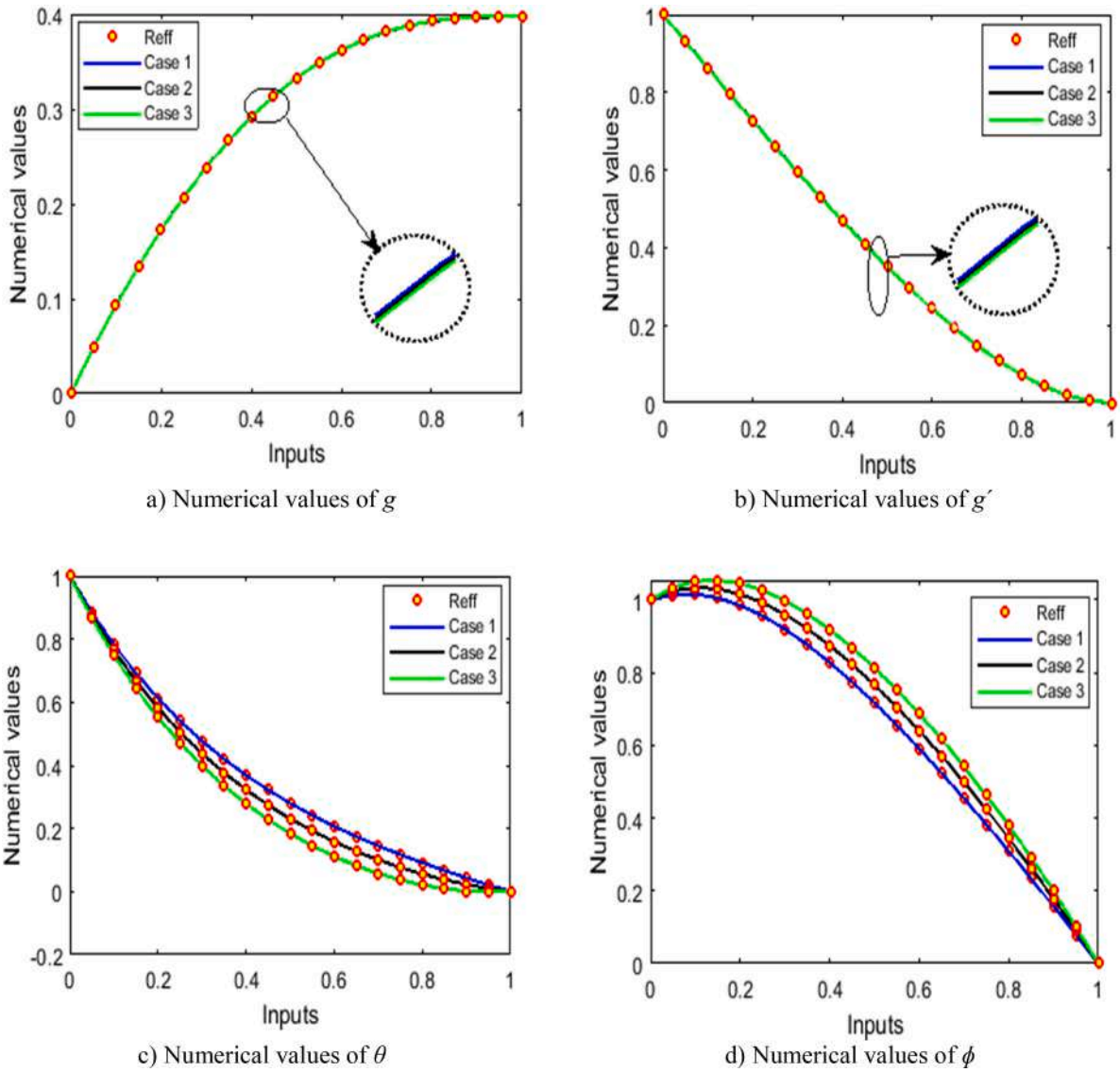


**Fig. 14.** Numerical values for scenario 3 of cu with all cases obtained through SNNT-GA-SQP.

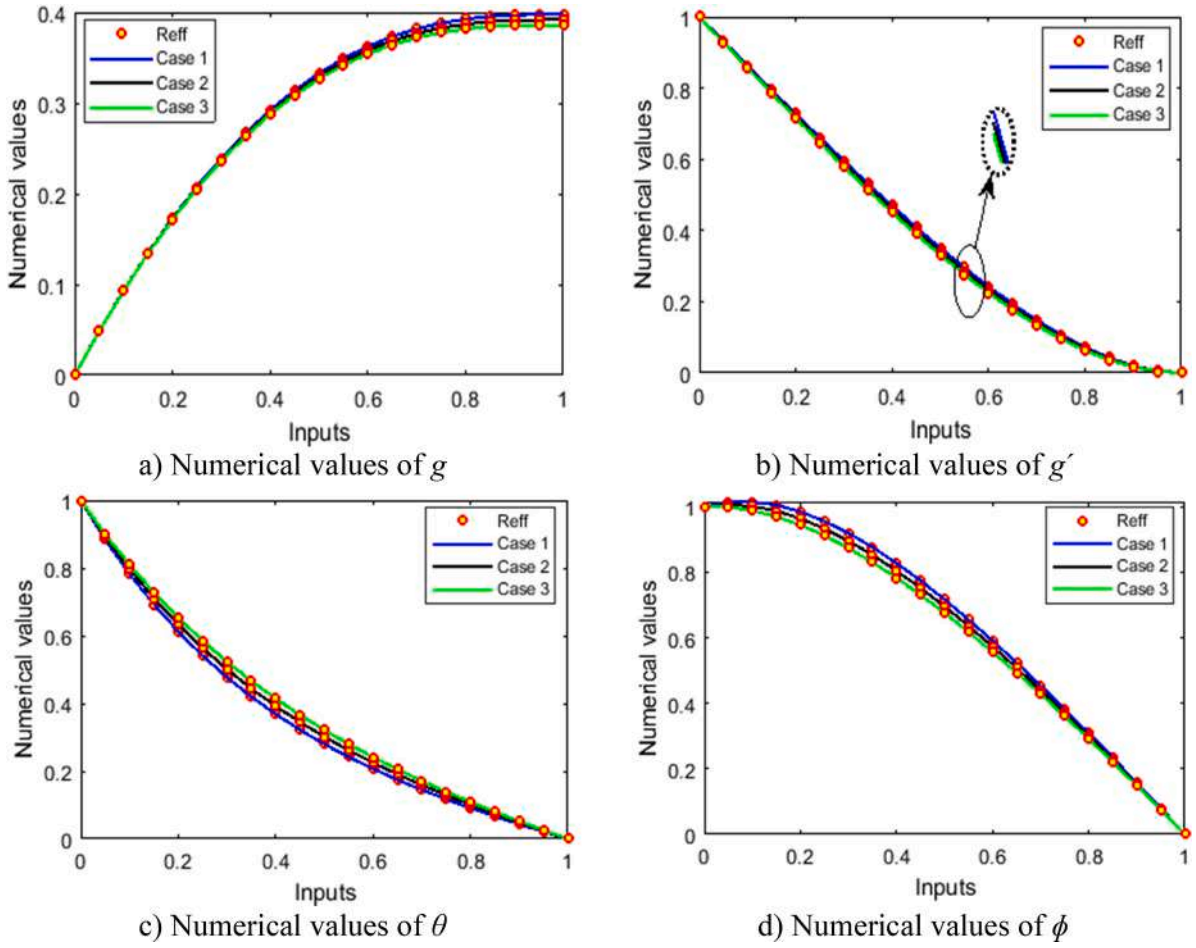


**Fig. 15.** Numerical values for scenario 4 of cu with all cases obtained through SNNT-GA-SQP.

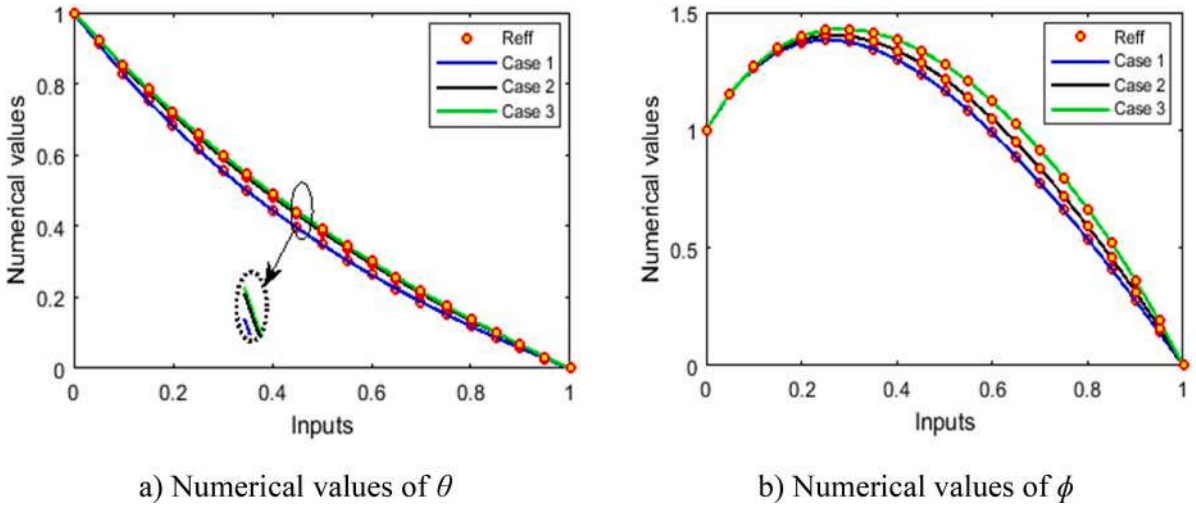


**Fig. 16.** Numerical values for scenario 5 of cu with all cases obtained through SNNT-GA-SQP.

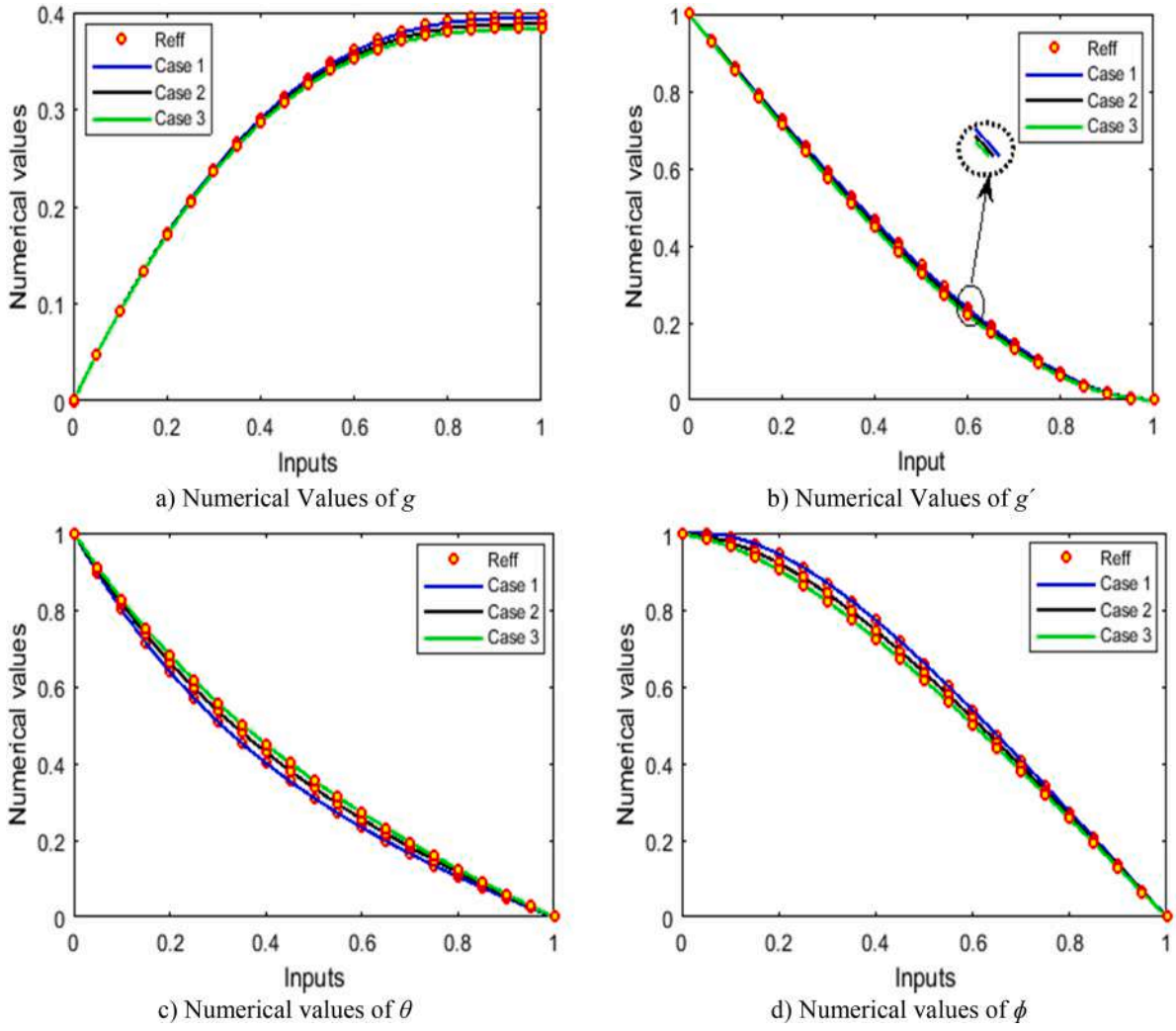


**Fig. 17.** Numerical values for scenario 1 of $Al_2O_3$ with all cases obtained through SNNT-GA-SQP.

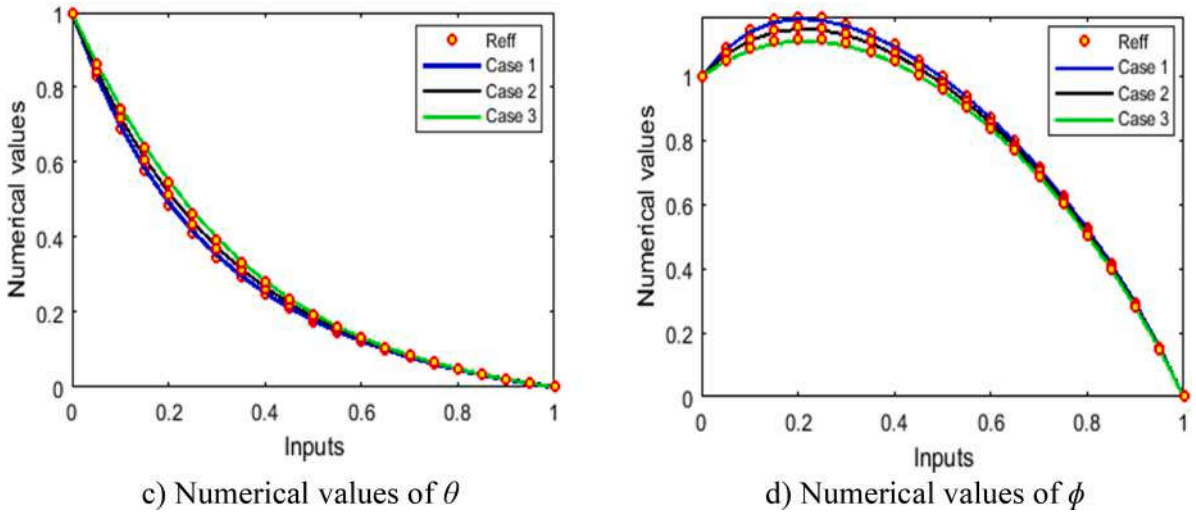


**Fig. 18.** Numerical values for scenario 2 of $Al_2O_3$ with all cases obtained through SNNT-GA-SQP.

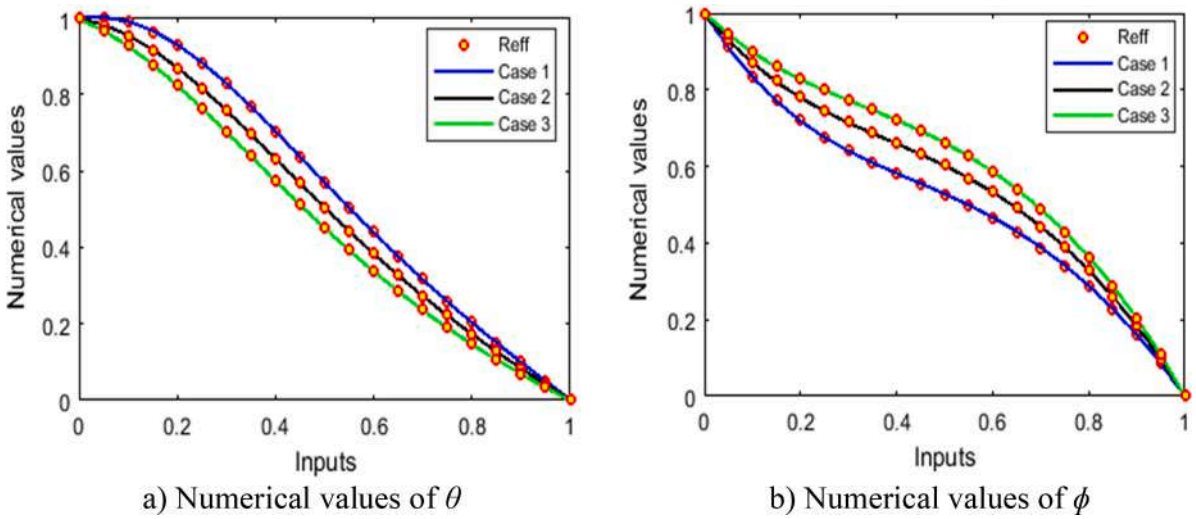


**Fig. 19.** Numerical values for scenario 3 of $Al_2O_3$ with all cases obtained through SNNT-GA-SQP.

The complete and detailed analysis related to SNNT-GA-SQP performance is scrutinized and illustrated through Figs. 23-42 in case of cu while this representation is through Figs. 3–18 (in Appendix) for $Al_2O_3$. This error analysis is carried out using quite reliable performance operators E-TIC, RMSE, E-$R^2$ and E-NSE for all scenarios of cu and $Al_2O_3$ and the best values with the corresponding iteration numbers for cu in tabulated form are presented in Tables 3–7. The performance grades in the case of all scenarios of cu are expressed through different ranges in Table 13.

The list of these grades is given below. The values obtained through the above-listed statistical operators are very close to zero for every scenario of MNP-CF problem for all velocity and temperature fields. The reliability of the proposed solver SNNT-GA-SQP is explained through fitness ε for both cu and $Al_2O_3$ and illustrated in Figs. 43–45. For all scenarios of cu and $Al_2O_3$, $\varepsilon \leq 10^{-4}, 10^{-5}, 10^{-6}$. The analysis of the convergence of proposed solver SNNT-GA-SQP is also demonstrated through function count and time consumed to perform complete runs by the solver.

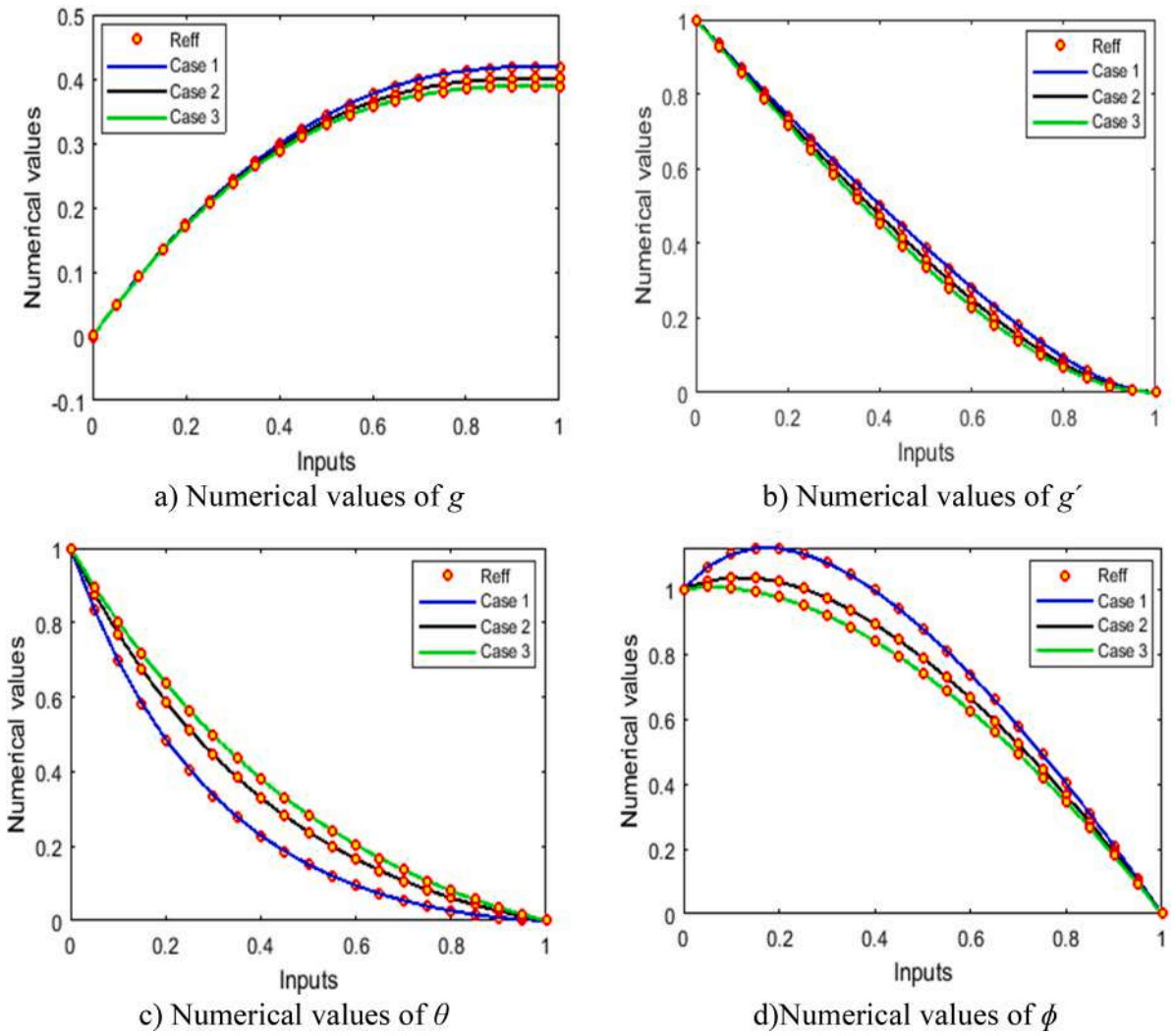


**Fig. 20.** Numerical values for scenario 4 of $Al_2O_3$ with all cases obtained through SNNT-GA-SQP.

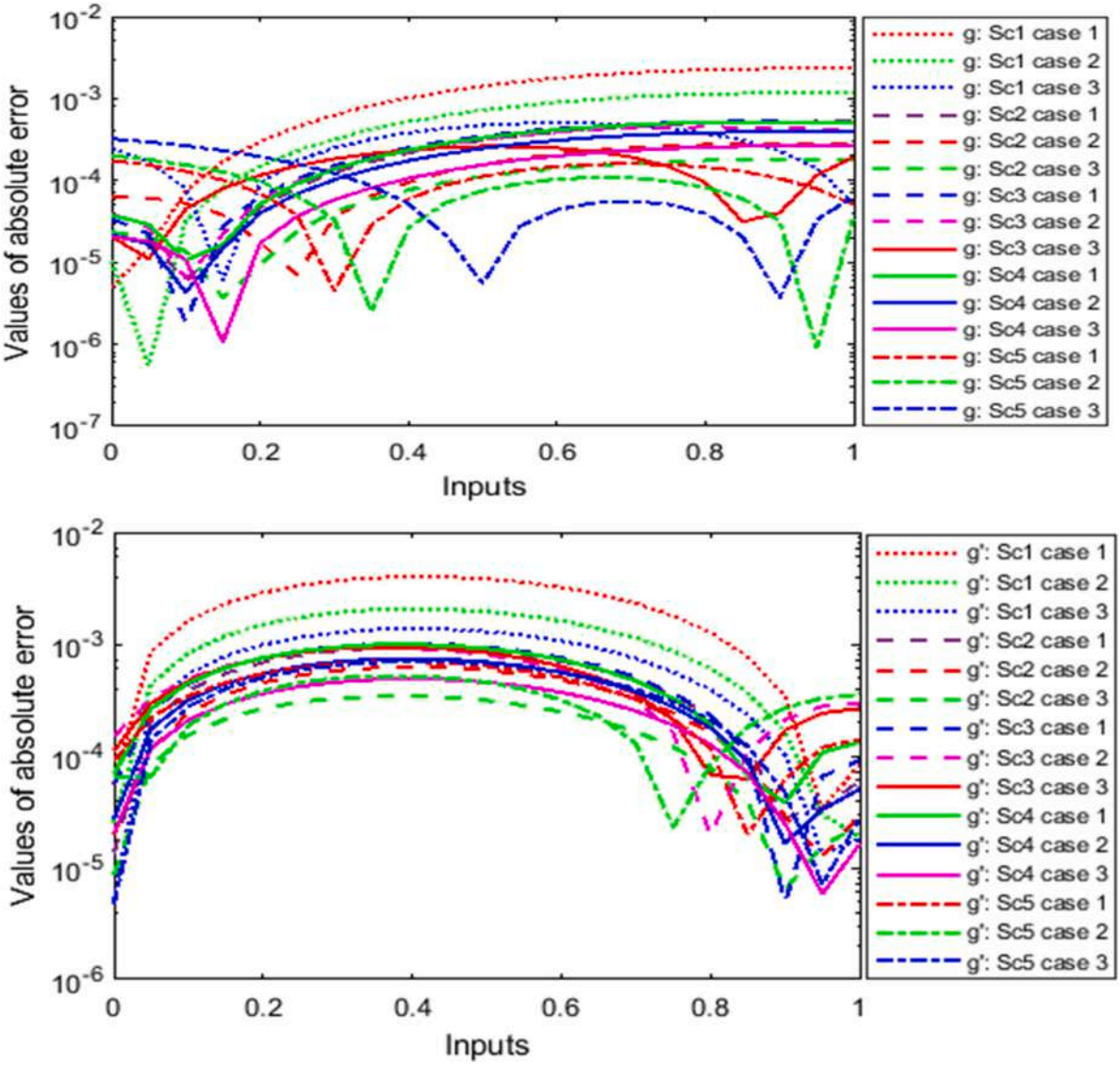


**Fig. 21.** Absolute errors in the values of $g$ and $g'$ for all scenarios of cu.

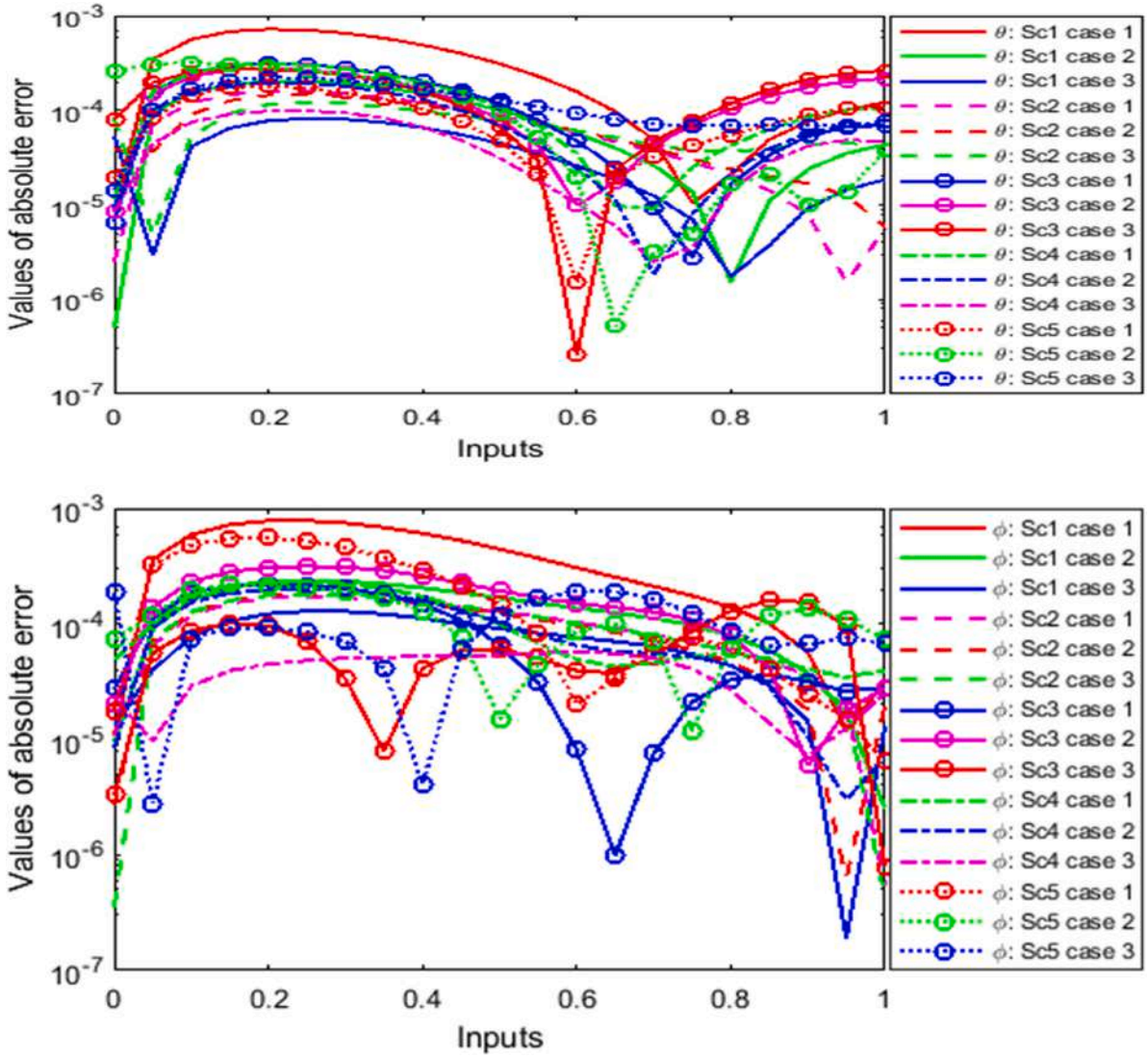


**Fig. 22.** Absolute errors in the values of $\theta$ and $\phi$ for all scenarios of cu.

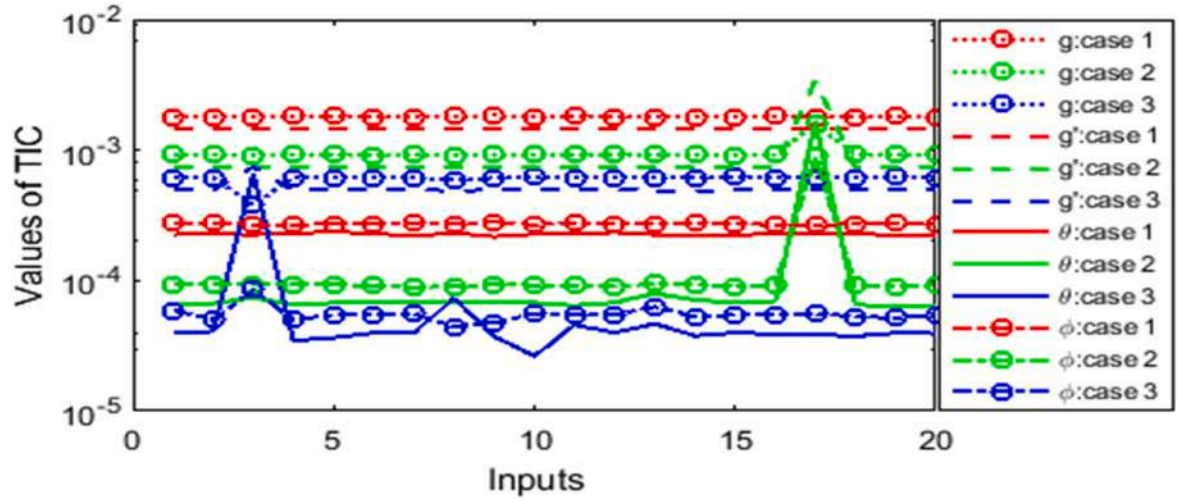


**Fig. 23.** E-TIC for cases (I, II, III) of scenario 1 in case of cu.

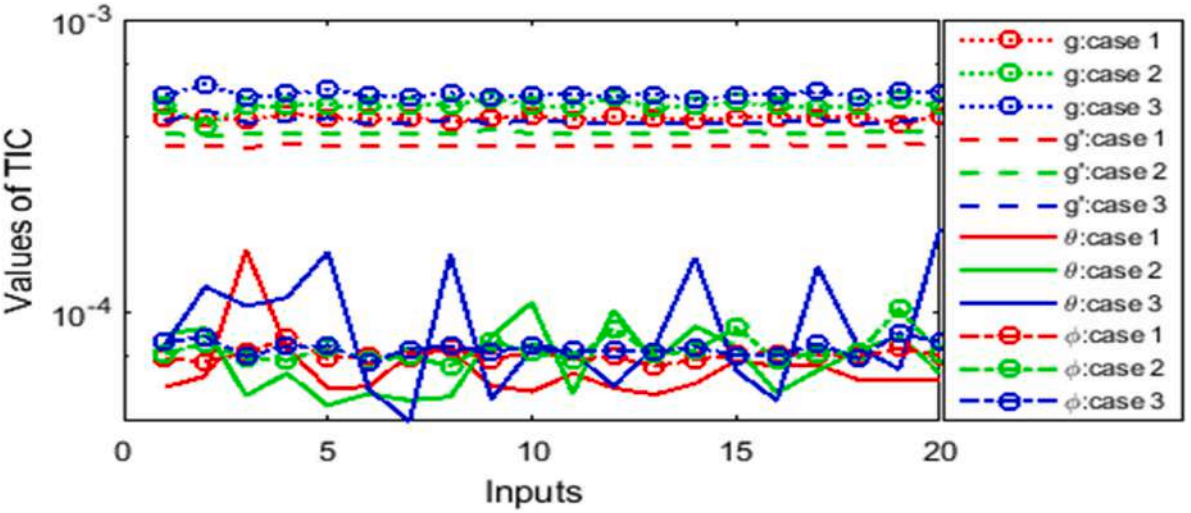


**Fig. 24.** E-TIC for cases (I, II, III) of scenario 2 in case of cu.

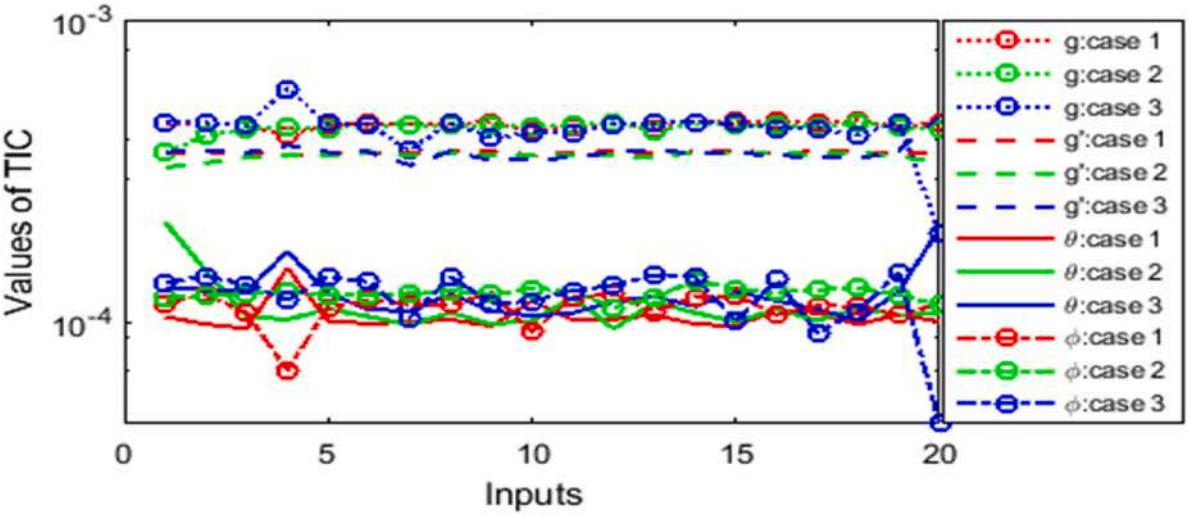


**Fig. 25.** E-TIC for cases (I, II, III) of scenario 3 in case of cu.

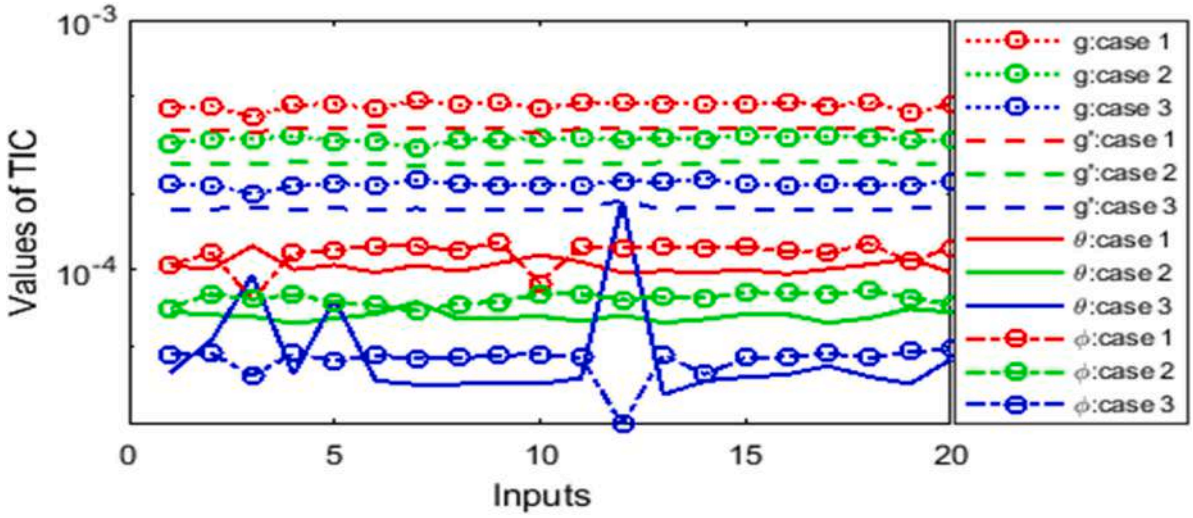


**Fig. 26.** E-TIC for cases (I, II, III) of scenario 4 in case of cu.

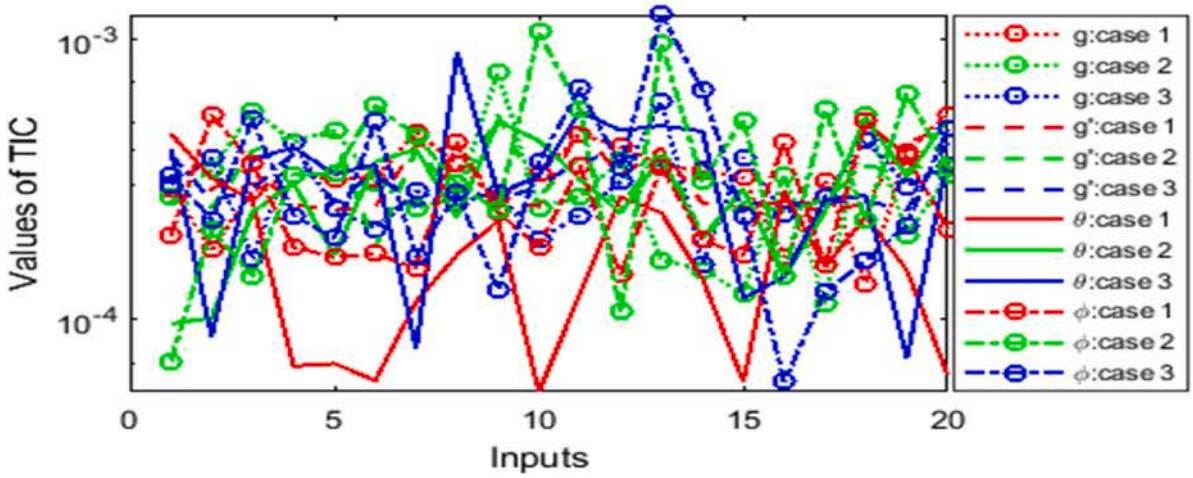


**Fig. 27.** E-TIC for cases (I, II, III) of scenario 5 in case of cu.

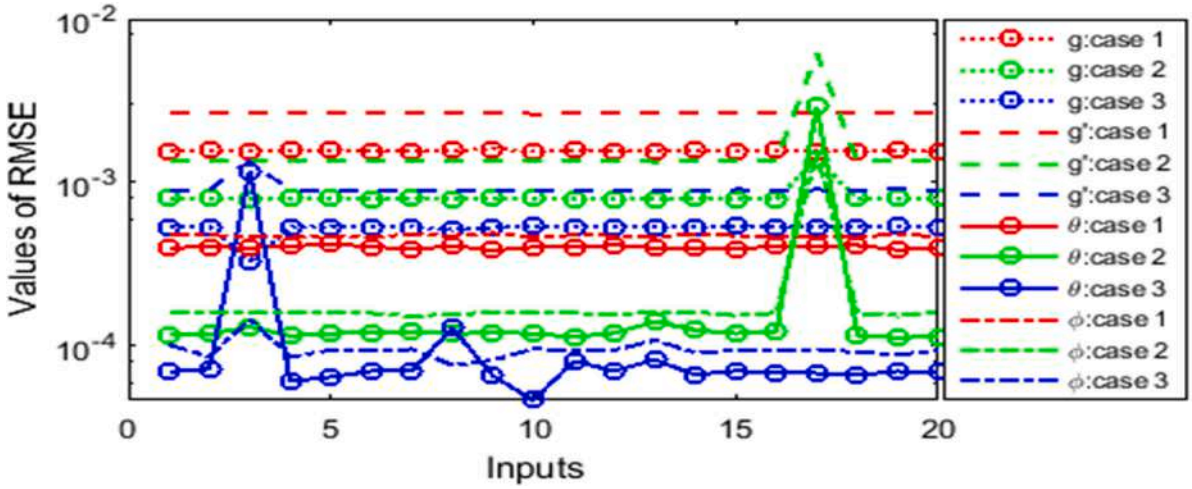


**Fig. 28.** RMSE for cases (I, II, III) of scenario 1 in case of cu.

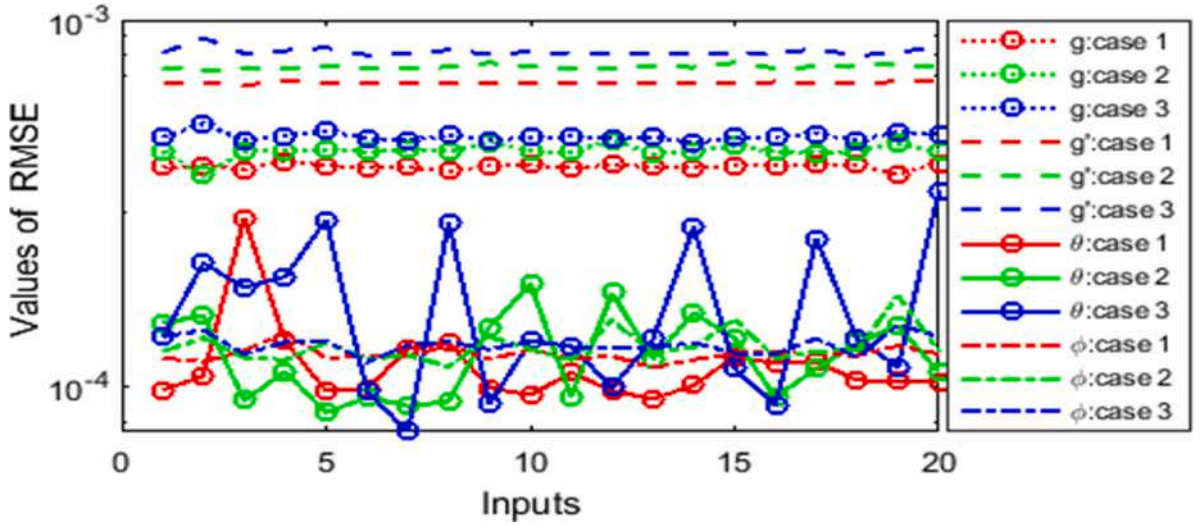


**Fig. 29.** RMSE for cases (I, II, III) of scenario 2 in case of cu.

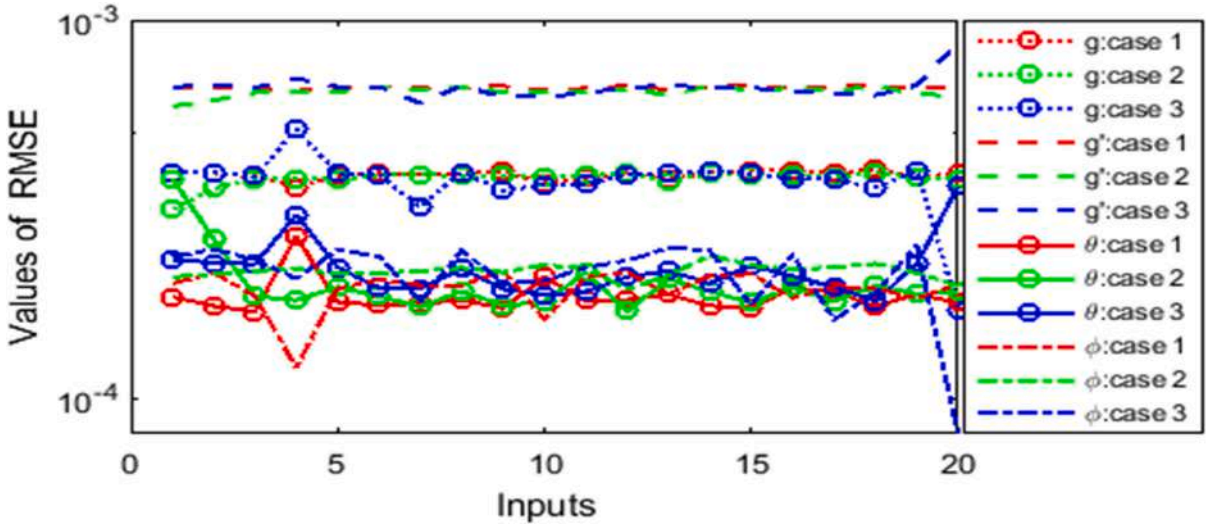


**Fig. 30.** RMSE for cases (I, II, III) of scenario 3 in case of cu.

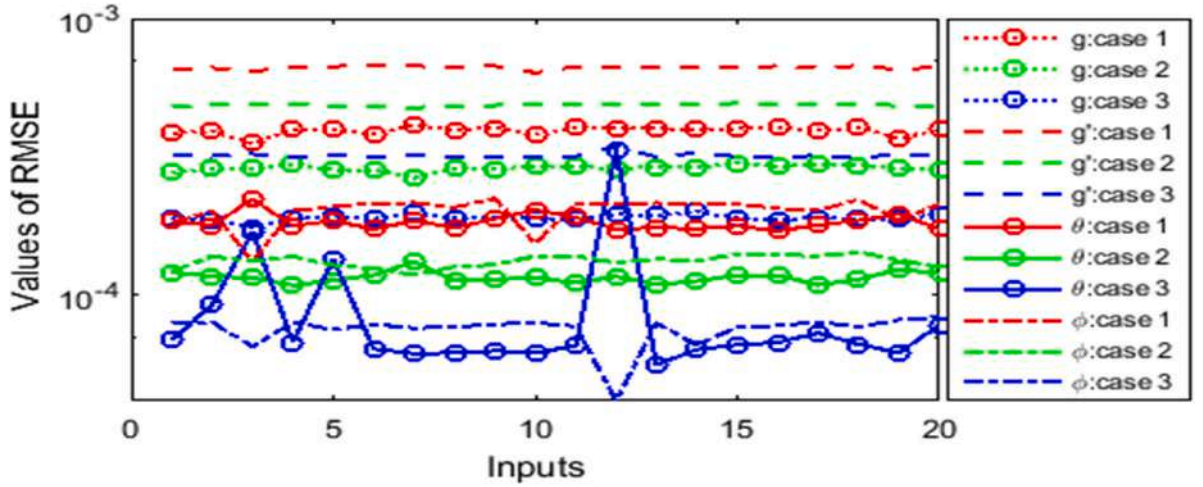


**Fig. 31.** RMSE for cases (I, II, III) of scenario 4 in case of cu.

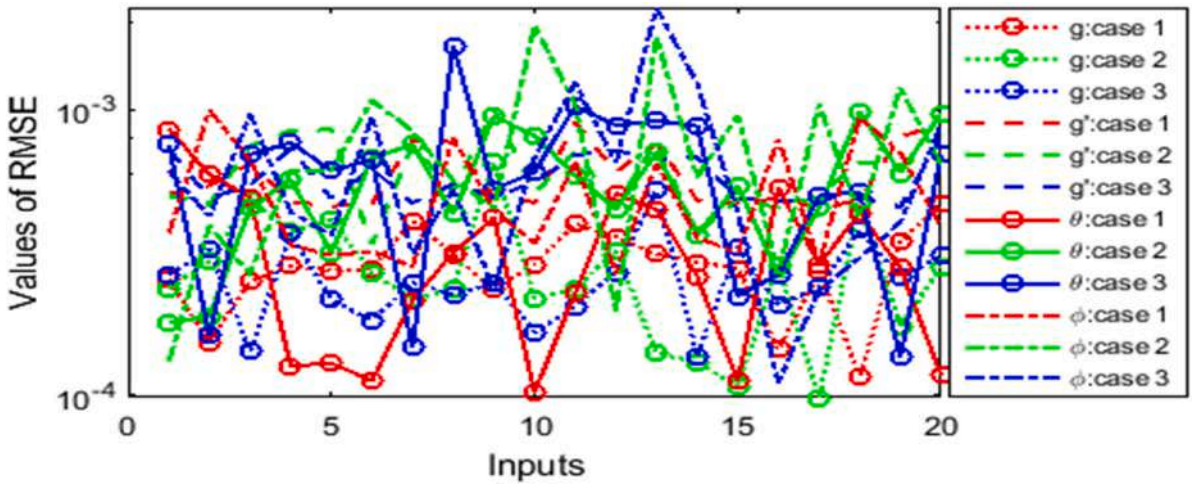


**Fig. 32.** RMSE for cases (I, II, III) of scenario 5 in case of cu.

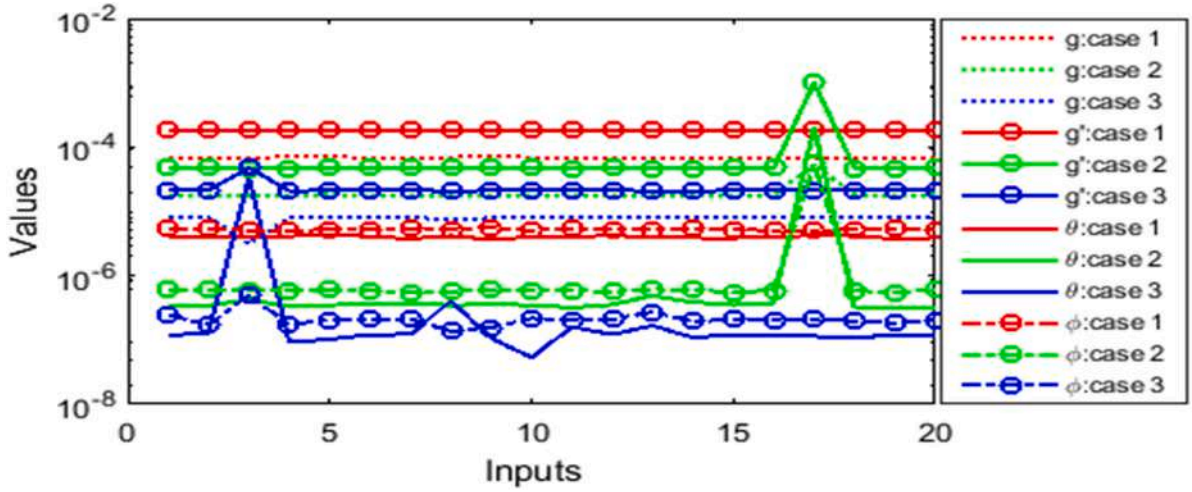


**Fig. 33.** E-$R^2$ for cases (I, II, III) of scenario 1 in case of cu.

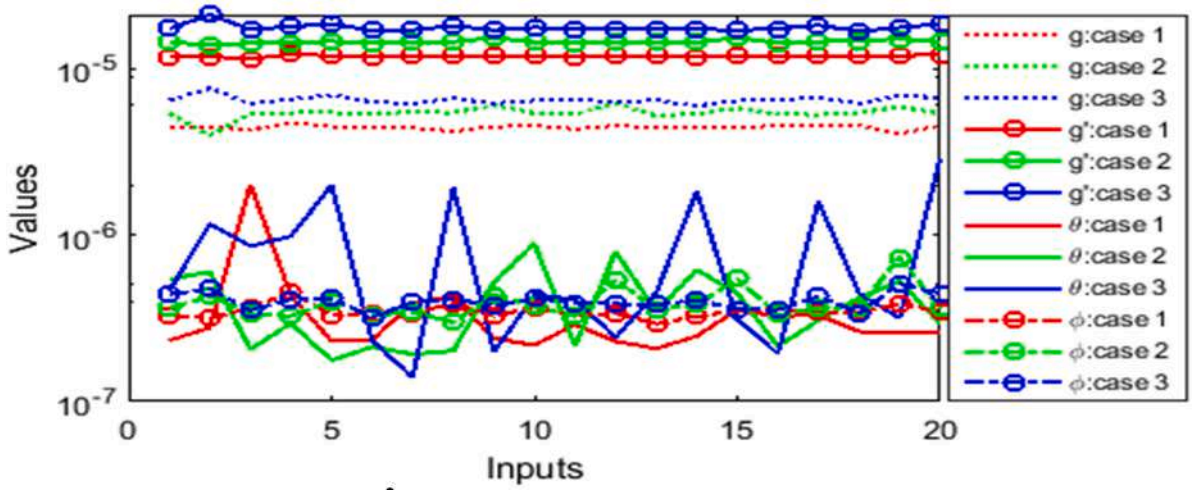


**Fig. 34.** E-$R^2$ for cases (I, II, III) of scenario 2 in case of cu.

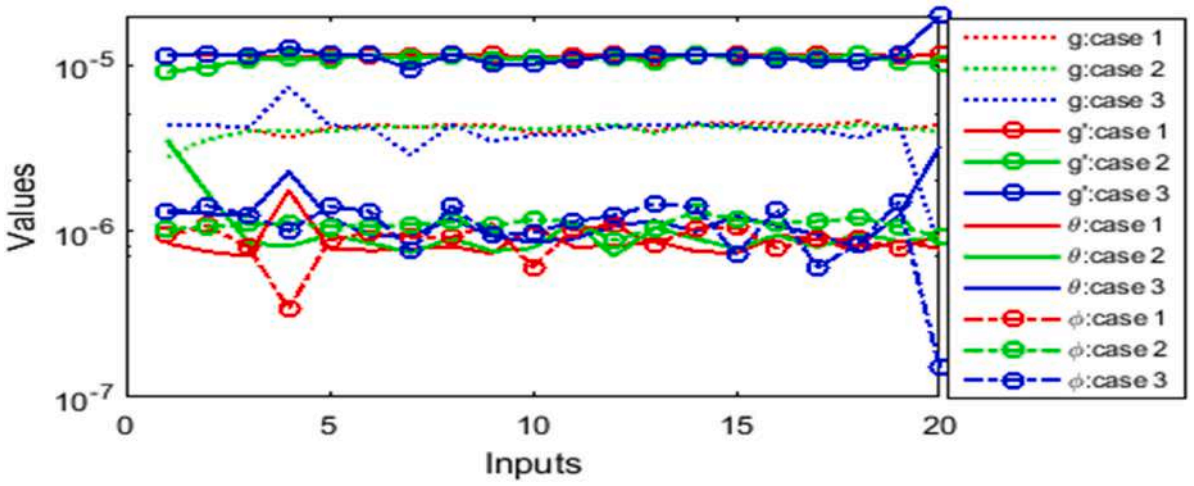


**Fig. 35.** E-$R^2$ for cases (I, II, III) of scenario 3 in case of cu.

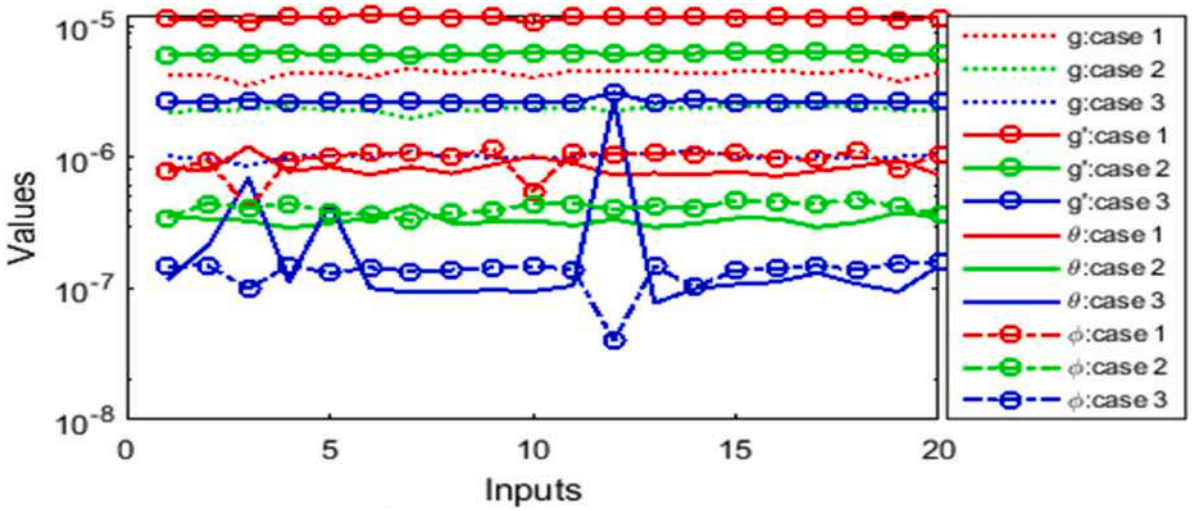


**Fig. 36.** E-$R^2$ for cases (I, II, III) of scenario 4 in case of cu.

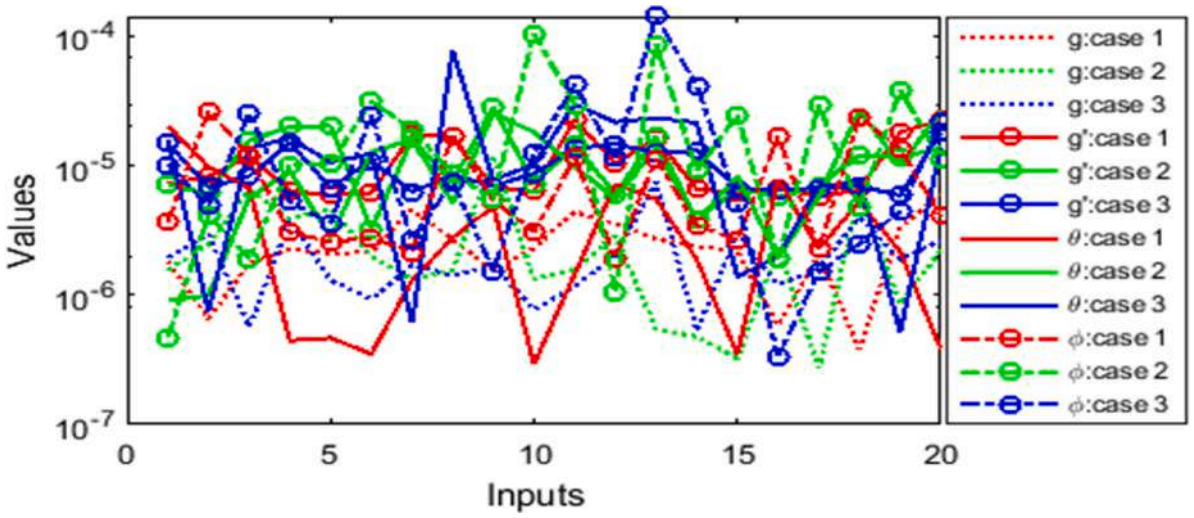


**Fig. 37.** E-$R^2$ for cases (I, II, III) of scenario 5 in case of cu.

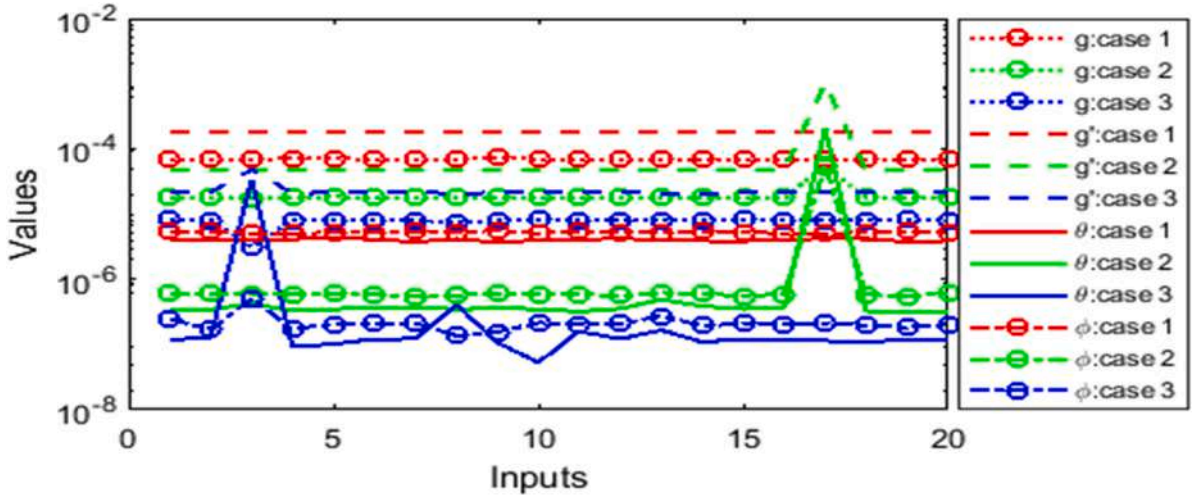


**Fig. 38.** E-NSE for cases (I, II, III) of scenario 1 in case of cu.

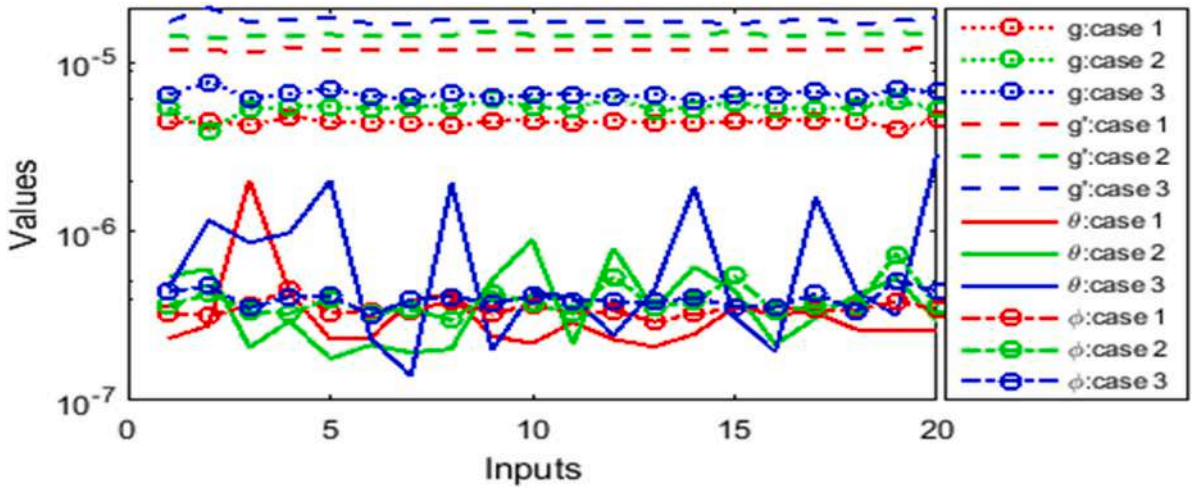


**Fig. 39.** E-NSE for cases (I, II, III) of scenario 2 in case of cu.

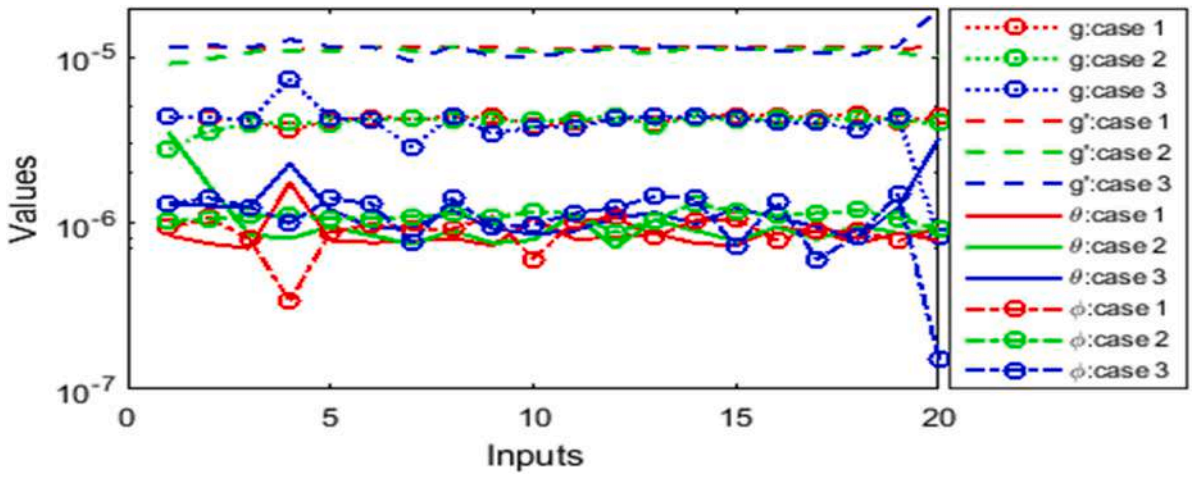


**Fig. 40.** E-NSE for cases (I, II, III) of scenario 3 in case of cu.

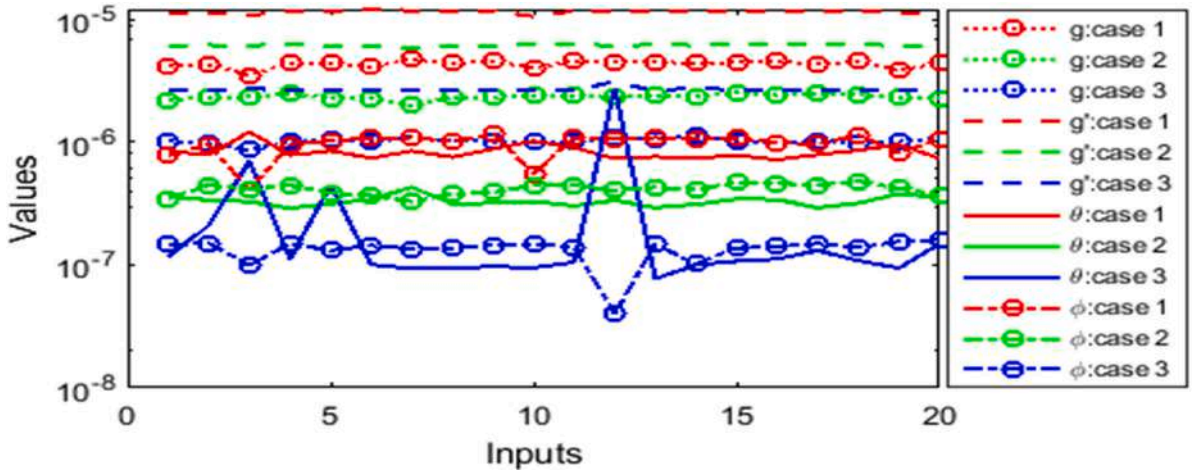


**Fig. 41.** E-NSE for cases (I, II, III) of scenario 4 in case of cu.

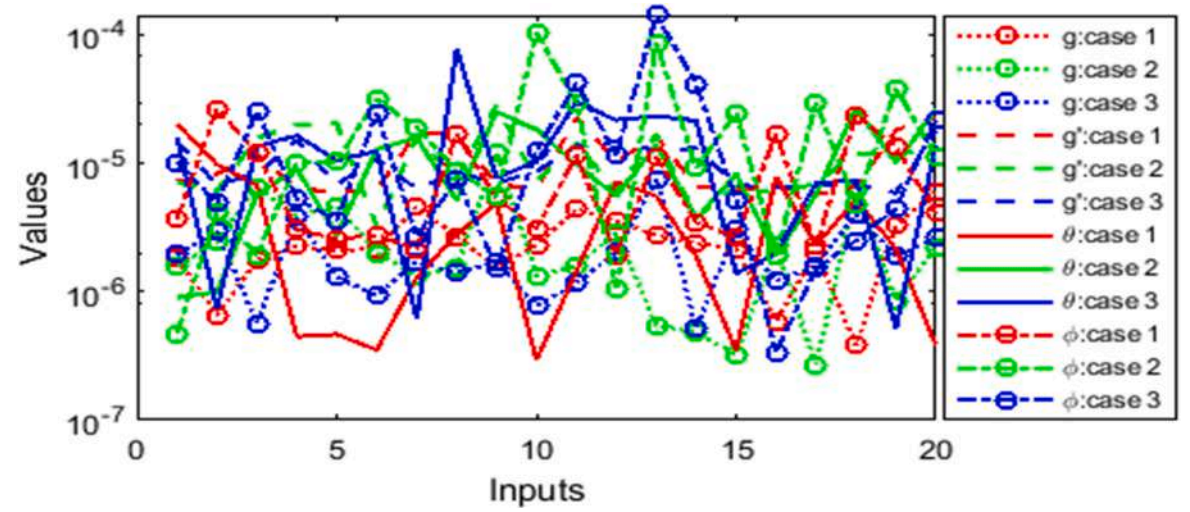


**Fig. 42.** E-NSE for cases (I, II, III) of scenario 5 in case of cu.

## 5. Conclusion

The approximate numerical results of the MNP-CNF problem are obtained through SNNT-GA-SQP with five scenarios of cu and four scenarios of $Al_2O_3$. Each scenario has three cases, and every case is based on physical parameters with ten neurons. The suggested solver runs independently twenty times, and its convergence, accuracy, and effectiveness are verified in different ways. On the strength of obtained numerical results and through their simulation, we can end up with the following conclusions:

- The flow $\widehat{g}(\eta)$and velocity $\widehat{g}'(\eta)$have an inverse relation with Casson fluid parameter $\beta$ but with the temperature field, $\widehat{\theta}(\eta)$this relation is directly proportional.
- The concentration $\widehat{\phi}(\eta)$of nano-particles has a direct relation with the temperature field $\widehat{\theta}(\eta)$in case when Schmidt number Sc increases otherwise this relation of $\widehat{\phi}(\eta)$and $\widehat{\theta}(\eta)$is always an inverse relation.
- The suggested solver generates results that match with a strong accuracy up to $10^{-7}$ decimal places when compared with the proposed reference solutions.
- The values obtained through used statistical operators closely match with the reference solution which reveals that the suggested solver is robust and strongly reliable.
- The convergence rate calculated through function count, time taken by iterations, and fitness values attained for all scenarios of cu and $Al_2O_3$ shows the suggested solver successfully attained the stiff criteria which also shows the efficiency of the solver.

**Table 3**
Illustration of best values for different operators on Cu scenario 1.

| Index | $g$ | | | | | | $g'$ | | | | | |
|---|---|---|---|---|---|---|---|---|---|---|---|---|
| | $Case_1$ | | $Case_2$ | | $Case_3$ | | $Case_1$ | | $Case_2$ | | $Case_3$ | |
| | Best | It# | Best | It# | Best | It# | Best | It# | Best | It# | Best | It# |
| **MAES** | 1.3026678E−3 | 17 | 1.323732E−3 | 3 | 1.346836E−3 | 3 | 1.3045894E−3 | 10 | 1.303483E−3 | 13 | 1.307180E−3 | 14 |
| **RMSE** | 1.5651528E−3 | 20 | 1.583744E−3 | 3 | 1.604494E−3 | 3 | 1.5665231E−3 | 10 | 1.565069E−3 | 13 | 1.565026E−3 | 14 |
| **E_TIC** | 1.8072756E−3 | 20 | 1.828725E−3 | 3 | 1.852647E−3 | 3 | 1.8088647E−3 | 10 | 1.807168E−3 | 13 | 1.807129E−3 | 14 |
| **E_NSE** | 6.8591689E−5 | 20 | 7.023082E−5 | 3 | 7.208320E−5 | 3 | 6.8711851E−5 | 10 | 6.858435E−5 | 13 | 6.858061E−5 | 14 |
| **E_VAF** | 3.1615914E−6 | 10 | 3.175103E−6 | 3 | 3.193814E−6 | 3 | 3.1585730E−6 | 17 | 3.151566E−6 | 13 | 3.110472E−6 | 8 |
| **E_$R^2$** | 6.8591689E−5 | 20 | 7.023082E−5 | 3 | 7.208320E−5 | 3 | 6.8711851E−5 | 10 | 6.858435E−5 | 13 | 6.858061E−5 | 14 |
| **Index** | $\Theta$ | | | | | | $\phi$ | | | | | |
| | $Case_1$ | | $Case_2$ | | $Case_3$ | | $Case_1$ | | $Case_2$ | | $Case_3$ | |
| | Best | It# | Best | It# | Best | It# | Best | It# | Best | It# | Best | It# |
| **MAES** | 1.3007967E−3 | 14 | 1.299653E−3 | 18 | 1.313037E−3 | 10 | 1.3284744E−3 | 10 | 1.305993E−3 | 7 | 1.303438E−3 | 9 |
| **RMSE** | 1.5624961E−3 | 9 | 1.561380E−3 | 19 | 1.572934E−3 | 10 | 1.5856709E−3 | 4 | 1.569149E−3 | 7 | 1.565446E−3 | 8 |
| **E_TIC** | 1.8042141E−3 | 9 | 1.802913E−3 | 19 | 1.816249E−3 | 10 | 1.8309512E−3 | 4 | 1.811896E−3 | 7 | 1.807620E−3 | 8 |
| **E_NSE** | 6.8359031E−5 | 9 | 6.826139E−5 | 19 | 6.927543E−5 | 10 | 7.0401864E−5 | 4 | 6.894239E−5 | 7 | 6.861741E−5 | 8 |
| **E_VAF** | 3.1471523E−6 | 19 | 3.144999E−6 | 19 | 3.150233E−6 | 10 | 3.1479335E−6 | 16 | 3.177761E−6 | 7 | 3.157015E−6 | 8 |
| **E_$R^2$** | 6.8359031E−5 | 9 | 6.826139E−5 | 19 | 6.927543E−5 | 10 | 7.0401864E−5 | 4 | 6.894239E−5 | 7 | 6.861741E−5 | 8 |

**Table 4**
Illustration of best values for different operators on Cu scenario 2.

| Index | $g$ | | | | | | $g^{'}$ | | | | | |
|---|---|---|---|---|---|---|---|---|---|---|---|---|
| | $Case_1$ | | $Case_2$ | | $Case_3$ | | $Case_1$ | | $Case_2$ | | $Case_3$ | |
| | Best | It# | Best | It# | Best | It# | Best | It# | Best | It# | Best | It# |
| **MAES** | 1.3040259E−3 | 19 | 1.295088E−3 | 2 | 2.240050E−3 | 14 | 1.3058511E−3 | 3 | 1.300109E−3 | 2 | 2.237354E−3 | 18 |
| **RMSE** | 1.5647876E−3 | 19 | 1.557985E−3 | 2 | 2.646760E−3 | 14 | 1.5673687E−3 | 3 | 1.561028E−3 | 2 | 2.644299E−3 | 18 |
| **E_TIC** | 1.8068565E−3 | 19 | 1.798996E−3 | 2 | 1.454473E−3 | 14 | 1.8098397E−3 | 3 | 1.802510E−3 | 2 | 1.453119E−3 | 18 |
| **E_NSE** | 6.8559690E−5 | 19 | 6.796488E−5 | 2 | 1.829610E−4 | 14 | 6.8786048E−5 | 3 | 6.823064E−5 | 2 | 1.826209E−4 | 18 |
| **E_VAF** | 3.1419230E−6 | 3 | 3.150269E−6 | 2 | 1.031864E−5 | 14 | 3.1558696E−6 | 8 | 3.135408E−6 | 19 | 1.031371E−5 | 19 |
| **E_$R^2$** | 6.8559690E−5 | 19 | 6.796488E−5 | 2 | 1.829610E−4 | 14 | 6.8786048E−5 | 3 | 6.823064E−5 | 2 | 1.826209E−4 | 18 |
| **Index** | $\Theta$ | | | | | | $\phi$ | | | | | |
| | $Case_1$ | | $Case_2$ | | $Case_3$ | | $Case_1$ | | $Case_2$ | | $Case_3$ | |
| | Best | It# | Best | It# | Best | It# | Best | It# | Best | It# | Best | It# |
| **MAES** | 1.3020164E−3 | 13 | 1.309170E−3 | 5 | 2.232333E−3 | 7 | 1.3120863E−3 | 13 | 1.295133E−3 | 8 | 2.240210E−3 | 6 |
| **RMSE** | 1.5630279E−3 | 13 | 1.569713E−3 | 5 | 2.639112E−3 | 7 | 1.5727944E−3 | 13 | 1.555895E−3 | 8 | 2.647305E−3 | 6 |
| **E_TIC** | 1.8048173E−3 | 13 | 1.812541E−3 | 5 | 1.450256E−3 | 7 | 1.8160975E−3 | 13 | 1.796571E−3 | 8 | 1.454851E−3 | 6 |
| **E_NSE** | 6.8405571E−5 | 13 | 6.899194E−5 | 5 | 1.819051E−4 | 7 | 6.9263103E−5 | 13 | 6.778265E−5 | 8 | 1.830364E−4 | 6 |
| **E_VAF** | 3.1407996E−6 | 4 | 3.150305E−6 | 15 | 1.028795E−5 | 9 | 3.1588700E−6 | 13 | 3.122449E−6 | 11 | 1.032990E−5 | 14 |
| **E_$R^2$** | 6.8405571E−5 | 13 | 6.899194E−5 | 5 | 1.819051E−4 | 7 | 6.9263103E−5 | 13 | 6.778265E−5 | 8 | 1.830364E−4 | 6 |

**Table 5**
Illustration of best values for different operators on Cu scenario 3.

| Index | $G$ | | | | | | $g'$ | | | | | |
|---|---|---|---|---|---|---|---|---|---|---|---|---|
| | $Case_1$ | | $Case_2$ | | $Case_3$ | | $Case_1$ | | $Case_2$ | | $Case_3$ | |
| | Best | It# | Best | It# | Best | It# | Best | It# | Best | It# | Best | It# |
| **MAES** | 2.2460538E−3 | 4 | 2.254580E−3 | 1 | 2.233837E−3 | 20 | 2.2414010E−3 | 10 | 2.221916E−3 | 1 | 2.236825E−3 | 7 |
| **RMSE** | 2.6525634E−3 | 4 | 2.660365E−3 | 1 | 2.640815E−3 | 20 | 2.6480251E−3 | 4 | 2.630375E−3 | 1 | 2.643751E−3 | 7 |
| **E_TIC** | 1.4576874E−3 | 4 | 1.461989E−3 | 1 | 1.451226E−3 | 20 | 1.4552025E−3 | 4 | 1.445503E−3 | 1 | 1.452823E−3 | 7 |
| **E_NSE** | 1.8376418E−4 | 4 | 1.848468E−4 | 1 | 1.821399E−4 | 20 | 1.8313593E−4 | 4 | 1.807027E−4 | 1 | 1.825452E−4 | 7 |
| **E_VAF** | 1.0338472E−5 | 4 | 1.035444E−5 | 1 | 1.029975E−5 | 20 | 1.0321982E−5 | 4 | 1.028980E−5 | 1 | 1.031096E−5 | 7 |
| **E_$R^2$** | 1.8376418E−4 | 4 | 1.848468E−4 | 1 | 1.821399E−4 | 20 | 1.8313593E−4 | 4 | 1.807027E−4 | 1 | 1.825452E−4 | 7 |
| **Index** | $\Theta$ | | | | | | $\phi$ | | | | | |
| | $Case_1$ | | $Case_2$ | | $Case_3$ | | $Case_1$ | | $Case_2$ | | $Case_3$ | |
| | Best | It# | Best | It# | Best | It# | Best | It# | Best | It# | Best | It# |
| **MAES** | 2.2353988E−3 | 3 | 2.234567E−3 | 12 | 2.235128E−3 | 18 | 2.2455686E−3 | 4 | 2.237169E−3 | 12 | 2.244511E−3 | 20 |
| **RMSE** | 2.6430632E−3 | 3 | 2.641623E−3 | 12 | 2.642114E−3 | 18 | 2.6502188E−3 | 4 | 2.644108E−3 | 12 | 2.651008E−3 | 20 |
| **E_TIC** | 1.4524482E−3 | 3 | 1.451653E−3 | 12 | 1.451944E−3 | 18 | 1.4563592E−3 | 4 | 1.453014E−3 | 12 | 1.456865E−3 | 20 |
| **E_NSE** | 1.8245024E−4 | 3 | 1.822514E−4 | 12 | 1.823192E−4 | 18 | 1.8343947E−4 | 4 | 1.825945E−4 | 12 | 1.835488E−4 | 20 |
| **E_VAF** | 1.0325185E−5 | 9 | 1.030496E−5 | 12 | 1.030541E−5 | 20 | 1.0285237E−5 | 4 | 1.031276E−5 | 1 | 1.033162E−5 | 20 |
| **E_$R^2$** | 1.8245024E−4 | 3 | 1.822514E−4 | 12 | 1.823192E−4 | 18 | 1.8343947E−4 | 4 | 1.825945E−4 | 12 | 1.835488E−4 | 20 |

**Table 6**
Illustration of best values for different operators on Cu scenario 4.

| Index | $g$ | | | | | | $g'$ | | | | | |
|---|---|---|---|---|---|---|---|---|---|---|---|---|
| | $Case_1$ | | $Case_2$ | | $Case_3$ | | $Case_1$ | | $Case_2$ | | $Case_3$ | |
| | Best | It# | Best | It# | Best | It# | Best | It# | Best | It# | Best | It# |
| **MAES** | 2.2370095E−3 | 3 | 3.041854E−4 | 7 | 3.315606E−4 | 3 | 2.2319021E−3 | 10 | 3.056078E−4 | 7 | 3.179945E−4 | 13 |
| **RMSE** | 2.6410327E−3 | 3 | 4.000217E−4 | 7 | 4.202236E−4 | 3 | 2.6391056E−3 | 10 | 4.025356E−4 | 7 | 4.064699E−4 | 13 |
| **E_TIC** | 1.4513002E−3 | 3 | 2.253730E−4 | 7 | 2.367551E−4 | 3 | 1.4502816E−3 | 10 | 2.267894E−4 | 7 | 2.290132E−4 | 13 |
| **E_NSE** | 1.8217001E−4 | 3 | 3.940896E−6 | 7 | 4.348994E−6 | 3 | 1.8190427E−4 | 10 | 3.990584E−6 | 7 | 4.068972E−6 | 13 |
| **E_VAF** | 1.0232080E−5 | 3 | 4.363814E−7 | 7 | 4.309947E−7 | 3 | 1.0297751E−5 | 10 | 4.438186E−7 | 7 | 4.144533E−7 | 3 |
| **E_$R^2$** | 1.8217001E−4 | 3 | 3.940896E−6 | 7 | 4.348994E−6 | 3 | 1.8190427E−4 | 10 | 3.990584E−6 | 7 | 4.068972E−6 | 13 |
| **Operator** | $\Theta$ | | | | | | $\phi$ | | | | | |
| | $Case_1$ | | $Case_2$ | | $Case_3$ | | $Case_1$ | | $Case_2$ | | $Case_3$ | |
| | Best | It# | Best | It# | Best | It# | Best | It# | Best | It# | Best | It# |
| **MAES** | 2.2356371E−3 | 16 | 3.080259E−4 | 13 | 3.097676E−4 | 13 | 2.2299797E−3 | 3 | 3.112258E−4 | 7 | 3.135751E−4 | 12 |
| **RMSE** | 2.6425067E−3 | 16 | 3.992254E−4 | 4 | 3.895565E−4 | 13 | 2.6371573E−3 | 3 | 4.086681E−4 | 7 | 4.109468E−4 | 12 |
| **E_TIC** | 1.4521497E−3 | 16 | 2.249261E−4 | 4 | 2.194792E−4 | 13 | 1.4492192E−3 | 3 | 2.302509E−4 | 7 | 2.315301E−4 | 12 |
| **E_NSE** | 1.8237342E−4 | 16 | 3.925223E−6 | 4 | 3.737393E−6 | 13 | 1.8163578E−4 | 3 | 4.113102E−6 | 7 | 4.159097E−6 | 12 |
| **E_VAF** | 1.0304381E−5 | 18 | 4.170635E−7 | 7 | 3.607922E−7 | 7 | 1.0288913E−5 | 3 | 4.535780E−7 | 1 | 4.561630E−7 | 12 |
| **E_$R^2$** | 1.8237342E−4 | 16 | 3.925223E−6 | 4 | 3.737393E−6 | 13 | 1.8163578E−4 | 3 | 4.113102E−6 | 7 | 4.159097E−6 | 12 |

**Table 7**
Illustration of best values for different operators on Cu scenario 5.

| Index | $g$ | | | | | | $g'$ | | | | | |
|---|---|---|---|---|---|---|---|---|---|---|---|---|
| | $Case_1$ | | $Case_2$ | | $Case_3$ | | $Case_1$ | | $Case_2$ | | $Case_3$ | |
| | Best | It# | Best | It# | Best | It# | Best | It# | Best | It# | Best | It# |
| **MAES** | 3.0396804E−4 | 18 | 3.090833E−4 | 17 | 3.138858E−4 | 3 | 3.0604559E−4 | 17 | 3.032763E−4 | 6 | 3.152552E−4 | 19 |
| **RMSE** | 3.8503527E−4 | 18 | 3.986692E−4 | 17 | 4.115371E−4 | 14 | 4.0244156E−4 | 17 | 3.962716E−4 | 6 | 4.132645E−4 | 19 |
| **E_TIC** | 2.1693049E−4 | 18 | 2.246148E−4 | 17 | 2.318604E−4 | 14 | 2.2673600E−4 | 17 | 2.232610E−4 | 6 | 2.328386E−4 | 19 |
| **E_NSE** | 3.6511439E−6 | 18 | 3.914292E−6 | 17 | 4.171056E−6 | 14 | 3.9887203E−6 | 17 | 3.867352E−6 | 6 | 4.206144E−6 | 19 |
| **E_VAF** | 3.6116248E−7 | 18 | 4.099746E−7 | 15 | 4.580421E−7 | 10 | 4.4159775E−7 | 18 | 4.206437E−7 | 6 | 4.616838E−7 | 3 |
| **E_$R^2$** | 3.6511439E−6 | 18 | 3.914292E−6 | 17 | 4.171056E−6 | 14 | 3.9887203E−6 | 17 | 3.867352E−6 | 6 | 4.206144E−6 | 19 |
| **Index** | $\Theta$ | | | | | | $\phi$ | | | | | |
| | $Case_1$ | | $Case_2$ | | $Case_3$ | | $Case_1$ | | $Case_2$ | | $Case_3$ | |
| | Best | It# | Best | It# | Best | It# | Best | It# | Best | It# | Best | It# |
| **MAES** | 3.0644972E−4 | 10 | 3.153943E−4 | 1 | 3.117987E−4 | 19 | 3.1875023E−4 | 17 | 3.234608E−4 | 1 | 3.159967E−4 | 16 |
| **RMSE** | 4.0298511E−4 | 10 | 3.946079E−4 | 1 | 3.881135E−4 | 19 | 4.1593029E−4 | 12 | 4.073974E−4 | 1 | 3.973217E−4 | 16 |
| **E_TIC** | 2.2704107E−4 | 10 | 2.223277E−4 | 1 | 2.186664E−4 | 19 | 2.3433693E−4 | 12 | 2.295383E−4 | 1 | 2.238575E−4 | 16 |
| **E_NSE** | 3.9995021E−6 | 10 | 3.834949E−6 | 1 | 3.709757E−6 | 19 | 4.2605830E−6 | 12 | 4.087562E−6 | 1 | 3.887877E−6 | 16 |
| **E_VAF** | 4.4282798E−7 | 10 | 3.636601E−7 | 2 | 3.453731E−7 | 15 | 4.6164877E−7 | 12 | 3.966616E−7 | 1 | 3.750970E−7 | 16 |
| **E_$R^2$** | 3.9995021E−6 | 10 | 3.834949E−6 | 1 | 3.709757E−6 | 19 | 4.2605830E−6 | 12 | 4.087562E−6 | 1 | 3.887877E−6 | 16 |

**Table 8**
Absolute error of all the cases in scenario 1 of cu for MNP-CNF problem.

| η | g | | | g′ | | |
|---|---|---|---|---|---|---|
| | $Case_1$ | $Case_2$ | $Case_3$ | $Case_1$ | $Case_2$ | $Case_3$ |
| 0.0 | 6.12414E−6 | 9.25932E−5 | 1.64875E−5 | 3.59264E−5 | 4.30852E−4 | 9.94670E−5 |
| 0.1 | 8.47734E−5 | 9.36463E−5 | 3.15230E−5 | 1.61308E−3 | 1.11891E−3 | 6.17707E−4 |
| 0.2 | 3.13083E−4 | 1.77464E−4 | 1.07382E−4 | 2.88523E−3 | 1.65595E−3 | 1.03816E−3 |
| 0.3 | 6.46455E−4 | 3.22646E−4 | 2.25676E−4 | 3.69975E−3 | 1.95723E−3 | 1.29810E−3 |
| 0.4 | 1.03619E−3 | 5.11981E−4 | 3.60854E−4 | 4.01111E−3 | 1.99205E−3 | 1.37463E−3 |
| 0.5 | 1.43250E−3 | 7.02135E−4 | 4.94668E−4 | 3.83865E−3 | 1.94195E−3 | 1.27399E−3 |
| 0.6 | 1.78996E−3 | 8.86950E−4 | 6.10744E−4 | 3.24865E−3 | 1.74207E−3 | 1.02683E−3 |
| 0.7 | 2.07193E−3 | 1.04471E−3 | 6.96859E−4 | 2.35145E−3 | 1.39504E−3 | 7.49308E−4 |
| 0.8 | 2.25552E−3 | 1.16389E−3 | 7.46950E−4 | 1.31510E−3 | 9.86871E−4 | 4.44146E−4 |
| 0.9 | 2.33860E−3 | 1.24375E−3 | 7.63027E−4 | 3.92817E−4 | 6.29522E−4 | 1.89701E−4 |
| 1.0 | 2.35059E−3 | 1.29619E−3 | 7.57039E−4 | 3.08671E−5 | 4.93258E−4 | 1.03582E−4 |
| **η** | **Θ** | | | **ϕ** | | |
| | $Case_1$ | $Case_2$ | $Case_3$ | $Case_1$ | $Case_2$ | $Case_3$ |
| 0.0 | 2.36377E−5 | 2.07049E−4 | 2.18335E−5 | 6.97280E−6 | 4.96168E−5 | 1.19813E−5 |
| 0.1 | 5.72689E−4 | 3.08027E−4 | 1.00593E−4 | 5.89480E−4 | 2.42661E−4 | 9.32082E−5 |
| 0.2 | 7.26224E−4 | 3.20536E−4 | 1.30004E−4 | 7.80286E−4 | 3.28780E−4 | 1.34467E−4 |
| 0.3 | 6.58532E−4 | 2.85721E−4 | 1.27741E−4 | 7.52456E−4 | 3.42877E−4 | 1.41901E−4 |
| 0.4 | 4.94311E−4 | 2.34075E−4 | 1.11245E−4 | 6.25198E−4 | 3.13135E−4 | 1.28850E−4 |
| 0.5 | 3.11955E−4 | 1.86864E−4 | 9.46097E−5 | 4.70695E−4 | 2.62913E−4 | 1.08265E−4 |
| 0.6 | 1.57016E−4 | 1.66571E−4 | 9.31964E−5 | 3.34765E−4 | 2.08952E−4 | 8.83002E−5 |
| 0.7 | 5.85118E−5 | 1.68631E−4 | 9.73417E−5 | 2.37131E−4 | 1.56063E−4 | 7.60925E−5 |
| 0.8 | 5.36618E−5 | 1.90132E−4 | 1.08852E−4 | 1.63873E−4 | 9.82511E−5 | 5.84113E−5 |
| 0.9 | 8.47132E−5 | 2.34615E−4 | 1.26992E−4 | 8.37183E−5 | 4.97263E−5 | 3.23263E−5 |
| 1.0 | 1.25378E−4 | 2.79552E−4 | 1.50643E−4 | 7.97820E−6 | 4.38640E−5 | 1.41047E−5 |

**Table 9**
Absolute error of all the cases in scenario 2 of cu for MNP-CNF problem.

| *η* | *g* | | | *g′* | | |
|---|---|---|---|---|---|---|
| | $Case_1$ | $Case_2$ | $Case_3$ | $Case_1$ | $Case_2$ | $Case_3$ |
| **0.0** | 3.86015E−6 | 1.16412E−5 | 5.29391E−6 | 1.31839E−5 | 4.11789E−5 | 3.82291E−5 |
| **0.1** | 1.86513E−5 | 2.63098E−5 | 2.10086E−5 | 4.05007E−4 | 4.19069E−4 | 4.62975E−4 |
| **0.2** | 7.66441E−5 | 8.38185E−5 | 8.89583E−5 | 7.45694E−4 | 7.98636E−4 | 8.76293E−4 |
| **0.3** | 1.63289E−4 | 1.77346E−4 | 1.91568E−4 | 9.64535E−4 | 1.04751E−3 | 1.14963E−3 |
| **0.4** | 2.64829E−4 | 2.88203E−4 | 3.13351E−4 | 1.04249E−3 | 1.14372E−3 | 1.25785E−3 |
| **0.5** | 3.67207E−4 | 4.01070E−4 | 4.37651E−4 | 9.83714E−4 | 1.09004E−3 | 1.20224E−3 |
| **0.6** | 4.57792E−4 | 5.02006E−4 | 5.49144E−4 | 8.12104E−4 | 9.10812E−4 | 1.00772E−3 |
| **0.7** | 5.27201E−4 | 5.80469E−4 | 6.36082E−4 | 5.68213E−4 | 6.49228E−4 | 7.20459E−4 |
| **0.8** | 5.70836E−4 | 6.31073E−4 | 6.92297E−4 | 3.06759E−4 | 3.64771E−4 | 4.05553E−4 |
| **0.9** | 5.90160E−4 | 6.55084E−4 | 7.18965E−4 | 9.38016E−5 | 1.30506E−4 | 1.44261E−4 |
| **1.0** | 5.93703E−4 | 6.61632E−4 | 7.26068E−4 | 1.04167E−5 | 3.36392E−5 | 3.73402E−5 |
| *η* | **Θ** | | | ***ϕ*** | | |
| | $Case_1$ | $Case_2$ | $Case_3$ | $Case_1$ | $Case_2$ | $Case_3$ |
| **0.0** | 1.82828E−5 | 3.30517E−5 | 6.21298E−5 | 3.92713E−6 | 6.44220E−6 | 5.57589E−6 |
| **0.1** | 1.15253E−4 | 1.06338E−4 | 9.02188E−5 | 1.32091E−4 | 1.38327E−4 | 1.38271E−4 |
| **0.2** | 1.65100E−4 | 1.65033E−4 | 1.65606E−4 | 1.82752E−4 | 1.94061E−4 | 1.97148E−4 |
| **0.3** | 1.64525E−4 | 1.69271E−4 | 1.82893E−4 | 1.84506E−4 | 1.96646E−4 | 1.98758E−4 |
| **0.4** | 1.43019E−4 | 1.49143E−4 | 1.76896E−4 | 1.64711E−4 | 1.75106E−4 | 1.76243E−4 |
| **0.5** | 1.18872E−4 | 1.27193E−4 | 1.69272E−4 | 1.38585E−4 | 1.46971E−4 | 1.48639E−4 |
| **0.6** | 9.79817E−5 | 1.09005E−4 | 1.62419E−4 | 1.11651E−4 | 1.17142E−4 | 1.17344E−4 |
| **0.7** | 8.21728E−5 | 9.46602E−5 | 1.58823E−4 | 8.65622E−5 | 8.81740E−5 | 8.46463E−5 |
| **0.8** | 7.41677E−5 | 8.95563E−5 | 1.69932E−4 | 6.42514E−5 | 6.39596E−5 | 6.05367E−5 |
| **0.9** | 7.17830E−5 | 9.35117E−5 | 1.94964E−4 | 3.93615E−5 | 3.96422E−5 | 4.18149E−5 |
| **1.0** | 6.54144E−5 | 9.02925E−5 | 2.08064E−4 | 3.45942E−6 | 8.90219E−6 | 6.01401E−6 |

**Table 10**
Absolute error of all the cases in scenario 3 of cu for MNP-CNF problem.

| $\eta$ | $g$ | | | $g'$ | | |
|---|---|---|---|---|---|---|
| | $Case_1$ | $Case_2$ | $Case_3$ | $Case_1$ | $Case_2$ | $Case_3$ |
| **0.0** | 7.22980E−6 | 6.38462E−6 | 1.37039E−5 | 3.44588E−5 | 5.83784E−5 | 7.88402E−5 |
| **0.1** | 1.77110E−5 | 2.12950E−5 | 2.47373E−5 | 4.31583E−4 | 4.43676E−4 | 4.53538E−4 |
| **0.2** | 7.75984E−5 | 8.13585E−5 | 8.46620E−5 | 7.52611E−4 | 7.53017E−4 | 7.52813E−4 |
| **0.3** | 1.64049E−4 | 1.67279E−4 | 1.70066E−4 | 9.54492E−4 | 9.43571E−4 | 9.33501E−4 |
| **0.4** | 2.63966E−4 | 2.65562E−4 | 2.66863E−4 | 1.02113E−3 | 9.99483E−4 | 9.79890E−4 |
| **0.5** | 3.63902E−4 | 3.62831E−4 | 3.61711E−4 | 9.57161E−4 | 9.25595E−4 | 8.96872E−4 |
| **0.6** | 4.51750E−4 | 4.47070E−4 | 4.42644E−4 | 7.84256E−4 | 7.43857E−4 | 7.39756E−4 |
| **0.7** | 5.18327E−4 | 5.09223E−4 | 5.00685E−4 | 5.39037E−4 | 4.91212E−4 | 5.24032E−4 |
| **0.8** | 5.58831E−4 | 5.44659E−4 | 5.31327E−4 | 2.72505E−4 | 2.19367E−4 | 2.87264E−4 |
| **0.9** | 5.74310E−4 | 5.54664E−4 | 5.40021E−4 | 5.83610E−5 | 4.73957E−5 | 1.45663E−4 |
| **1.0** | 5.73287E−4 | 5.48071E−4 | 5.43243E−4 | 4.23143E−5 | 9.69756E−5 | 1.53711E−4 |
| $\eta$ | $\Theta$ | | | $\phi$ | | |
| | $Case_1$ | $Case_2$ | $Case_3$ | $Case_1$ | $Case_2$ | $Case_3$ |
| **0.0** | 4.14771E−5 | 2.98470E−5 | 7.40834E−5 | 7.09839E−6 | 1.02532E−5 | 2.34950E−5 |
| **0.1** | 2.74256E−4 | 2.38730E−4 | 2.84089E−4 | 2.51495E−4 | 2.47502E−4 | 2.26899E−4 |
| **0.2** | 3.26470E−4 | 2.84438E−4 | 3.37723E−4 | 3.24746E−4 | 3.30016E−4 | 3.08840E−4 |
| **0.3** | 2.90724E−4 | 2.48884E−4 | 3.20297E−4 | 3.14543E−4 | 3.33338E−4 | 3.15789E−4 |
| **0.4** | 2.10238E−4 | 1.77802E−4 | 2.64185E−4 | 2.56280E−4 | 2.87406E−4 | 2.83904E−4 |
| **0.5** | 1.17013E−4 | 1.04232E−4 | 1.94594E−4 | 1.79345E−4 | 2.27464E−4 | 2.37295E−4 |
| **0.6** | 4.51348E−5 | 6.80314E−5 | 1.38351E−4 | 1.22301E−4 | 1.87421E−4 | 1.99952E−4 |
| **0.7** | 3.70342E−5 | 8.36827E−5 | 1.07661E−4 | 9.78427E−5 | 1.61454E−4 | 1.73078E−4 |
| **0.8** | 5.93496E−5 | 1.30677E−4 | 9.40280E−5 | 7.52691E−5 | 1.13581E−4 | 1.31369E−4 |
| **0.9** | 9.47940E−5 | 2.01074E−4 | 1.02280E−4 | 3.09856E−5 | 4.32945E−5 | 6.85113E−5 |
| **1.0** | 1.14436E−4 | 2.49984E−4 | 1.11260E−4 | 9.13021E−6 | 9.44526E−6 | 1.66673E−5 |

**Table 11**
Absolute error of all the cases in scenario 4 of cu for MNP-CNF problem.

| $\eta$ | $g$ | | | $g'$ | | |
|---|---|---|---|---|---|---|
| | $Case_1$ | $Case_2$ | $Case_3$ | $Case_1$ | $Case_2$ | $Case_3$ |
| **0.0** | 6.82126E−6 | 4.27535E−6 | 3.66440E−6 | 2.78976E−5 | 1.82426E−5 | 2.09782E−5 |
| **0.1** | 2.12360E−5 | 1.52739E−5 | 1.19053E−5 | 4.22938E−4 | 3.11741E−4 | 2.10510E−4 |
| **0.2** | 7.89496E−5 | 5.85576E−5 | 3.99874E−5 | 7.47923E−4 | 5.49942E−4 | 3.64582E−4 |
| **0.3** | 1.65128E−4 | 1.21890E−4 | 8.18235E−5 | 9.53729E−4 | 7.00548E−4 | 4.61574E−4 |
| **0.4** | 2.65162E−4 | 1.95315E−4 | 1.30108E−4 | 1.02423E−3 | 7.51114E−4 | 4.93083E−4 |
| **0.5** | 3.65597E−4 | 2.68874E−4 | 1.78320E−4 | 9.63992E−4 | 7.04953E−4 | 4.61300E−4 |
| **0.6** | 4.54306E−4 | 3.33618E−4 | 2.20623E−4 | 7.94591E−4 | 5.78535E−4 | 3.77415E−4 |
| **0.7** | 5.22078E−4 | 3.82824E−4 | 2.52687E−4 | 5.52545E−4 | 3.99727E−4 | 2.60242E−4 |
| **0.8** | 5.64073E−4 | 4.13082E−4 | 2.72412E−4 | 2.88736E−4 | 2.06791E−4 | 1.35402E−4 |
| **0.9** | 5.81286E−4 | 4.25315E−4 | 2.80557E−4 | 7.59046E−5 | 4.81993E−5 | 3.45088E−5 |
| **1.0** | 5.82162E−4 | 4.25808E−4 | 2.81316E−4 | 3.24999E−5 | 1.83987E−5 | 8.93853E−6 |
| $\eta$ | $\Theta$ | | | $\phi$ | | |
| | $Case_1$ | $Case_2$ | $Case_3$ | $Case_1$ | $Case_2$ | $Case_3$ |
| **0.0** | 3.51058E−5 | 1.57877E−5 | 2.32007E−5 | 9.00241E−6 | 3.24915E−6 | 3.46307E−6 |
| **0.1** | 2.64038E−4 | 1.62228E−4 | 8.81327E−5 | 2.55310E−4 | 1.62508E−4 | 8.52620E−5 |
| **0.2** | 3.16769E−4 | 1.99050E−4 | 9.88978E−5 | 3.33986E−4 | 2.14194E−4 | 1.14922E−4 |
| **0.3** | 2.78892E−4 | 1.80506E−4 | 8.39806E−5 | 3.25022E−4 | 2.13159E−4 | 1.18050E−4 |
| **0.4** | 1.95023E−4 | 1.30987E−4 | 5.90752E−5 | 2.67593E−4 | 1.78610E−4 | 1.01738E−4 |
| **0.5** | 9.84619E−5 | 7.12523E−5 | 4.03407E−5 | 1.92916E−4 | 1.30526E−4 | 7.82604E−5 |
| **0.6** | 3.65593E−5 | 3.16720E−5 | 4.15064E−5 | 1.36187E−4 | 9.53849E−5 | 6.35334E−5 |
| **0.7** | 4.17996E−5 | 2.71004E−5 | 5.59332E−5 | 1.07805E−4 | 7.88886E−5 | 5.60767E−5 |
| **0.8** | 7.70481E−5 | 3.89395E−5 | 7.95128E−5 | 7.92213E−5 | 5.76434E−5 | 3.77611E−5 |
| **0.9** | 1.21209E−4 | 6.81710E−5 | 1.11849E−4 | 3.20518E−5 | 2.01746E−5 | 9.63936E−6 |
| **1.0** | 1.46628E−4 | 8.24964E−5 | 1.25694E−4 | 9.49156E−6 | 3.46846E−6 | 5.41272E−6 |

**Table 12**
Absolute error of all the cases in scenario 5 of cu for MNP-CNF problem.

| $\eta$ | $g$ | | | $g^{'}$ | | |
|---|---|---|---|---|---|---|
| | $Case_1$ | $Case_2$ | $Case_3$ | $Case_1$ | $Case_2$ | $Case_3$ |
| **0.0** | 4.00076E−5 | 1.45873E−4 | 1.67229E−4 | 5.15548E−4 | 5.95912E−4 | 4.70675E−4 |
| **0.1** | 5.45459E−5 | 1.44533E−4 | 1.31660E−4 | 6.68650E−4 | 7.18871E−4 | 6.26376E−4 |
| **0.2** | 1.08266E−4 | 1.65260E−4 | 1.30617E−4 | 7.68047E−4 | 7.94166E−4 | 7.38581E−4 |
| **0.3** | 1.76746E−4 | 2.05736E−4 | 1.52716E−4 | 7.87658E−4 | 7.89637E−4 | 7.70617E−4 |
| **0.4** | 2.52387E−4 | 2.54894E−4 | 1.92532E−4 | 7.19634E−4 | 6.97626E−4 | 7.14277E−4 |
| **0.5** | 3.17425E−4 | 3.01397E−4 | 2.36726E−4 | 5.68086E−4 | 5.22368E−4 | 5.73486E−4 |
| **0.6** | 3.63684E−4 | 3.30948E−4 | 2.78612E−4 | 3.47277E−4 | 2.78664E−4 | 3.68205E−4 |
| **0.7** | 3.85379E−4 | 3.42173E−4 | 3.05551E−4 | 2.09009E−4 | 1.94071E−4 | 2.41069E−4 |
| **0.8** | 3.79802E−4 | 3.29016E−4 | 3.12918E−4 | 3.34046E−4 | 3.54655E−4 | 2.99700E−4 |
| **0.9** | 3.48892E−4 | 2.93582E−4 | 3.03615E−4 | 4.46247E−4 | 5.40374E−4 | 4.20417E−4 |
| **1.0** | 3.01635E−4 | 2.56551E−4 | 3.00286E−4 | 5.00179E−4 | 6.27542E−4 | 4.76308E−4 |
| $\eta$ | $\Theta$ | | | $\phi$ | | |
| | $Case_1$ | $Case_2$ | $Case_3$ | $Case_1$ | $Case_2$ | $Case_3$ |
| **0.0** | 3.33046E−4 | 7.32736E−4 | 4.94050E−4 | 3.69450E−5 | 9.91054E−5 | 5.05108E−5 |
| **0.1** | 3.45760E−4 | 5.87790E−4 | 5.31649E−4 | 4.04515E−4 | 5.44827E−4 | 4.40353E−4 |
| **0.2** | 2.97954E−4 | 4.67259E−4 | 5.02783E−4 | 5.89590E−4 | 8.20816E−4 | 6.57405E−4 |
| **0.3** | 2.60146E−4 | 4.09911E−4 | 4.83958E−4 | 6.16143E−4 | 9.01131E−4 | 7.43349E−4 |
| **0.4** | 2.17921E−4 | 3.57352E−4 | 4.57955E−4 | 6.10490E−4 | 9.26253E−4 | 7.78595E−4 |
| **0.5** | 1.85283E−4 | 3.00483E−4 | 4.30211E−4 | 6.75120E−4 | 9.99047E−4 | 8.52728E−4 |
| **0.6** | 1.77528E−4 | 2.92912E−4 | 4.48794E−4 | 6.56072E−4 | 1.01455E−3 | 9.04323E−4 |
| **0.7** | 2.31143E−4 | 3.85302E−4 | 5.49085E−4 | 4.71906E−4 | 7.94229E−4 | 7.72380E−4 |
| **0.8** | 3.40686E−4 | 5.33763E−4 | 7.10055E−4 | 2.13170E−4 | 4.27992E−4 | 4.79348E−4 |
| **0.9** | 4.15217E−4 | 6.45984E−4 | 8.53552E−4 | 6.83038E−5 | 1.45984E−4 | 2.02973E−4 |
| **1.0** | 4.46134E−4 | 7.16216E−4 | 9.72902E−4 | 2.96385E−5 | 8.86465E−5 | 5.53679E−5 |

**Table 13**
Performance grades of various statistical operators.

| **Scenarios.** | **Ranges (in decimal places)** | | | | |
|---|---|---|---|---|---|
| | E-TIC | RMSE | E-R2 | E-NSE | |
| 1. | $10^{-2}$ to $10^{-5}$ | $10^{-2}$ to $10^{-4}$ | $10^{-2}$ to $10^{-8}$ | $10^{-2}$ to $10^{-8}$ | for cu |
| 2. | $10^{-3}$ to $10^{-4}$ | $10^{-3}$ to $10^{-4}$ | $10^{-5}$ to $10^{-7}$ | $10^{-5}$ to $10^{-7}$ | |
| 3. | $10^{-3}$ to $10^{-4}$ | $10^{-3}$ to $10^{-4}$ | $10^{-5}$ to $10^{-7}$ | $10^{-5}$ to $10^{-7}$ | |
| 4. | $10^{-3}$ to $10^{-4}$ | $10^{-3}$ to $10^{-4}$ | $10^{-5}$ to $10^{-8}$ | $10^{-5}$ to $10^{-8}$ | |
| 5. | $10^{-3}$ to $10^{-4}$ | $10^{-3}$ to $10^{-4}$ | $10^{-4}$ to $10^{-7}$ | $10^{-4}$ to $10^{-7}$ | |
| 1. | $10^{-3}$ to $10^{-4}$ | $10^{-3}$ to $10^{-4}$ | $10^{-3}$ to $10^{-7}$ | $10^{-3}$ to $10^{-7}$ | For $Al_2O_3$ |
| 2. | $10^{-3}$ to $10^{-4}$ | $10^{-3}$ to $10^{-4}$ | $10^{-2}$ to $10^{-4}$ | $10^{-2}$ to $10^{-4}$ | |
| 3. | $10^{-3}$ to $10^{-4}$ | $10^{-2}$ to $10^{-3}$ | $10^{-2}$ to $10^{-5}$ | $10^{-2}$ to $10^{-5}$ | |
| 4. | $10^{-3}$ to $10^{-4}$ | $10^{-3}$ to $10^{-4}$ | $10^{-3}$ to $10^{-6}$ | $10^{-3}$ to $10^{-6}$ | |

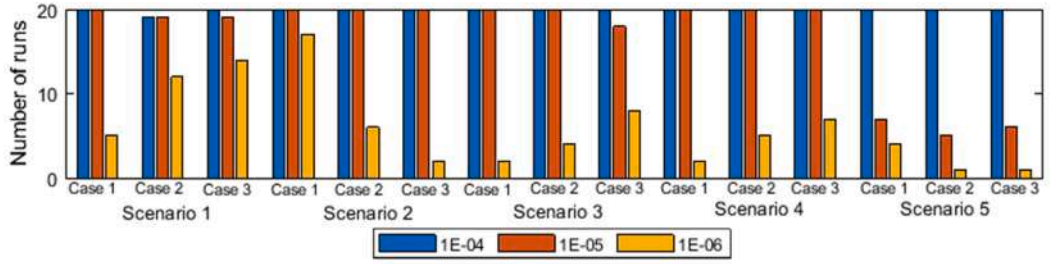


Convergence rate according to Fitness evaluation of all scenarios of cu for twenty runs

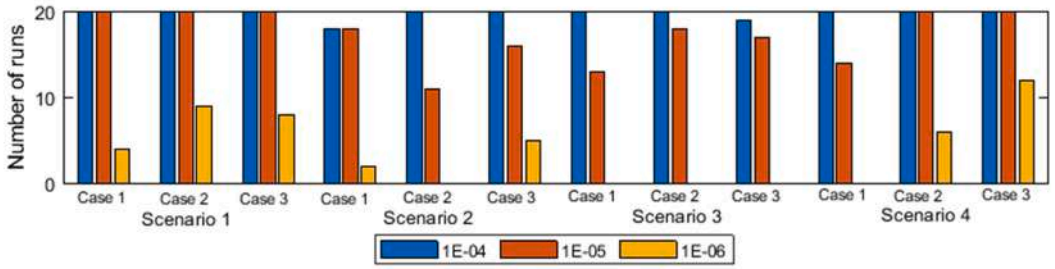


Convergence rate according to Fitness evaluation of all scenarios of $Al_2O_3$ for twenty runs

**Fig. 43.** Convergence rate based on fitness of SNNT-GA-SQP solver for both cu and $Al_2O_3$.

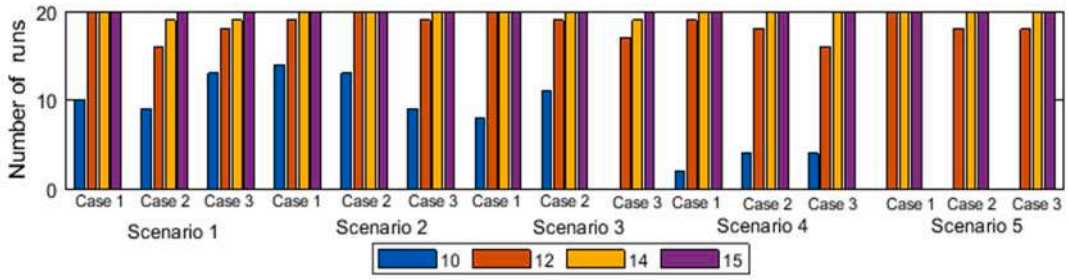


Convergence rate according to Time evaluation of all scenarios of cu for twenty runs

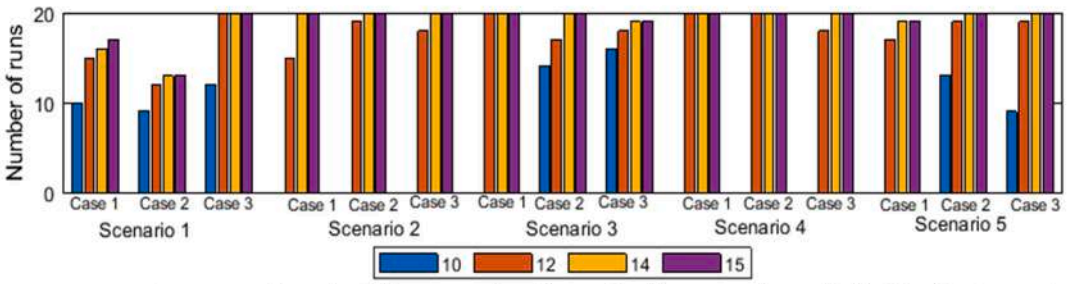


Convergence rate according to Time evaluation of all scenarios of $Al_2O_3$ for twenty runs

**Fig. 44.** Convergence rate via consumed time of SNNT-GA-SQP solver for both cu and $Al_2O_3$.

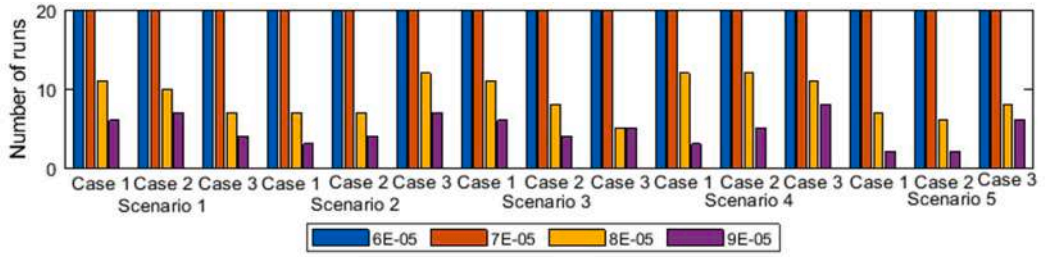


Convergence rate according to Function count of all scenarios of cu for twenty runs

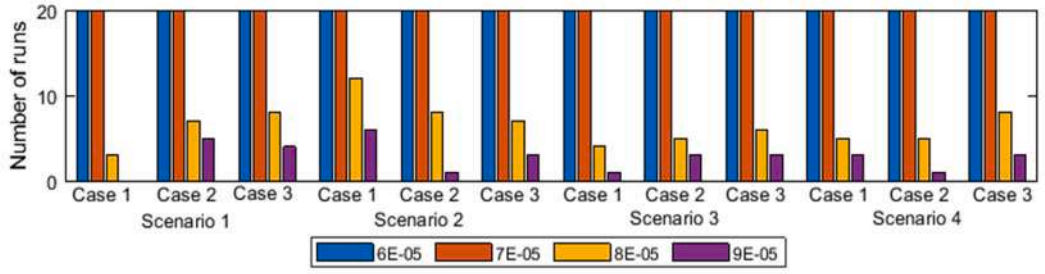


Convergene rate according to Function count of all scenarios of $Al_2O_3$ for twenty runs

**Fig. 45.** Convergence rate through function count of SNNT-GA-SQP solver for both cu and $Al_2O_3$.

## Declaration of competing interest

The authors declare that they have no known competing financial interests or personal relationships that could have appeared to influence the work reported in this paper.

## Appendix

The approximately calculated numerical results of MNP-CNF problem obtained through SNNT-GA-SQP solver for all scenarios of cu and $Al_2O_3$ are calculated by substituting the obtained values of weights in Eq. 20. The mathematical formulation of calculated numerical results are as follows (Figs. A1–A18):

Scenario 1 for cu:

$$\widehat{g}(\eta)_{cu:s1c1} = \frac{0.049148}{1+e^{-(13.43345-9.09074\eta)}} + \frac{-6.45588}{1+e^{-(11.68868-6.1737\eta)}} + \ldots + \frac{4.395779}{1+e^{-(0.466104+1.580071\eta)}}$$

$$\widehat{\theta}(\eta)_{cu:s1c1} = \frac{-1.35902}{1+e^{-(1.530398+0.106599\eta)}} + \frac{0.436291}{1+e^{-(-1.66216+2.208554\eta)}} + \ldots + \frac{0.063277}{1+e^{-(5.000147-4.62631\eta)}}$$

$$\widehat{\phi}(\eta)_{cu:s1c1} = \frac{-6.43972}{1+e^{-(-3.4058+1.694809\eta)}} + \frac{-4.53554}{1+e^{-(0.744951-0.54591\eta)}} + \ldots + \frac{0.674663}{1+e^{-(1.008031+1.454169\eta)}}$$

$$\widehat{g}(\eta)_{cu:s1c2} = \frac{5.640606}{1+e^{-(-5.92897+1.299262\eta)}} + \frac{-7.16138}{1+e^{-(-1.29734-1.0295\eta)}} + \ldots + \frac{-4.51165}{1+e^{-(-4.34728+1.654937\eta)}}$$

$$\widehat{\theta}(\eta)_{cu:s1c2} = \frac{2.86699}{1+e^{-(-0.47549-2.00496\eta)}} + \frac{-0.29541}{1+e^{-(-0.59471+0.178205\eta)}} + \ldots + \frac{-2.14445}{1+e^{-(7.366978+0.416505\eta)}}$$

$$\widehat{\phi}(\eta)_{cu:s1c2} = \frac{0.894028}{1+e^{-(-0.09935+0.30909\eta)}} + \frac{-3.4758}{1+e^{-(-3.43744-3.56208\eta)}} + \ldots + \frac{-0.77755}{1+e^{-(1.232356-1.32242\eta)}}$$

$$\widehat{g}(\eta)_{cu:s1c3} = \frac{-1.02793}{1+e^{-(1.802438+0.726027\eta)}} + \frac{-5.121}{1+e^{-(-1.64185-1.56831\eta)}} + \ldots + \frac{1.714745}{1+e^{-(-1.55251+0.76984\eta)}}$$

$$\widehat{\theta}(\eta)_{cu:s1c3} = \frac{3.550087}{1+e^{-(-0.17949-0.94202\eta)}} + \frac{3.894875}{1+e^{-(-3.56068-3.12199\eta)}} + \ldots + \frac{0.944371}{1+e^{-(-0.45795-0.73326\eta)}}$$

$$\widehat{\phi}(\eta)_{cu:s1c3} = \frac{-7.70781}{1+e^{-(-7.50136-0.56256\eta)}} + \frac{-2.44429}{1+e^{-(1.028038+1.124175\eta)}} + \ldots + \frac{-1.20597}{1+e^{-(4.253434+1.096078\eta)}}$$

Scenario 2 for cu:

$$\widehat{g}(\eta)_{cu:s2c1} = \frac{-5.80638}{1+e^{-(7.307139+2.579693\eta)}} + \frac{-29.4386}{1+e^{-(5.998028-1.77578\eta)}} + ... + \frac{18.6162}{1+e^{-(19.27481-0.89382\eta)}}$$

$$\widehat{\theta}(\eta)_{cu:s2c1} = \frac{-3.02404}{1+e^{-(-1.55826+0.686548\eta)}} + \frac{0.408588}{1+e^{-(-3.00513+-4.44318\eta)}} + ... + \frac{-1.23679}{1+e^{-(1.575059-1.8452\eta)}}$$

$$\widehat{\phi}(\eta)_{cu:s2c1} = \frac{5.046668}{1+e^{-(0.503502-1.45128\eta)}} + \frac{0.874573}{1+e^{-(0.221847-1.43504\eta)}} + ... + \frac{-4.32654}{1+e^{-(10.5408-0.56026\eta)}}$$

$$\widehat{g}(\eta)_{cu:s2c2} = \frac{3.523557}{1+e^{-(3.577508+1.520767\eta)}} + \frac{-5.50976}{1+e^{-(-5.77569-3.60537\eta)}} + ... + \frac{5.273557}{1+e^{-(2.951189-0.60829\eta)}}$$

$$\widehat{\theta}(\eta)_{cu:s2c2} = \frac{1.569605}{1+e^{-(2.31207-0.56963\eta)}} + \frac{1.173862}{1+e^{-(0.098893+1.814157\eta)}} + ... + \frac{5.713924}{1+e^{-(-6.13748-1.9941\eta)}}$$

$$\widehat{\phi}(\eta)_{cu:s2c2} = \frac{-6.61902}{1+e^{-(-6.65462+2.596159\eta)}} + \frac{1.862091}{1+e^{-(4.912653-0.11692\eta)}} + ... + \frac{-2.13909}{1+e^{-(2.905926-1.4627\eta)}}$$

$$\widehat{g}(\eta)_{cu:s2c3} = \frac{4.457833}{1+e^{-(3.746333+0.14124\eta)}} + \frac{7.773672}{1+e^{-(5.278984+3.647992\eta)}} + ... + \frac{-1.54925}{1+e^{-(2.934446-1.48789\eta)}}$$

$$\widehat{\theta}(\eta)_{cu:s2c3} = \frac{-1.28428}{1+e^{-(2.989929+4.843423\eta)}} + \frac{-0.17227}{1+e^{-(-1.24867+0.096264\eta)}} + ... + \frac{2.248511}{1+e^{-(-0.60953+0.154106\eta)}}$$

$$\widehat{\phi}(\eta)_{cu:s1c3} = \frac{-1.34074}{1+e^{-(0.663581-2.0486\eta)}} + \frac{0.007855}{1+e^{-(-1.34346+0.102432\eta)}} + ... + \frac{0.365788}{1+e^{-(0.776609+0.089761\eta)}}$$

Scenario 3 for cu:

$$g(\eta)_{cu:s3c1} = \frac{-12.03407927}{1+e^{-(7.658520071-3.510084132\eta)}} + \frac{6.276096015}{1+e^{-(6.185969777-3.129143257\eta)}} + ... + \frac{2.482276816}{1+e^{-(0.783319851-1.589083426\eta)}}$$

$$\theta(\eta)_{cu:s3c1} = \frac{1.639137276}{1+e^{-(-0.030812348-1.645467787\eta)}} + \frac{4.810007157}{1+e^{-(0.525109098-1.241583163\eta)}} + ... + \frac{-7.73804632}{1+e^{-(3.855745839+5.283436168\eta)}}$$

$$\widehat{\phi(\eta)}_{cu:s3c1} = \frac{-2.767847456}{1+e^{-(0.36172634+0.182177686\eta)}} + \frac{-4.301490821}{1+e^{-(-0.044715486-2.264071767\eta)}} + ... + \frac{8.210991608}{1+e^{-(3.546063164+4.87931826\eta)}}$$

$$\widehat{g(\eta)}_{cu:s3c2} = \frac{-1.737140648}{1+e^{-(4.39357869-3.191574714\eta)}} + \frac{3.993003697}{1+e^{-(2.146514592+1.641622037\eta)}} + ... + \frac{4.941515256}{1+e^{-(2.893236386-0.930276348\eta)}}$$

$$\widehat{\theta(\eta)}_{cu:s3c2} = \frac{10.10303886}{1+e^{-(-17.61188076-21.07020095\eta)}} + \frac{17.0781469}{1+e^{-(-4.776201851-5.803236344\eta)}} + ... + \frac{8.263764326}{1+e^{-(-2.339851984+0.581444436\eta)}}$$

$$\widehat{\phi(\eta)}_{cu:s3c2} = \frac{-3.028765361}{1+e^{-(-1.085996481-3.409215803\eta)}} + \frac{-5.035382316}{1+e^{-(-0.728058706-0.838400843\eta)}} + ... + \frac{2.606451529}{1+e^{-(6.117056947-1.122222538\eta)}}$$

$$\widehat{g(\eta)}_{cu:scs3} = \frac{-1.534156207}{1+e^{-(4.81152443+0.138226079\eta)}} + \frac{0.620056913}{1+e^{-(-0.828265233-0.356496506\eta)}} + ... + \frac{2.291975191}{1+e^{-(-3.518676505-0.084253072\eta)}}$$

$$\widehat{\theta(\eta)}_{cu:s3c3} = \frac{0.074610562}{1+e^{-(0.964408787+0.395442756\eta)}} + \frac{6.282961385}{1+e^{-(-3.236766111+1.379772645\eta)}} + ... + \frac{-19.00272412}{1+e^{-(0.547245261+1.347721478\eta)}}$$

$$\widehat{\phi(\eta)}_{cu:s3c3} = \frac{-1.13490843}{1+e^{-(-0.979917717-1.18439907\eta)}} + \frac{3.616585235}{1+e^{-(7.825782539-2.350313222\eta)}} + ... + \frac{-4.601192885}{1+e^{-(-1.695699642-3.270378303\eta)}}$$

Scenario 4 of cu:

$$g(\eta)_{cu:s4c1} = \frac{3.57708}{1+e^{-(1.22506-0.60822\eta)}} + \frac{-1.77460}{1+e^{-(-2.42801+1.73296\eta)}} + \ldots + \frac{11.35870}{1+e^{-(-9.16228+3.86514\eta)}}$$

$$\theta(\eta)_{cu:s4c1} = \frac{11.88122}{1+e^{-(-22.36461-12.51077\eta)}} + \frac{4.39493}{1+e^{-(3.22109+0.91635\eta)}} + \ldots + \frac{-0.88692}{1+e^{-(3.27161+1.51388\eta)}}$$

$$\widehat{\phi(\eta)}_{cu:s4c1} = \frac{-10.52668}{1+e^{-(-2.07185-3.29584\eta)}} + \frac{-4.42940}{1+e^{-(1.54919+4.01053\eta)}} + \ldots + \frac{-12.47631}{1+e^{-(-4.91949+-2.19929\eta)}}$$

$$\widehat{g(\eta)}_{cu:s4c2} = \frac{-0.877767072}{1+e^{-(-2.620359635+1.845895277\eta)}} + \frac{6.384187297}{1+e^{-(-0.005569489+0.823605558\eta)}} + \ldots + \frac{-8.723694794}{1+e^{-(-6.410422946+2.656787232\eta)}}$$

$$\widehat{\theta(\eta)}_{cu:s4c2} = \frac{1.147059585}{1+e^{-(-0.995511232-0.192223436\eta)}} + \frac{1.453906172}{1+e^{-(-1.229059637+0.654160338\eta)}} + \ldots + \frac{0.212817195}{1+e^{-(5.319602798+4.479003772\eta)}}$$

$$\widehat{\phi(\eta)}_{cu:s4c2} = \frac{-1.585558507}{1+e^{-(-4.759794201-2.502730509\eta)}} + \frac{-3.134789159}{1+e^{-(1.290520689+1.200877842\eta)}} + \ldots + \frac{-0.392989216}{1+e^{-(3.595133072-3.37080653\eta)}}$$

$$\widehat{g(\eta)}_{cu:s4c3} = \frac{-7.089362756}{1+e^{-(5.123410815-2.650158068\eta)}} + \frac{0.284539737}{1+e^{-(2.700308713-0.245834325\eta)}} + \ldots + \frac{-3.537045902}{1+e^{-(-2.901161727+1.741233694\eta)}}$$

$$\widehat{\theta(\eta)}_{cu:s4c3} = \frac{-0.200493503}{1+e^{-(-0.128759584+0.951440152\eta)}} + \frac{-1.420781542}{1+e^{-(0.625261655+2.092578364\eta)}} + \ldots + \frac{3.134632988}{1+e^{-(-0.144234775-1.56839148\eta)}}$$

$$\widehat{\phi(\eta)}_{cu:54c3} = \frac{5.060430935}{1+e^{-(-0.979917717-1.600478113\eta)}} + \frac{-1.650907579}{1+e^{-(7.825782539+1.38815308\eta)}} + \ldots + \frac{-3.837518355}{1+e^{-(-1.695699642-1.985380476\eta)}}$$

Scenario 5 of cu:

$$g(\eta)_{cu:s5c1} = \frac{0.179237852}{1+e^{-(-2.745521541-0.424880283\eta)}} + \frac{0.394615119}{1+e^{-(2.341923422-\eta)}} + \ldots + \frac{10.54394859}{1+e^{-(6.386410048-2.555729897\eta)}}$$

$$\theta(\eta)_{cu:s5c1} = \frac{1.140214598}{1+e^{-(1.79062241+1.219890132\eta)}} + \frac{5.587865286}{1+e^{-(-4.579034788-8.474745147\eta)}} + \ldots + \frac{0.901233166}{1+e^{-(-0.56063334-0.856335704\eta}}$$

$$\widehat{\phi(\eta)}_{cu:s5c1} = \frac{-12.16467876}{1+e^{-(4.788785265+9.303112187\eta)}} + \frac{5.397051246}{1+e^{-(4.4726734+3.107500516\eta)}} + \ldots + \frac{7.039163288}{1+e^{-(2.136206727+4.04631856\eta)}}$$

$$\widehat{g(\eta)}_{cu:s5c2} = \frac{-4.795699009}{1+e^{-(0.36420427+0.234505401\eta)}} + \frac{9.671121047}{1+e^{-(3.823185413-3.06286288\eta)}} + \ldots + \frac{2.396036444}{1+e^{-(-4.676784523+4.346214188\eta)}}$$

$$\widehat{\theta(\eta)}_{cu:s5c2} = \frac{3.413371337}{1+e^{-(0.148583409-2.537795243\eta)}} + \frac{-5.356132608}{1+e^{-(5.183958396+9.63418424\eta)}} + \ldots + \frac{-1.646614344}{1+e^{-(-2.016633736+1.749914797\eta)}}$$

$$\widehat{\phi(\eta)}_{cu:s5c2} = \frac{-7.138908544}{1+e^{-(-1.763155697+1.399672155\eta)}} + \frac{-1.261573618}{1+e^{-(-2.400104734-4.397154664\eta)}} + \ldots + \frac{-5.566822158}{1+e^{-(-2.643556222-6.106673078\eta)}}$$

$$\widehat{g(\eta)}_{cu:s5c3} = \frac{-6.495665884}{1+e^{-(10.03313864-5.281071585\eta)}} + \frac{-3.479138188}{1+e^{-(-4.570048716+2.648585249\eta)}} + \ldots + \frac{9.274992038}{1+e^{-(7.099583871-0.477489039\eta)}}$$

$$\widehat{\theta(\eta)}_{cu:s5c3} = \frac{-2.184082544}{1+e^{-(-0.004022166-1.313851154\eta)}} + \frac{-1.217180227}{1+e^{-(4.379226274-1.002944725\eta)}} + \ldots + \frac{0.861786677}{1+e^{-(2.056066874+0.018626139\eta)}}$$

$$\widehat{\phi(\eta)}_{cu:s5c3} = \frac{1.816269399}{1+e^{-(5.049346846-2.173374991\eta)}} + \frac{-15.75326497}{1+e^{-(-3.716025778-6.601206811\eta)}} + \ldots + \frac{-2.607986878}{1+e^{-(0.394228449-0.398828565\eta)}}$$

Scenario 1 of $Al_2O_3$:

$$g(\eta)_{Al:s1c1} = \frac{2.807861132}{1+e^{-(4.105841813-1.549846748\eta)}} + \frac{10.76690602}{1+e^{-(9.940416298-4.121074558\eta)}} + \ldots + \frac{1.299019846}{1+e^{-(3.970920131+0.503398928\eta)}}$$

$$\theta(\eta)_{Al:s1c1} = \frac{0.73511953}{1+e^{-(-0.604139565-2.007860077\eta)}} + \frac{5.826518094}{1+e^{-(-0.690687371-0.66178471\eta)}} + \ldots + \frac{-1.491588813}{1+e^{-(3.528420602+0.574250647\eta)}}$$

$$\widehat{\phi(\eta)}_{Al:s1c1} = \frac{6.929491344}{1+e^{-(1.280179253+0.066450027\eta)}} + \frac{-5.809723102}{1+e^{-(0.376099596+1.145299575\eta)}} + \ldots + \frac{-1.555008293}{1+e^{-(-0.927818854+4.74645115\eta)}}$$

$$\widehat{g(\eta)}_{Al::1c1} = \frac{-10.84093673}{1+e^{-(-0.211161833-1.756475069\eta)}} + \frac{-0.593096298}{1+e^{-(-3.149775899-0.470339141\eta)}} + \ldots + \frac{-3.294090107}{1+e^{-(9.160377868+8.614227511\eta)}}$$

$$\widehat{\theta(\eta)}_{Al:s1c2} = \frac{1.275703614}{1+e^{-(3.376813186-3.381546775\eta)}} + \frac{0.156423168}{1+e^{-(-1.62118823-2.553568456\eta)}} + \ldots + \frac{-1.635955907}{1+e^{-(-2.742909022-1.778360404\eta)}}$$

$$\widehat{\phi(\eta)}_{Al:51c2} = \frac{-7.473638618}{1+e^{-(-2.736632884+1.243952062\eta)}} + \frac{-4.539814214}{1+e^{-(0.836079696-2.312598683\eta)}} + \ldots + \frac{-4.274286882}{1+e^{-(-1.943358192-3.775393189\eta)}}$$

$$\widehat{g(\eta)}_{Al:s1c3} = \frac{0.070144751}{1+e^{-(9.654452679-1.371718668\eta)}} + \frac{1.494225925}{1+e^{-(3.392247053+1.764770941\eta)}} + \ldots + \frac{3.0963365}{1+e^{-(2.444223791-4.82628665\eta)}}$$

$$\widehat{\theta(\eta)}_{Al:51c3} = \frac{6.462008631}{1+e^{-(-1.062517966-1.521818477\eta)}} + \frac{4.473511187}{1+e^{-(7.173762766+8.467819921\eta)}} + \ldots + \frac{-4.535802254}{1+e^{-(0.057709693-4.453642784\eta)}}$$

$$\widehat{\phi(\eta)}_{Al:s1c3} = \frac{-5.176920508}{1+e^{-(-0.367944913-0.065808994\eta)}} + \frac{4.495429753}{1+e^{-(-2.924710614-0.349057773\eta)}} + \ldots + \frac{-4.184512818}{1+e^{-(-1.100055614-3.763645292\eta)}}$$

Scenario 2 of $Al_2O_3$:

$$g(\eta)_{Al:s2c1} = \frac{3.35501939}{1+e^{-(-0.809261982-0.173599036\eta)}} + \frac{0.153861162}{1+e^{-(4.527984104-4.267125775\eta)}} + \ldots + \frac{1.1684222}{1+e^{-(1.411617073-0.435952636\eta)}}$$

$$\theta(\eta)_{Al:s2c1} = \frac{-4.42075064}{1+e^{-(-6.163332947-10.0751811\eta)}} + \frac{-0.284305738}{1+e^{-(1.216792049+0.428165617\eta)}} + \ldots + \frac{-9.88547333}{1+e^{-(2.411898324+0.266810824\eta)}}$$

$$\widehat{\phi(\eta)}_{Al:s2c1} = \frac{-0.688190669}{1+e^{-(1.375143358+4.417795508\eta)}} + \frac{-0.364043384}{1+e^{-(-10.00707645+4.720889025\eta)}} + \ldots + \frac{-0.364043384}{1+e^{-(-3.922814111+2.927707585\eta)}}$$

$$\widehat{g(\eta)}_{Al:s2c1} = \frac{-3.608841926}{1+e^{-(1.218513642-0.685585791\eta)}} + \frac{1.087820062}{1+e^{-(-4.469560756-3.262491197\eta)}} + \ldots + \frac{-5.039558308}{1+e^{-(-1.441471065-2.086599055\eta)}}$$

$$\widehat{\theta(\eta)}_{Al:s2c2} = \frac{0.075576484}{1+e^{-(7.900185265+3.83832965\eta)}} + \frac{1.686248998}{1+e^{-(4.679599628-2.123806798\eta)}} + \ldots + \frac{-3.64827888}{1+e^{-(9.892680484-3.64827888\eta)}}$$

$$\widehat{\phi(\eta)}_{Al:s2c2} = \frac{-15.73462321}{1+e^{-(-15.22455607+0.233241826\eta)}} + \frac{-6.634241159}{1+e^{-(-6.70180866-3.37843002\eta)}} + \ldots + \frac{2.753599397}{1+e^{-(2.159219549-2.331593146\eta)}}$$

$$\widehat{g(\eta)}_{Al:s2c3} = \frac{6.227061911}{1+e^{-(1.304245977-0.390065608\eta)}} + \frac{-7.522549034}{1+e^{-(-0.643360053+0.51366384\eta)}} + \ldots + \frac{-11.44353648}{1+e^{-(-6.802802248-1.979430858\eta)}}$$

$$\widehat{\theta(\eta)}_{Al::sc3} = \frac{1.90716792}{1+e^{-(4.646527983+4.585398851\eta)}} + \frac{-0.985882706}{1+e^{-(-6.316076937-3.348559025\eta)}} + \ldots + \frac{1.284520745}{1+e^{-(-2.437314858+3.07116354\eta)}}$$

$$\widehat{\phi(\eta)}_{Al:s2c3} = \frac{-7.75554042}{1+e^{-(2.354979355+1.047485194\eta)}} + \frac{7.537330194}{1+e^{-(5.37900877+8.492736238\eta)}} + \ldots + \frac{8.7781327}{1+e^{-(8.794382203-5.232776775\eta)}}$$

Scenario 3 of $Al_2O_3$:

$$g(\eta)_{Al:s3c1} = \frac{-1.654343682}{1+e^{-(1.248392716-1.520035341\eta)}} + \frac{2.031372868}{1+e^{-(2.746845984+2.780981318\eta)}} + \ldots + \frac{5.36273364}{1+e^{-(1.235510173+0.027465054\eta)}}$$

$$\theta(\eta)_{Al:s3c1} = \frac{-1.79634399}{1+e^{-(-0.562949038-0.827172022\eta)}} + \frac{1.956623026}{1+e^{-(-1.024606532+3.064344464\eta)}} + \ldots + \frac{-2.078689848}{1+e^{-(1.69820669-3.219766823\eta)}}$$

$$\widehat{\phi(\eta)}_{Al:53c1} = \frac{7.842745845}{1+e^{-(-1.268424476-0.544518947\eta)}} + \frac{2.843908297}{1+e^{-(-4.187571186-2.639394418\eta)}} + \ldots + \frac{-5.494740626}{1+e^{-(-3.601988776+0.416277855\eta)}}$$

$$\widehat{g(\eta)}_{\text{Al:s3c1}} = \frac{-2.894022639}{1+e^{-(7.500459778-3.850891481\eta)}} + \frac{2.753369396}{1+e^{-(-1.8532773+2.778952741\eta)}} + \ldots + \frac{3.32109313}{1+e^{-(-2.469737015-1.8532773\eta)}}$$

$$\widehat{\theta(\eta)}_{Al:53c2} = \frac{2.416818207}{1+e^{-(-0.544156543+2.023161359\eta)}} + \frac{-1.834936564}{1+e^{-(-1.466841176+2.997522969\eta)}} + \ldots + \frac{-1.806991772}{1+e^{-(-0.978120616+0.833276196\eta)}}$$

$$\widehat{\phi(\eta)}_{Al:s3c2} = \frac{-8.33478266}{1+e^{-(-7.823509679+4.165646242\eta)}} + \frac{-3.985295595}{1+e^{-(1.141189758+0.716100419\eta)}} + \ldots + \frac{4.229514856}{1+e^{-(1.767064013-0.435764463\eta)}}$$

$$\widehat{g(\eta)}_{Al:53c3} = \frac{0.005655086}{1+e^{-(-1.584147081+4.216307532\eta)}} + \frac{0.745635916}{1+e^{-(-0.890396943+2.687481729\eta)}} + \ldots + \frac{4.999440383}{1+e^{-(-6.96645598+3.213058618\eta)}}$$

$$\widehat{\theta(\eta)}_{Al:53c3} = \frac{2.706703067}{1+e^{-(7.121118311-2.237740615\eta)}} + \frac{2.374391174}{1+e^{-(1.338694983+2.017944105\eta)}} + \ldots + \frac{-1.604894924}{1+e^{-(0.627488051-0.168166825\eta)}}$$

$$\widehat{\phi(\eta)}_{Al::3c3} = \frac{-17.17416634}{1+e^{-(1.580183366+2.205466802\eta)}} + \frac{-3.94746792}{1+e^{-(2.125590589+0.632210175\eta)}} + \ldots + \frac{-9.446759974}{1+e^{-(4.713347202+4.531603022\eta)}}$$

Scenario 4 of $Al_2O_3$:

$$g(\eta)_{Al:54c1} = \frac{-3.022207767}{1+e^{-(-1.244797907+1.262206141\eta)}} + \frac{-2.018839832}{1+e^{-(1.535551369+2.955016435\eta)}} + \ldots + \frac{-5.243197274}{1+e^{-(2.788616949+2.587731151\eta)}}$$

$$\theta(\eta)_{Al:54c1} = \frac{1.598173702}{1+e^{-(1.075943547-0.766505008\eta)}} + \frac{-10.10444132}{1+e^{-(6.400803099-2.163789883\eta)}} + \ldots + \frac{3.763277233}{1+e^{-(1.811668878+1.61543428\eta)}}$$

$$\widehat{\phi(\eta)}_{Al:54c1} = \frac{-6.589765613}{1+e^{-(2.665701213+0.460835076\eta)}} + \frac{-6.077559537}{1+e^{-(3.850854005-0.436646636\eta)}} + \ldots + \frac{2.857880621}{1+e^{-(-13.53041846-0.523978644\eta)}}$$

$$\widehat{g(\eta)}_{Al:s4c1} = \frac{8.356463615}{1+e^{-(6.079588345+0.805419806\eta)}} + \frac{-13.47918544}{1+e^{-(9.591657188-4.089108077\eta)}} + \ldots + \frac{2.437154254}{1+e^{-(2.650106716-1.713597521\eta)}}$$

$$\widehat{\theta(\eta)}_{Al:s4c2} = \frac{1.471923475}{1+e^{-(6.005977502+6.451844118\eta)}} + \frac{3.150984357}{1+e^{-(-2.362869375+1.732658829\eta)}} + \ldots + \frac{0.793105491}{1+e^{-(1.061909207-1.027407127\eta)}}$$

$$\widehat{\phi(\eta)}_{Al:s4c2} = \frac{9.179205278}{1+e^{-(2.333592378+4.752332484\eta)}} + \frac{-2.450679833}{1+e^{-(-0.867158373+0.181514638\eta)}} + \ldots + \frac{1.03072982}{1+e^{-(19.05836866+5.824217414\eta)}}$$

$$\widehat{g(\eta)}_{Al:54c3} = \frac{1.100846862}{1+e^{-(-1.893628767+0.97382238\eta)}} + \frac{3.00302062}{1+e^{-(0.533933974+0.107470861\eta)}} + \ldots + \frac{-0.692404437}{1+e^{-(0.275849684-1.592287849\eta)}}$$

$$\widehat{\theta(\eta)}_{Al:54c3} = \frac{-2.885741191}{1+e^{-(2.120196165+2.676168983\eta)}} + \frac{3.094182594}{1+e^{-(2.129646274-0.263129912\eta)}} + \ldots + \frac{0.741439524}{1+e^{-(1.724053474+1.436723248\eta)}}$$

$$\widehat{\phi(\eta)}_{Al:54c3} = \frac{-3.065853841}{1+e^{-(-1.458067038-0.203523584\eta)}} + \frac{-8.044196539}{1+e^{-(-2.910116393-2.690148563\eta)}} + \ldots + \frac{1.512960281}{1+e^{-(0.841052679+1.157570956\eta)}}$$

**Table A1**
Pseudo code based on SNNT-GA-SQP for system optimization.

**Start of GAs**
**Inputs:**
The chromosomes manifestation with equal number of inputs of networks as:
$W = [W_g, W_\theta, W_\phi] = [(a_g, b_g, c_g), (a_\theta, b_\theta, c_\theta), (a_\phi, b_\phi, c_\phi)]$,
$a_g = [a_{g,1}, a_{g,2}, ..., a_{g,n}], a_\theta = [a_{\theta,1}, a_{\theta,2}, ..., a_{\theta,n}], a_\phi = [a_{\phi,1}, a_{\phi,2}, ..., a_{\phi,n}]$,
$b_g = [b_{g,1}, b_{g,2}, ..., b_{g,n}], b_\theta = [b_{\theta,1}, b_{\theta,2}, ..., b_{\theta,n}], b_\phi = [b_{\phi,1}, b_{\phi,2}, ..., b_{\phi,n}]$,
$c_g = [c_{g,1}, c_{g,2}, ..., c_{g,n}], c_\theta = [c_{\theta,1}, c_{\theta,2}, ..., c_{\theta,n}], c_\phi = [c_{\phi,1}, c_{\phi,2}, ..., c_{\phi,n}]$
**Population:** representation of chromosomes set:
$P_I = [(W_{g1}, W_{g2}, ..., W_{gn}), (W_{\theta 1}, W_{\theta 2}, ..., W_{\theta n}), (W_{\phi 1}, W_{\phi 2}, ..., W_{\phi n})]$,
$[W_{gl}, W_{\theta l}, W_{\phi l}] = [(a_{gl}, b_{gl}, c_{gl}), (a_{\theta l}, b_{\theta l}, c_{\theta l}), (a_{\phi l}, b_{\phi l}, c_{\phi l})]$
**Output:** $W_{GA\text{-}Best}$ represent GA best individual
**Initialization:** Construct $W$ vector based on finite real numbers to represent a chromosome in the form of an initial set $P_I$. Set declarations for "GAoptimset" in case of GA.
**Fitness Evaluation:** Obtain the fitness "$e$" using Eq. (*30*) for every $W$ in termination of $P_I$. Terminates the scheme applied on completion of the following.
'Generations =200', 'Fitness limit→$10^{-20}$','TolFun →$10^{-20}$','TolCon→$10^{-20}$','Populationsize=200','StallGenLimit →75
other settings are by default. If termination condition meets then go towards result storage step otherwise,
**Upgrading:**
**Ranking**
Each $W$ of $P_I$ ranked up to the best rate of fitness.
**Reproduction**
For each iteration the settings of new $P_I$ are
- 'Selection': "@selectionstochunif".
- 'Mutations': "@mutationadaptfeasible function".
- 'Crossover': "@crossoverheuristic 2".
- 'Elitism': "10".

**Storage**
Store $W_{GA\text{-}Best}$, generation, function count and time for GA's current run.
**End GAs**
**GA-SQP Process Start**
**Inputs:** Globally obtained best vector $W_{GA\text{-}Best}$
**Output:** Best weight through GA-SQP.
**Initialize:**
Start from $W_{GA\text{-}Best}$. Settings of bounds and declarations related "Optimset" and Fmincon
**Termination**
Algorithm stops if desired value meet.
'Fitness limit =e$\leq 10^{-20}$, MaxFunEvals$\leq$2050000,'total Iterations=2000','TolFun $\leq 10^{-20}$','TolX $\leq 10^{-23}$','TolCon $\leq 10^{-23}$
**While** (Terminate)
**Fitness evaluation**
Calculate fitness for $W_{GA\text{-}SQP}$ using Eq. (26-30).
**Adjustments**
Call"fmincon" using "SQP" algorithm and adjust the weight in each iteration of incremental phase.
**End**
Save the final weight vector $W_{GA\text{-}SQP}$ its time, fitness in case of current run $W_{GA\text{-}SQP}$.
**GA-SQP Procedure Stop**
**Statistics:** GA-SQP algorithm repeated 20 times and data obtained are used for necessary statistics.

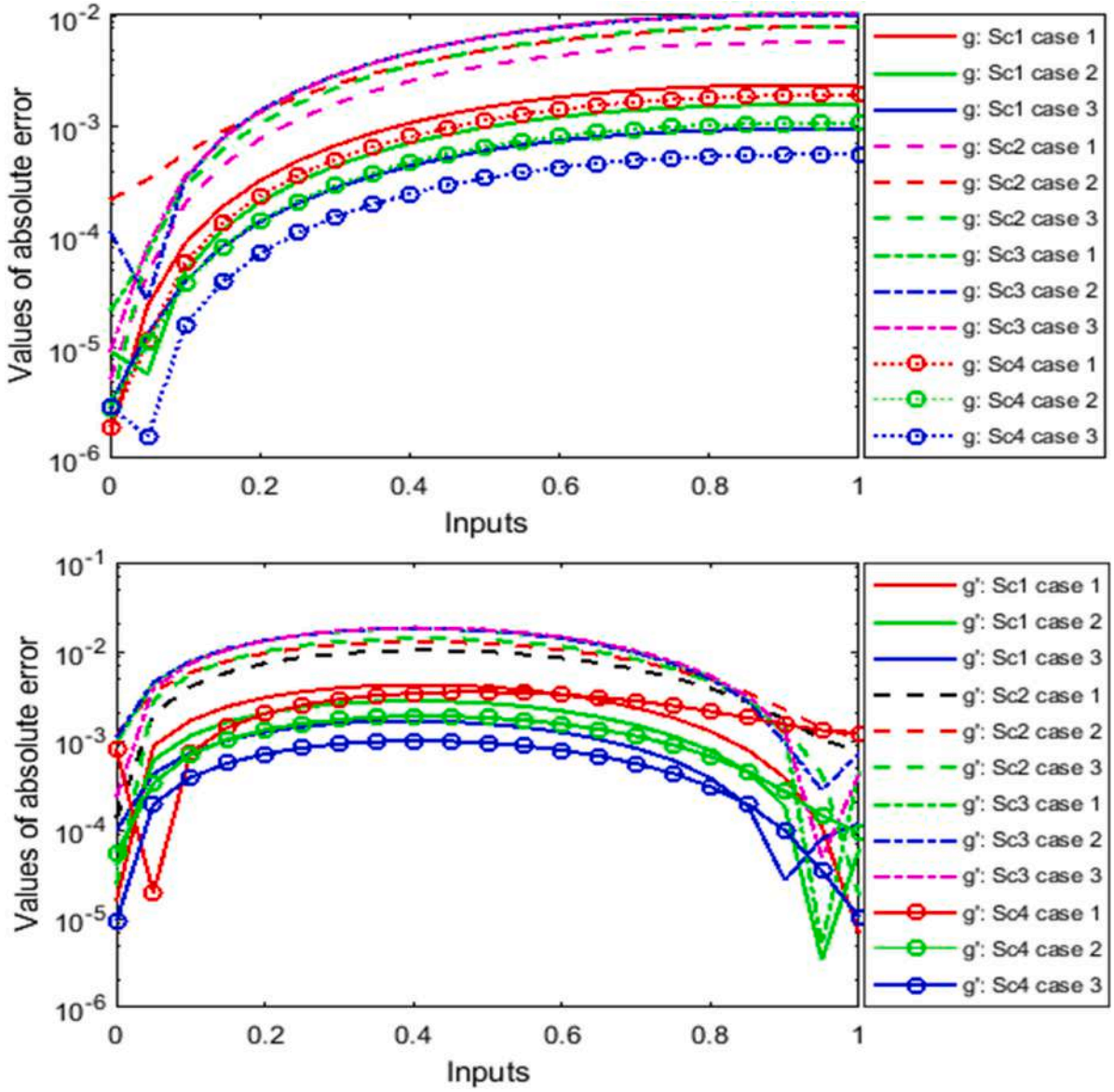


**Fig A1.** Absolute errors in the values of $g$ and $g'$ for all scenarios of $Al_2O_3$.

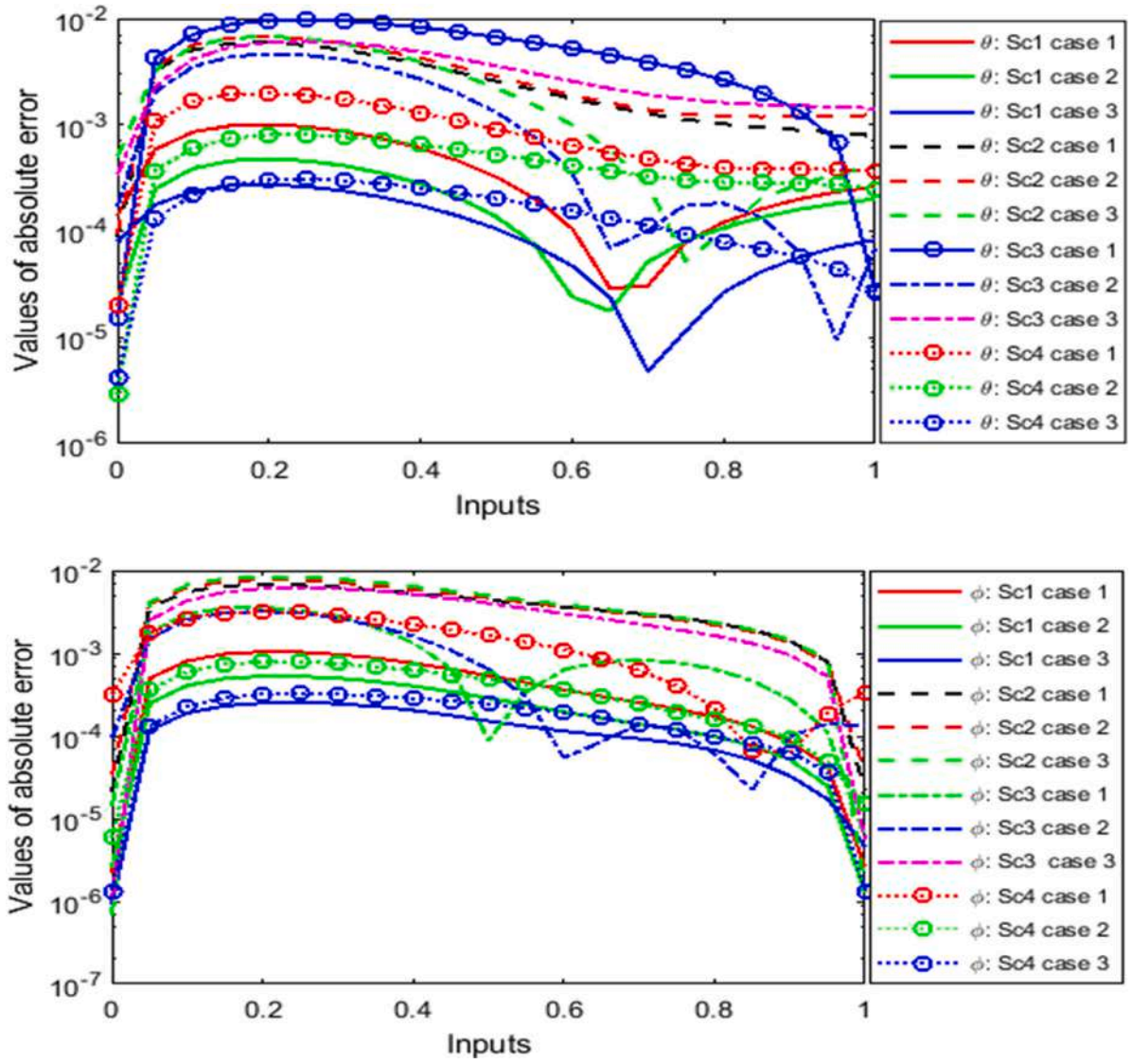


**Fig A2.** Absolute errors in the values of $\theta$ and $\phi$ for all scenarios of $Al_2O_3$.

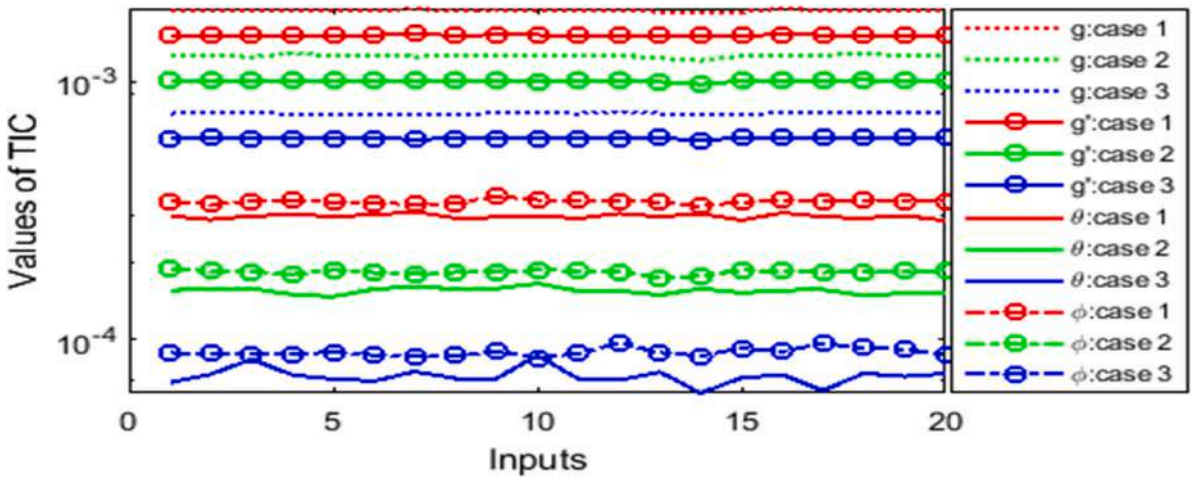


**Fig A3.** E-TIC for cases (I, II, III) of scenario 1 in case of $Al_2O_3$.

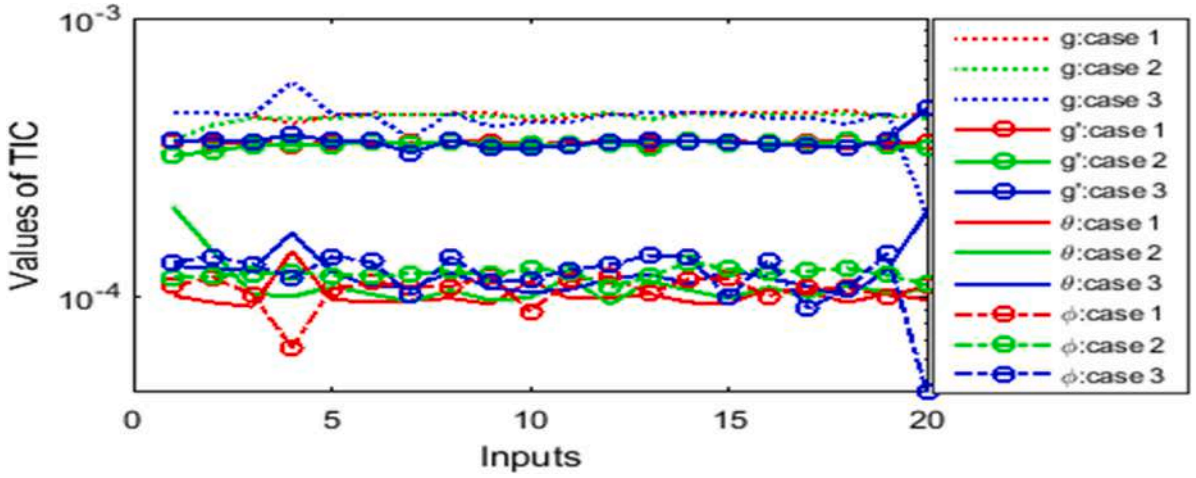


**Fig A4.** E-TIC for cases (I, II, III) of scenario 2 in case of $Al_2O_3$.

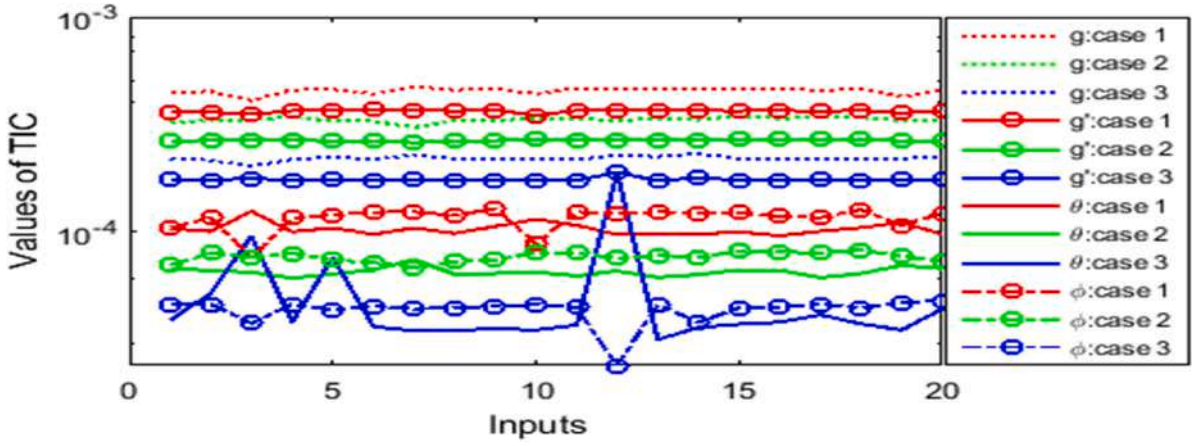


**Fig A5.** E-TIC for cases (I, II, III) of scenario 3 in case of $Al_2O_3$.

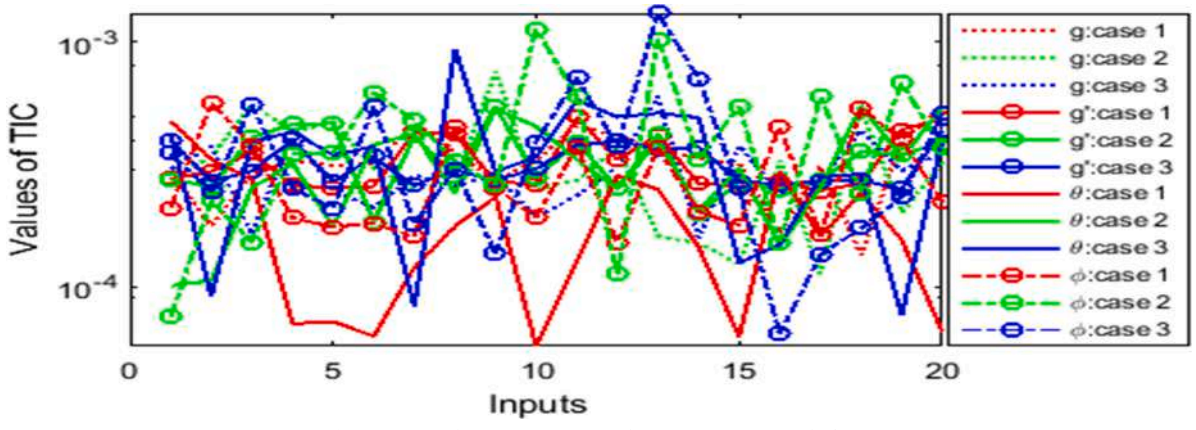


**Fig A6.** E-TIC for cases (I, II, III) of scenario 4 in case of $Al_2O_3$.

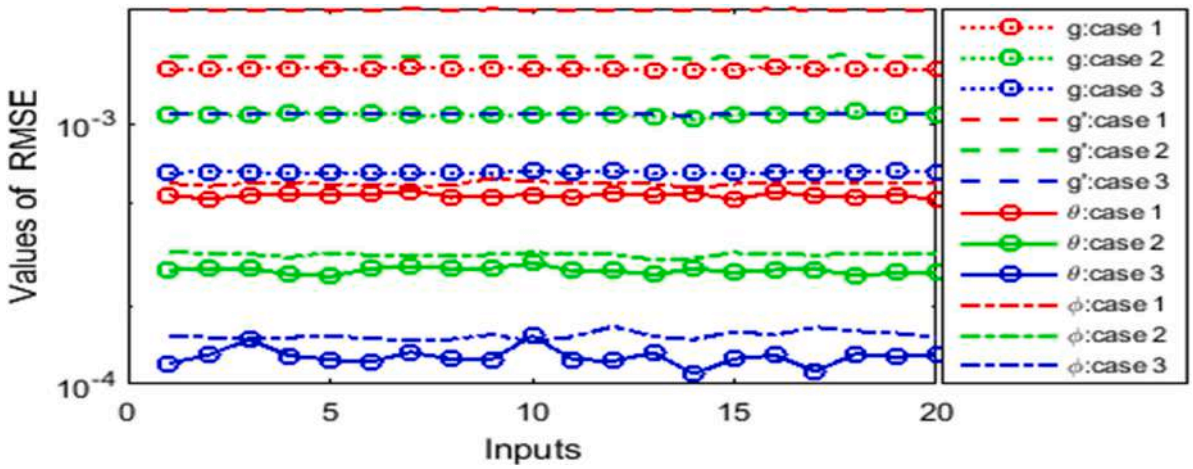


**Fig A7.** RMSE for cases (I, II, III) of scenario 1 in case of $Al_2O_3$.

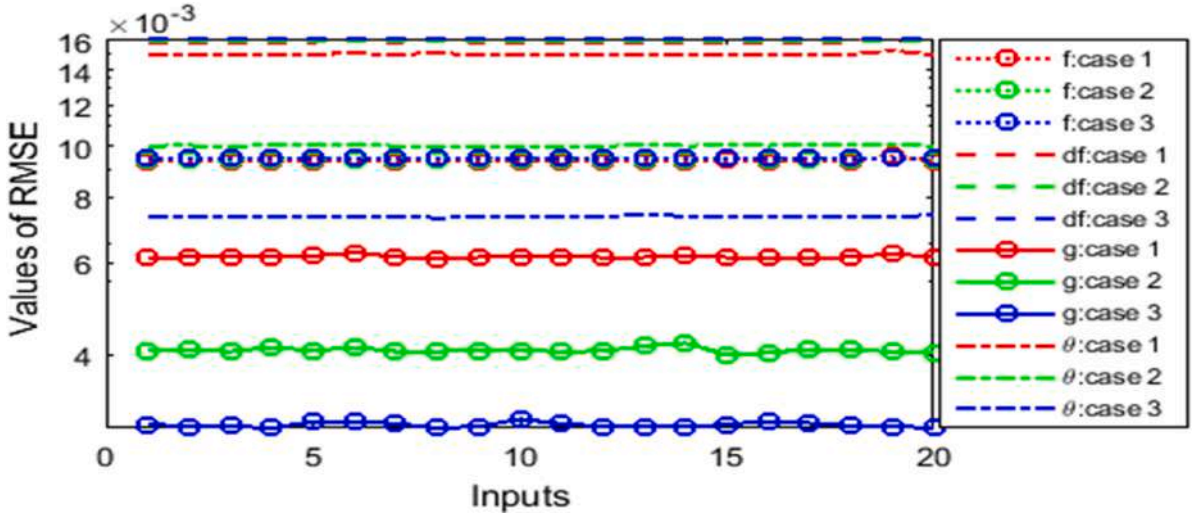


**Fig A8.** RMSE for cases (I, II, III) of scenario 2 in case of $Al_2O_3$.

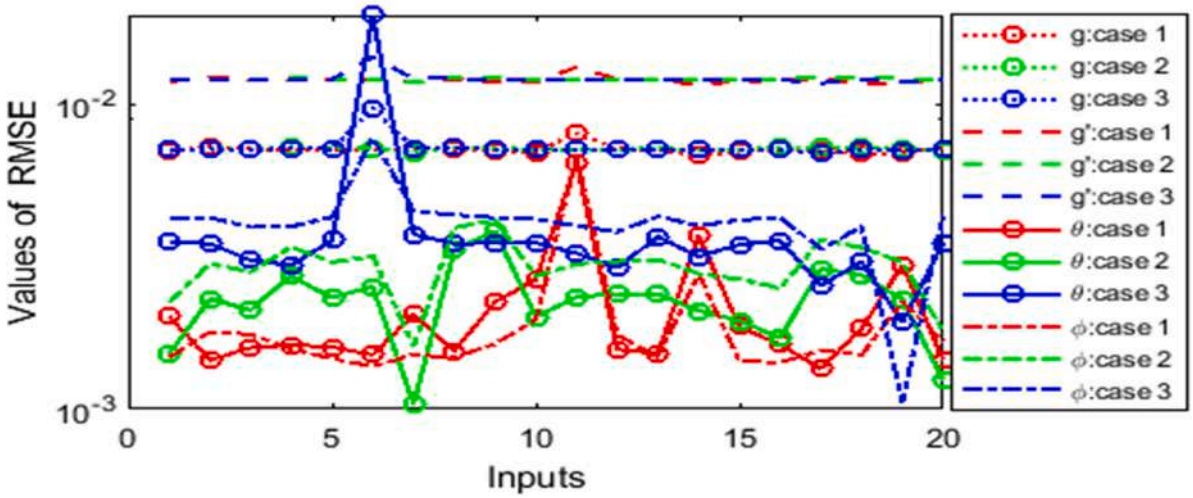


**Fig A9.** RMSE for cases (I, II, III) of scenario 3 in case of $Al_2O_3$.

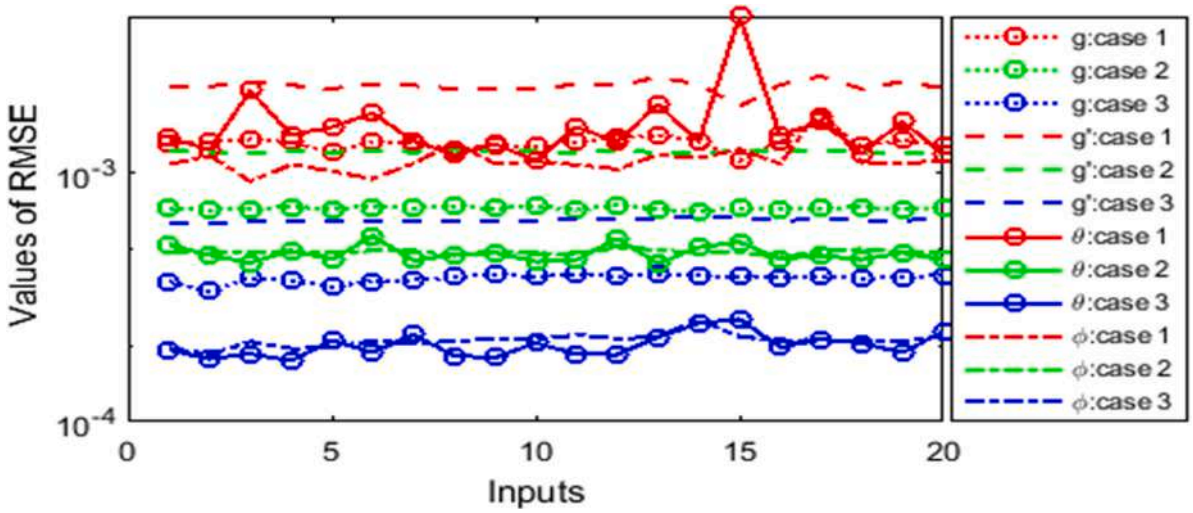


**Fig A10.** RMSE for cases (I, II, III) of scenario 4 in case of $Al_2O_3$.

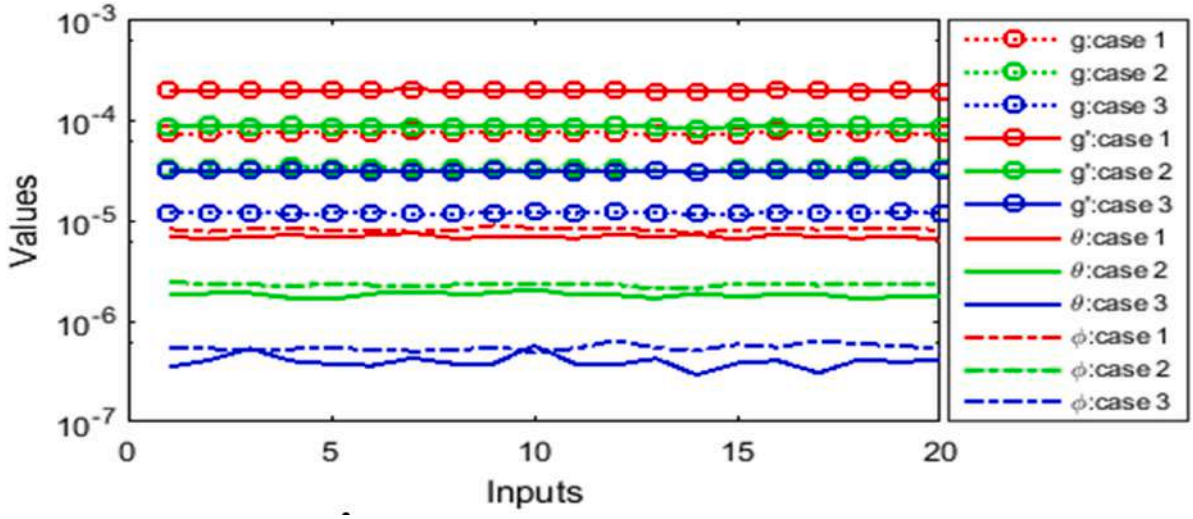


**Fig A11.** E-$R^2$ for cases (I, II, III) of scenario 1 in case of $Al_2O_3$.

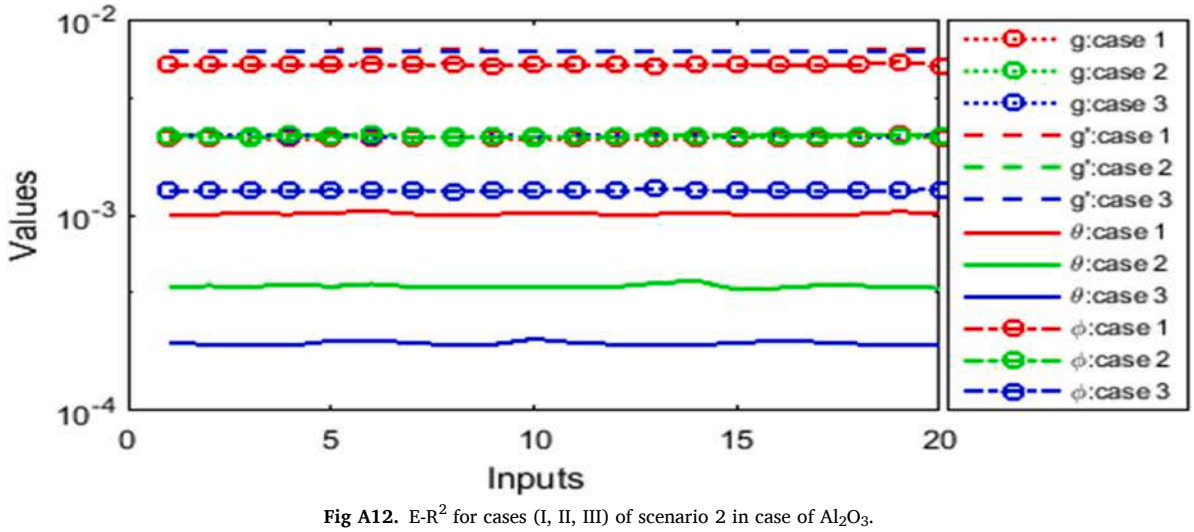


**Fig A12.** E-$R^2$ for cases (I, II, III) of scenario 2 in case of $Al_2O_3$.

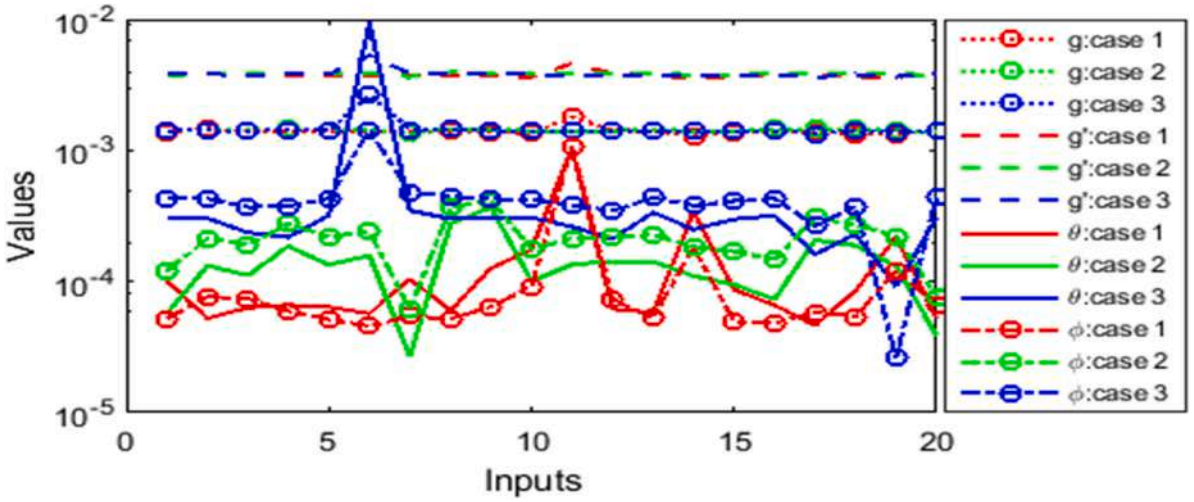


**Fig A13.** E-$R^2$ for cases (I, II, III) of scenario 3 in case of $Al_2O_3$.

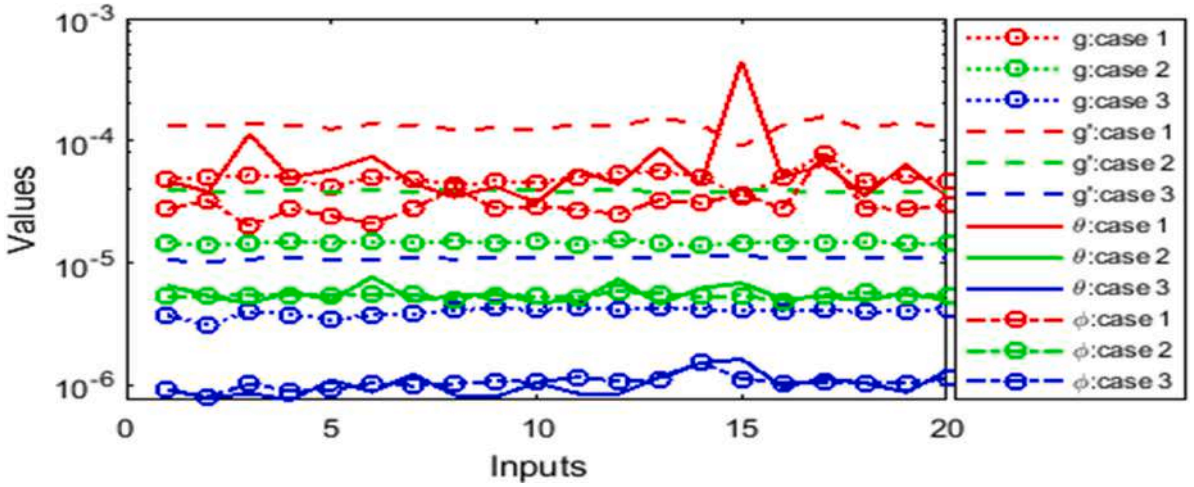


**Fig A14.** E-$R^2$ for cases (I, II, III) of scenario 4 in case of $Al_2O_3$.

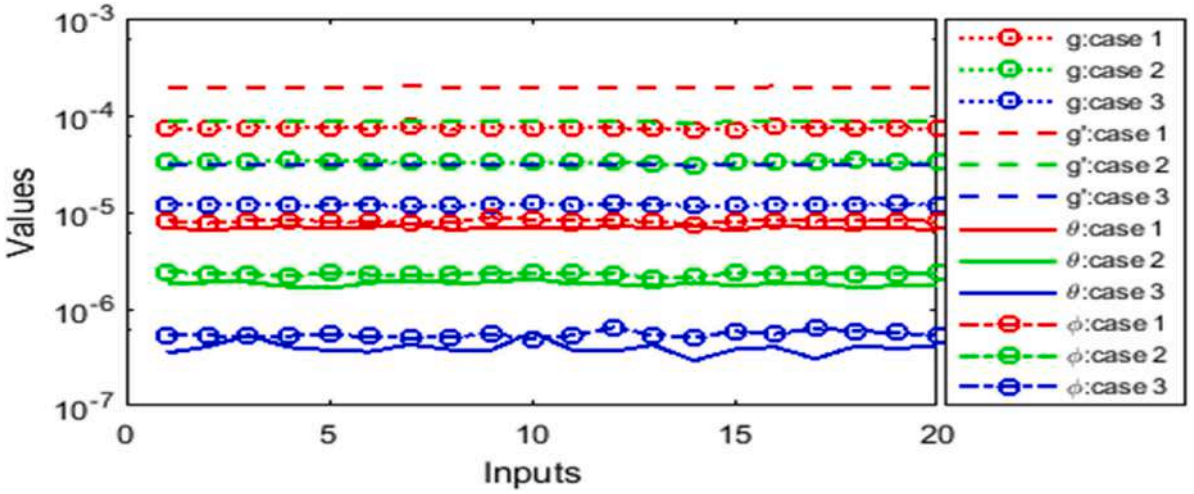


**Fig A15.** E-NSE for cases (I, II, III) of scenario 1 in case of $Al_2O_3$.

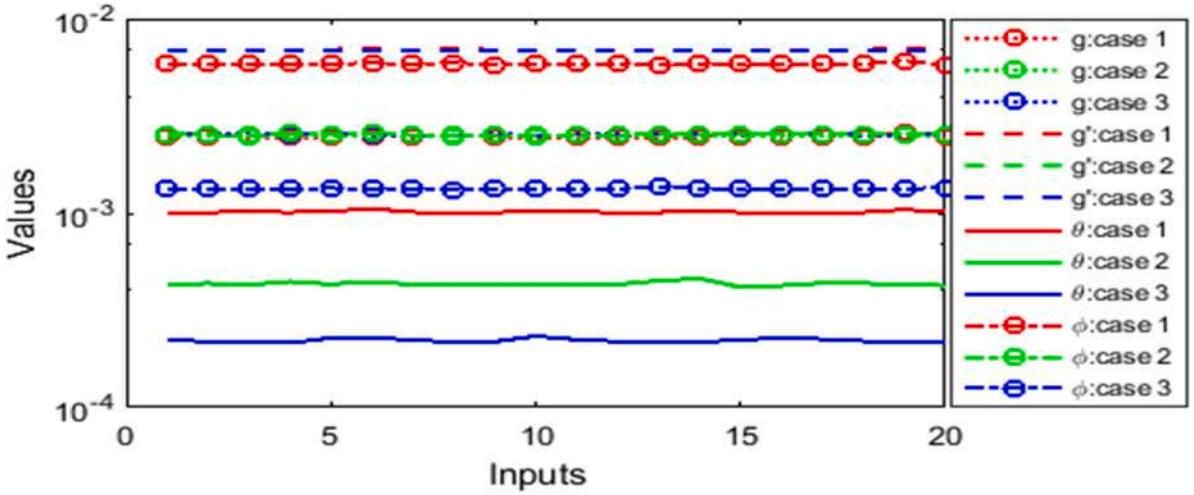


**Fig A16.** E-NSE for cases (I, II, III) of scenario 2 in case of $Al_2O_3$.

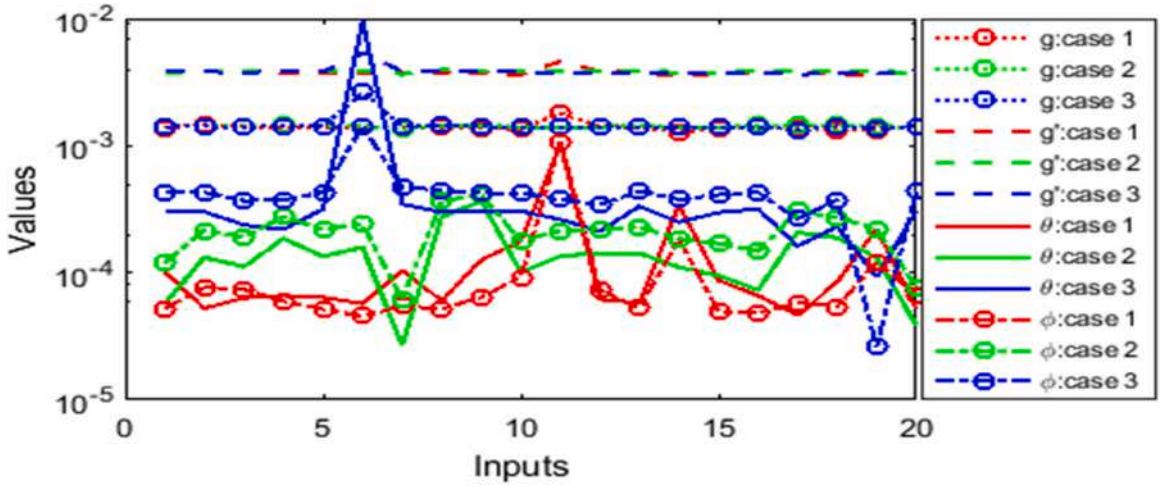


**Fig A17.** E-NSE for cases (I, II, III) of scenario 3 in case of $Al_2O_3$.

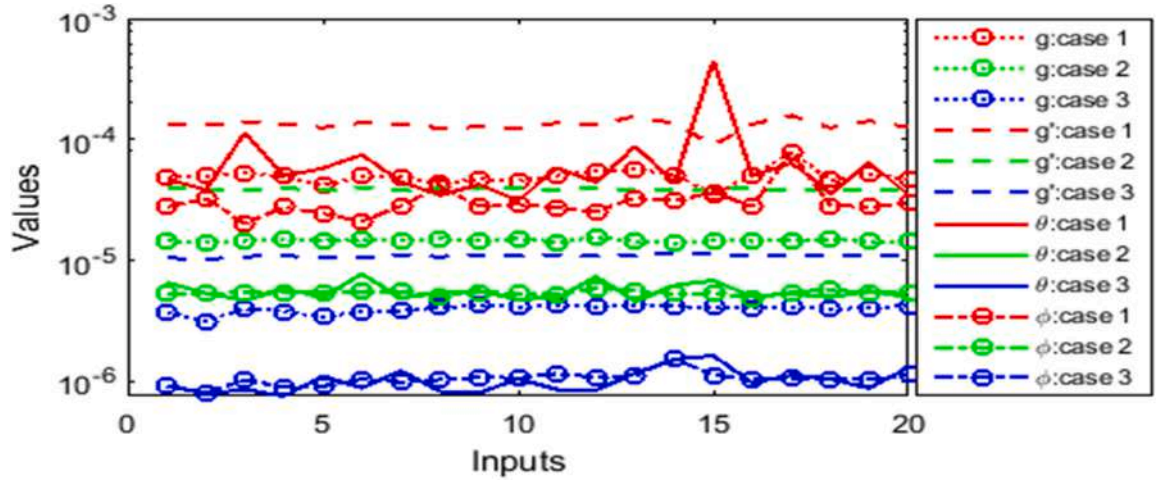


**Fig A18.** E-NSE for cases (I, II, III) of scenario 4 in case of $Al_2O_3$.

## References


[1] S.U. Choi, J.A. Eastman, Enhancing Thermal Conductivity of Fluids with Nanoparticles, Argonne National Lab, IL (United States), 1995 (No. ANL/MSD/CP-84938; CONF-951135-29).
[2] D.A. Nield, A.V. Kuznetsov, Forced convection in a parallel-plate channel occupied by a nanofluid or a porous medium saturated by a nanofluid, Int. J. Heat Mass Transf. 70 (2014) 430–433, https://doi.org/10.1016/j.ijheatmasstransfer.2013.11.016.
[3] M. Hatami, J. Hatami, D.D. Ganji, Computer simulation of MHD blood conveying gold nanoparticles as a third grade non-Newtonian nanofluid in a hollow porous vessel, Comput. Methods Programs Biomed. 113 (2) (2014) 632–641, https://doi.org/10.1016/j.cmpb.2013.11.001.
[4] D.L. Immaculate, R. Muthuraj, A.K. Shukla, S. Srinivas, MHD unsteady flow of a williamson nanofluid in a vertical porous space with oscillating wall temperature, Front. Heat Mass Transf. 7 (2016) 1–14, https://doi.org/10.5098/hmt.7.12.
[5] M.A. Sheremet, H.F. Oztop, I. Pop, MHD natural convection in an inclined wavy cavity with corner heater filled with a nanofluid, J. Magn. Magn. Mater. 416 (2016) 737–747, https://doi.org/10.1016/j.jmmm.2016.04.061.
[6] S. Srinivas, A. Vijayalakshmi, A. Subramanyam Redd y, Flow and heat transfer of gold-blood nanofluid in a porous channel with moving/stationary walls, J. Mech. 33 (3) (2017) 395–404, https://doi.org/10.1017/jmech.2016.102.
[7] M. Sheikholeslami, D.D. Ganji, Influence of electric field on Fe3O4-water nanofluid radiative and convective heat transfer in a permeable enclosure, J. Mol. Liq. 250 (2018) 404–412, https://doi.org/10.1016/j.molliq.2017.12.028.
[8] S.Z. Alamri, R. Ellahi, N. Shehzad, A. Zeeshan, Convective radiative plane Poiseuille flow of nanofluid through porous medium with slip: an application of Stefan blowing, J. Mol. Liq. 273 (2019) 292–304, https://doi.org/10.1016/j.molliq.2018.10.038.
[9] A. SubramanyamReddy, S. Srinivas, K. Jagadeshkumar, Blood-gold/coppernanofluid flow between expanding or contracting permeable walls with slip effects, Mater. Today: Proc. 9 (2019) 351–360, https://doi.org/10.1016/j.matpr.2019.02.164.
[10] Masuda, H., Ebata, A. and Teramae, K., 1993. Alteration of thermal conductivity and viscosity of liquid by dispersing ultra-fine particles. Dispersion of Al2O3, SiO2 and TiO2 ultra-fine particles. https://doi.org/10.2963/jjtp.7.227.
[11] Z.I. Butt, I. Ahmad, M. Shoaib, H. Ilyas, A.K. Kiani, M.A.Z. Raja, Neuro-evolution heuristics for Prandtl-Eyring nanofluid flow with homogenous/heterogeneous reaction across a linearly heated stretched sheet, Waves Random Complex Media (2023) 1–47, https://doi.org/10.1080/17455030.2022.2155325.
[12] T. Muhammad, A. Alsaedi, S.A. Shehzad, T. Hayat, A revised model for Darcy-Forchheimer flow of Maxwell nanofluid subject to convective boundary condition, Chin. J. Phys. 55 (3) (2017) 963–976, https://doi.org/10.1016/j.cjph.2017.03.006.
[13] S. Mandal, G.C. Shit, Entropy analysis on unsteady MHD bi-viscosity nanofluid flow with convective heat transfer in a permeable radiative stretchable rotating disk, Chin. J. Phys. 74 (2021) 239–255, https://doi.org/10.1016/j.cjph.2021.07.036.
[14] O.D. Makinde, A. Aziz, Boundary layer flow of a nanofluid past a stretching sheet with a convective boundary condition, Int. J. Therm. Sci. 50 (7) (2011) 1326–1332, https://doi.org/10.1016/j.ijthermalsci.2011.02.019.
[15] W.A. Khan, I. Pop, Boundary-layer flow of a nanofluid past a stretching sheet, Int. J. Heat Mass Transf. 53 (11-12) (2010) 2477–2483, https://doi.org/10.1016/j.ijheatmasstransfer.2010.01.032.
[16] P.K. Pattnaik, S.R. Mishra, O.Anwar Bég, Umar F. Khan, J.C. Umavathi, Axisymmetric radiative titanium dioxide magnetic nanofluid flow on a stretching cylinder with homogeneous/heterogeneous reactions in Darcy-Forchheimer porous media: Intelligent nanocoating simulation, Mater. Sci. Eng. B 277 (2022) 115589, https://doi.org/10.1016/j.mseb.2021.115589.
[17] J.C. Umavathi, O.A. Bég, T.A. Bég, A. Kadir, Swirling bioconvective nanofluid flow from a spinning stretchable disk in a permeable medium, Int. J. Model. Simul. 43 (5) (2023) 764–796, https://doi.org/10.1080/02286203.2022.2122928.
[18] M.Y. Malik, M. Naseer, S. Nadeem, A. Rehman, The boundary layer flow of Casson nanofluid over a vertical exponentially stretching cylinder, Appl. Nanosci. 4 (7) (2014) 869–873, https://doi.org/10.1007/s13204-013-0267-0.
[19] S. Nadeem, R. Mehmood, N.S. Akbar, Optimized analytical solution for oblique flow of a Casson-nano fluid with convective boundary conditions, Int. J. Therm. Sci. 78 (2014) 90–100, https://doi.org/10.1016/j.ijthermalsci.2013.12.001.
[20] W. Ibrahim, O.D. Makinde, Magnetohydrodynamic stagnation point flow and heat transfer of Casson nanofluid past a stretching sheet with slip and convective boundary condition, J. Aerosp. Eng. 29 (2) (2016) 04015037, https://doi.org/10.1061/(ASCE)AS.1943-5525.0000529.
[21] C.S.K. Raju, N. Sandeep, V. Sugunamma, M.J. Babu, J.R. Reddy, Heat and mass transfer in magnetohydrodynamic Casson fluid over an exponentially permeable stretching surface, Eng. Sci. Technol. 19 (1) (2016) 45–52, https://doi.org/10.1016/j.jestch.2015.05.010.
[22] M.J. Babu, N. Sandeep, Three-dimensional MHD slip flow of nanofluids over a slendering stretching sheet with thermophoresis and Brownian motion effects, Adv. Powder Technol. 27 (5) (2016) 2039–2050, https://doi.org/10.1016/j.apt.2016.07.013.
[23] S.S. Ghadikolaei, M. Yassari, H. Sadeghi, K. Hosseinzadeh, D.D. Ganji, Investigation on thermophysical properties of $TiO_2$–Cu/$H_2O$ hybrid nanofluid transport dependent on shape factor in MHD stagnation point flow, Powder Technol. 322 (2017) 428–438, https://doi.org/10.1016/j.powtec.2017.09.006.
[24] K.L. Hsiao, Micropolar nanofluid flow with MHD and viscous dissipation effects towards a stretching sheet with multimedia feature, Int. J. Heat Mass Transf. 112 (2017) 983–990, https://doi.org/10.1016/j.ijheatmasstransfer.2017.05.042.
[25] G.J. Reddy, B. Kethireddy, J.C. Umavathi, M.A. Sheremet, Heat flow visualization for unsteady Casson fluid past a vertical slender hollow cylinder, Therm. Sci. Eng. Progress 5 (2018) 172–181, https://doi.org/10.1016/j.tsep.2017.11.010.
[26] J.C. Umavathi, D.G. Prakasha, Y.M. Alanazi, M.M. Lashin, F.S. Al-Mubaddel, R. Kumar, R.P. Gowda, Magnetohydrodynamic squeezing Casson nanofluid flow between parallel convectively heated disks, Int. J. Mod. Phys. B 37 (04) (2023) 2350031, https://doi.org/10.1142/S0217979223500315.
[27] J.C. Umavathi, Hakan F. Oztop, Investigation of MHD and applied electric field effects in a conduit cramed with nanofluids, Int. Commun. Heat Mass Transf. 121 (2021) 105097, https://doi.org/10.1016/j.icheatmasstransfer.2020.105097.
[28] J.C. Umavathi, O.A. Bég, Double-diffusive convection in a dissipative electrically conducting nanofluid under orthogonal electric and magnetic fields: a numerical study, Nanosci. Technol. 12 (2) (2021), https://doi.org/10.1615/NanoSciTechnolIntJ.2021036786.
[29] J.C. Umavathi, O.Anwar Bég, Computation of Von Karman thermo-solutal swirling flow of a nanofluid over a rotating disk to a non-Darcian porous medium with hydrodynamic/thermal slip, J. Therm. Anal. Calorim. (2021) 1–16, https://doi.org/10.1007/s10973-021-11126-1.
[30] J.C. Umavathi, M.A. Sheremet, Chemical reaction influence on nanofluid flow in a porous layer: Stability analysis, Int. Commun. Heat Mass Transf. 138 (2022) 106353, https://doi.org/10.1016/j.icheatmasstransfer.2022.106353.
[31] J.C. Umavathi, Electrically conducting micropolar nanofluid with heat source/sink over a wedge: Ion and hall currents, J. Magn. Magn. Mater. 559 (2022) 169548, https://doi.org/10.1016/j.jmmm.2022.169548.
[32] J.C. H Umavathi, O.A. Bég, Computation of Von Karman thermo-solutal swirling flow of a nanofluid over a rotating disk to a non-Darcian porous medium with hydrodynamic/thermal slip, J. Therm. Anal. Calorim. (2021) 1–16, https://doi.org/10.1007/s10973-021-11126-1.
[33] J.C. Umavathi, A.J. Chamkha, Convective stability of a permeable nanofluid inside a horizontal conduit: Fast chemical reactions, Math. Comput. Simul 187 (2021) 155–170, https://doi.org/10.1016/j.matcom.2021.02.016.
[34] J.C. Umavathi, Computation of combined electrical and magnetic field effects on dissipative immiscible newtonian fluid/nanofluid dynamics, J. Magn. Magn. Mater. 573 (2023) 170656, https://doi.org/10.1016/j.jmmm.2023.170656.
[35] J. Prakash, D. Tripathi, O. Anwar Bég, Computation of EMHD ternary hybrid non-Newtonian nanofluid over a wedge embedded in a Darcy-Forchheimer porous medium with zeta potential and wall suction/injection effects, Int. J. Amb. Energy (2023) 1–15, https://doi.org/10.1080/01430750.2023.2224339.
[36] A.W. Butt, N.S. Akbar, D. Tripathi, J. Akram, Analytical investigation of electroosmotically regulated peristaltic propulsion of Cu-water nanofluid through a microtube, Iraqi J. Sci. (2023) 2354–2367, https://doi.org/10.24996/ijs.2023.64.5.21.
[37] S. Munawar, N. Saleem, D. Tripathi, Cilia and electroosmosis induced double diffusive transport of hybrid nanofluids through microchannel and entropy analysis, Nonlinear Eng. 12 (1) (2023) 20220287, https://doi.org/10.1515/nleng-2022-0287.

[38] K.B.S. Latha, M.G. Reddy, D. Tripathi, O.A. Bég, S. Kuharat, H. Ahmad, D.U. Ozsahin, S. Askar, Computation of stagnation coating flow of electro-conductive ternary Williamson hybrid GO-AU-Co 3 O 4/EO nanofluid with a Cattaneo–Christov heat flux model and magnetic induction, Sci. Rep. 13 (1) (2023) 10972, https://doi.org/10.1038/s41598-023-37197-8.

[39] Javaria Akram, Noreen Sher Akbar, Monairah Alansari, Dharmendra Tripathi, Electroosmotically modulated peristaltic propulsion of $TiO_2$/10W40 nanofluid in curved microchannel, Int. Commun. Heat Mass Transf. 136 (2022) 106208, https://doi.org/10.1016/j.icheatmasstransfer.2022.106208.

[40] Javaria Akram, Noreen Sher Akbar, Dharmendra Tripathi, Analysis of electroosmotic flow of silver-water nanofluid regulated by peristalsis using two different approaches for nanofluid, J. Comput. Sci. 62 (2022) 101696, https://doi.org/10.1016/j.jocs.2022.101696.

[41] V. Sridhar, K. Ramesh, D. Tripathi, V. Vivekanand, Analysis of thermal radiation, Joule heating, and viscous dissipation effects on blood-gold couple stress nanofluid flow driven by electroosmosis, Heat Transf. 51 (5) (2022) 4080–4101, https://doi.org/10.1002/htj.22490.

[42] P. Jayavel, D. Tripathi, O. Anwar Bég, A.K. Tiwari, R. Kumar, Thermo-electrokinetic rotating non-Newtonian hybrid nanofluid flow from an accelerating vertical surface, Heat Transf. 51 (2) (2022) 1746–1777, https://doi.org/10.1002/htj.22373.

[43] Javaria Akram, Noreen Sher Akbar, Dharmendra Tripathi, A theoretical investigation on the heat transfer ability of water-based hybrid (Ag–Au) nanofluids and Ag nanofluids flow driven by electroosmotic pumping through a microchannel, Arabian J. Sci. Eng. 46 (2021) 2911–2927, https://doi.org/10.1007/s13369-020-05265-0.

[44] V. Barathi, J. Prakash, D. Tripathi, O. Beg, A. Sharma, R.K. Sharma, Heat Transfer in EMHD Hyperbolic Tangent Ternary Hybrid Nanofluid Flow Over a Darcy-Forchheimer Porous Wedge Surface: Anumerical simulation, Springer, 2023.

[45] Mohit Pandya, A.K. Ansu, R.K. Sharma, D. Tripathi, V.V. Tyagi, Ahmet Sari, Investigation on thermal energy storage properties of polyethylene glycol with hybrid nanoparticles of $Al_2O_3$ and CuO for solar thermal energy storage, ECS J. Solid State Sci. Technol. 12 (7) (2023) 071004, https://doi.org/10.1149/2162-8777/ace477.

[46] A. Khalid, I. Khan, A. Khan, S. Shafie, Unsteady MHD free convection flow of Casson fluid past over an oscillating vertical plate embedded in a porous medium, Eng. Sci. Technol. 18 (3) (2015) 309–317, https://doi.org/10.1016/j.jestch.2014.12.006.

[47] S. Nadeem, R.U. Haq, N.S. Akbar, Z.H. Khan, MHD three-dimensional Casson fluid flow past a porous linearly stretching sheet, Alexand. Eng. J. 52 (4) (2013) 577–582, https://doi.org/10.1016/j.aej.2013.08.005.

[48] I. Ahmad, H. Ilyas, S.I. Hussain, M.A.Z. Raja, Evolutionary techniques for the solution of bio-heat equation arising in human dermal region model, Arabian J. Sci. Eng. (2023) 1–26, https://doi.org/10.1007/s13369-023-07907-5.

[49] I. Ahmad, S.I. Hussain, M.A.Z. Raja, M. Shoaib, Qurratulain, Transportation of hybrid $MoS_2$–$SiO_2$/EG nanofluidic system toward radially stretched surface, Arabian J. Sci. Eng. 48 (1) (2023) 953–966, https://doi.org/10.1007/s13369-022-07241-2.

[50] I. Ahmad, H. Ilyas, K. Kutlu, V. Anam, S.I. Hussain, J.L.G. Guirao, Numerical computing approach for solving Hunter-Saxton equation arising in liquid crystal model through sinc collocation method, Heliyon 7 (7) (2021), https://doi.org/10.1016/j.heliyon.2021.e07600.

[51] I. Ahmad, S.I. Hussain, M. Usman, H. Ilyas, On the solution of Zabolotskaya–Khokhlov and Diffusion of Oxygen equations using a sinc collocation method, Part. Diff. Equ. Appl. Math. 4 (2021) 100066, https://doi.org/10.1016/j.padiff.2021.100066.

[52] S.I. Hussain, I. Ahmad, M.A.Z. Raja, C.M.Z. Umer, A computational convection analysis of $SiO_2$/water and $MoS_2$-$SiO_2$/water based fluidic system in inverted cone, Eng. Rep. (2023) e12660, https://doi.org/10.1002/eng2.12660.

[53] I. Ahmad, S.U.I. Ahmad, K. Kutlu, H. Ilyas, S.I. Hussain, F. Rasool, On the dynamical behavior of nonlinear Fitzhugh–Nagumo and Bateman–Burger equations in quantum model using Sinc collocation scheme, Eur. Phys. J. Plus 136 (11) (2021) 1108, https://doi.org/10.1140/epjp/s13360-021-02103-6.

[54] T.N. Cheema, M.A.Z. Raja, I. Ahmad, S. Naz, H. Ilyas, M. Shoaib, Intelligent computing with Levenberg–Marquardt artificial neural networks for nonlinear system of COVID-19 epidemic model for future generation disease control, Eur. Phys. J. Plus 135 (11) (2020) 1–35, https://doi.org/10.1140/epjp/s13360-020-00910-x.

[55] F. Faisal, M. Shoaib, M.A.Z. Raja, A new heuristic computational solver for nonlinear singular Thomas–Fermi system using evolutionary optimized cubic splines, Eur. Phys. J. Plus 135 (1) (2020) 1–29, https://doi.org/10.1140/epjp/s13360-019-00066-3.

[56] M. Umar, M.A.Z. Raja, Z. Sabir, A.S. Alwabli, M. Shoaib, A stochastic computational intelligent solver for numerical treatment of mosquito dispersal model in a heterogeneous environment, Eur. Phys. J. Plus 135 (7) (2020) 1–23, https://doi.org/10.1140/epjp/s13360-020-00557-8.

[57] I. Jadoon, A. Ahmed, A. ur Rehman, M. Shoaib, M.A.Z. Raja, Integrated meta-heuristics finite difference method for the dynamics of nonlinear unipolar electrohydrodynamic pump flow model, Appl. Soft Comput. 97 (2020) 106791, https://doi.org/10.1016/j.asoc.2020.106791.

[58] A.H. Bukhari, M. Sulaiman, M.A.Z. Raja, S. Islam, M. Shoaib, P. Kumam, Design of a hybrid NAR-RBFs neural network for nonlinear dusty plasma system, Alexand. Eng. J. 59 (5) (2020) 3325–3345, https://doi.org/10.1016/j.aej.2020.04.051.

[59] M.A.Z. Raja, J.A. Khan, S.M. Shah, R. Samar, D. Behloul, Comparison of three unsupervised neural network models for first Painlevé Transcendent, Neural. Comput. Appl. 26 (5) (2015) 1055–1071, https://doi.org/10.1007/s00521-014-1774-y.

[60] M.A.Z. Raja, S. Azad, S.M. Shah, Bio-inspired computational heuristics to study the boundary layer flow of the Falkner-Scan system with mass transfer and wall stretching, Appl. Soft Comput. 57 (2017) 293–314, https://doi.org/10.1016/j.asoc.2017.03.047.

[61] M.A.Z. Raja, Solution of the one-dimensional Bratu equation arising in the fuel ignition model using ANN optimised with PSO and SQP, Connect. Sci. 26 (3) (2014) 195–214, https://doi.org/10.1080/09540091.2014.907555.

[62] M.A.Z. Raja, Stochastic numerical treatment for solving Troesch's problem, Inf. Sci. 279 (2014) 860–873, https://doi.org/10.1016/j.ins.2014.04.036.

[63] M.A.Z. Raja, I. Ahmad, I. Khan, M.I. Syam, A.M. Wazwaz, Neuro-heuristic computational intelligence for solving nonlinear pantograph systems, Front. Inf. Technol. Electron. Eng. 18 (4) (2017) 464–484, https://doi.org/10.1631/FITEE.1500393.

[64] M.A.Z. Raja, J. Mehmood, Z. Sabir, A.K. Nasab, M.A. Manzar, Numerical solution of doubly singular nonlinear systems using neural networks-based integrated intelligent computing, Neural. Comput. Appl. 31 (2019) 793–812, https://doi.org/10.1007/s00521-017-3110-9.

[65] M.A.Z. Raja, J.A. Khan, N.I. Chaudhary, E. Shivanian, Reliable numerical treatment of nonlinear singular Flierl–Petviashivili equations for unbounded domain using ANN, GAs, and SQP, Appl. Soft Comput. 38 (2016) 617–636, https://doi.org/10.1016/j.asoc.2015.10.017.

[66] S. Mall, S. Chakraverty, Hermite functional link neural network for solving the Van der Pol–duffing oscillator equation, Neural Comput. 28 (8) (2016) 1574–1598, https://doi.org/10.1162/NECO_a_00858.

[67] M. Umar, Kusen, M.A.Z. Raja, Z. Sabir, Q. Al-Mdallal, A computational framework to solve the nonlinear dengue fever SIR system, Comput. Meth. Biomech. Biomed. Eng. 25 (16) (2022) 1821–1834, https://doi.org/10.1080/10255842.2022.2039640.

[68] Binas, J., Neil, D., Indiveri, G., Liu, S.C. and Pfeiffer, M., 2016. Precise neural network computation with imprecise analog devices. arXiv preprint arXiv: 1606.07786. https://doi.org/10.48550/arXiv.1606.07786.

[69] M. Ibrahim, S. Jemei, G. Wimmer, D. Hissel, Nonlinear autoregressive neural network in an energy management strategy for battery/ultra-capacitor hybrid electrical vehicles, Electric Power Syst. Res. 136 (2016) 262–269, https://doi.org/10.1016/j.epsr.2016.03.005.

[70] X. Huang, X. Lou, B. Cui, A novel neural network for solving convex quadratic programming problems subject to equality and inequality constraints, Neurocomputing 214 (2016) 23–31, https://doi.org/10.1016/j.neucom.2016.05.032.

[71] M.A.Z. Raja, M.A. Manzar, R. Samar, An efficient computational intelligence approach for solving fractional order Riccati equations using ANN and SQP, Appl. Math. Modell. 39 (10-11) (2015) 3075–3093, https://doi.org/10.1016/j.apm.2014.11.024.

[72] M. Pakdaman, A. Ahmadian, S. Effati, S. Salahshour, D. Baleanu, Solving differential equations of fractional order using an optimization technique based on training artificial neural network, Appl. Math. Comput. 293 (2017) 81–95, https://doi.org/10.1016/j.amc.2016.07.021.

[73] M.A.Z. Raja, F.H. Shah, E.S. Alaidarous, M.I. Syam, Design of bio-inspired heuristic technique integrated with interior-point algorithm to analyze the dynamics of heartbeat model, Appl. Soft Comput. 52 (2017) 605–629, https://doi.org/10.1016/j.asoc.2016.10.009.

[74] M. Ibnkahla, Applications of neural networks to digital communications–a survey, Signal Process. 80 (7) (2000) 1185–1215, https://doi.org/10.1016/S0165-1684(00)00030-X.

[75] M.A.Z. Raja, A. Zameer, A.U. Khan, A.M. Wazwaz, A new numerical approach to solve Thomas–Fermi model of an atom using bio-inspired heuristics integrated with sequential quadratic programming, SpringerPlus 5 (1) (2016) 1–22, https://doi.org/10.1186/s40064-016-3093-5.

[76] N.A. Khan, S. Khan, A. Shaikh, M.A.Z. Raja, MHD stagnation point flow of nanofluids over an off centered rotating disk in a porous medium via haar wavelet, J. Nanofluids 5 (3) (2016) 444–458, https://doi.org/10.1166/jon.2016.1226.
[77] C.A. Ramseyer, T.L. Mote, Atmospheric controls on Puerto Rico precipitation using artificial neural networks, Clim. Dyn. 47 (7) (2016) 2515–2526, https://doi.org/10.1007/s00382-016-2980-3.
[78] M.A.Z. Raja, M.A.R. Khan, T. Mahmood, U. Farooq, N.I. Chaudhary, Design of bio-inspired computing technique for nanofluidics based on nonlinear Jeffery–Hamel flow equations, Can. J. Phys. 94 (5) (2016) 474–489, https://doi.org/10.1139/cjp-2015-0440.
[79] P.M. Kumar, R. Saravanakumar, A. Karthick, V. Mohanavel, Artificial neural network-based output power prediction of grid-connected semitransparent photovoltaic system, Environ. Sci. Pollut. Res. (2022) 1–10, https://doi.org/10.1007/s11356-021-16398-6.
[80] I. Ahmad, S.I. Hussain, H. Ilyas, J.L. García Guirao, A. Ahmed, S. Rehmat, T. Saeed, Numerical solutions of Schrödinger wave equation and Transport equation through Sinc collocation method, Nonlinear Dyn. 105 (1) (2021) 691–705, https://doi.org/10.1007/s11071-021-06596-9.
[81] I. Ahmad, S.I. Hussain, H. Ilyas, L. Zoubir, M. Javed, M.A. Zahoor Raja, Integrated stochastic investigation of singularly perturbed delay differential equations for the neuronal variability model, Int. J. Intell. Syst. 2023 (2023), https://doi.org/10.1155/2023/1918409.
[82] I. Ahmad, S.I. Hussain, H. Ilyas, S. Jabeen, A. Iqrar, On the applications of collocation method for numerically analyzing the nonlinear Degasperis–Procesi and Benjamin–Bona–Mahony equations, Int. J. Mod. Phys. B (2023) 2450264, https://doi.org/10.1142/S0217979224502643.
[83] I. Ahmad, F. Ahmad, M.A.Z. Raja, H. Ilyas, N. Anwar, Z. Azad, Intelligent computing to solve fifth-order boundary value problem arising in induction motor models, Neural. Comput. Appl. 29 (7) (2018) 449–466, https://doi.org/10.1007/s00521-016-2547-6.
[84] R. Sridhar, M. Chandrasekaran, C. Sriramya, T. Page, Optimization of heterogeneous Bin packing using adaptive genetic algorithm, in: IOP Conference Series: Materials Science and Engineering 183, IOP Publishing, 2017 012026, https://doi.org/10.1088/1757-899X/183/1/012026.
[85] B. Khan, P. Singh, Selecting a meta-heuristic technique for smart micro-grid optimization problem: a comprehensive analysis, IEEE Access 5 (2017) 13951–13977, https://doi.org/10.1109/ACCESS.2017.2728683.
[86] D. Tuhus-Dubrow, M. Krarti, Genetic-algorithm based approach to optimize building envelope design for residential buildings, Build. Environ. 45 (7) (2010) 1574–1581, https://doi.org/10.1016/j.buildenv.2010.01.005.
[87] J.C. Lee, W.M. Lin, G.C. Liao, T.P. Tsao, Quantum genetic algorithm for dynamic economic dispatch with valve-point effects and including wind power system, Int. J. Electr. Power Energy Syst. 33 (2) (2011) 189–197, https://doi.org/10.1016/j.ijepes.2010.08.014.
[88] Hoque, M.S., Mukit, M., Bikas, M. and Naser, A., 2012. An implementation of intrusion detection system using genetic algorithm. *arXiv preprint arXiv:1204.1336*. https://doi.org/10.5121/ijnsa.2012.4208.
[89] M.G. Ball, B. Qela, S. Wesolkowski, A review of the use of computational intelligence in the design of military surveillance networks. Recent Advances in Computational Intelligence in Defense and Security, 2016, pp. 663–693, https://doi.org/10.1007/978-3-319-26450-9_24.
[90] M.S.P. Subathra, S.E. Selvan, T.A.A. Victoire, A.H. Christinal, U. Amato, A hybrid with cross-entropy method and sequential quadratic programming to solve economic load dispatch problem, IEEE Syst. J. 9 (3) (2014) 1031–1044, https://doi.org/10.1109/JSYST.2013.2297471.
[91] Z. Sun, Y. Tian, H. Li, J. Wang, A superlinear convergence feasible sequential quadratic programming algorithm for bipedal dynamic walking robot via discrete mechanics and optimal control, Optim. Control Appl. Methods 37 (6) (2016) 1139–1161, https://doi.org/10.1002/oca.2228.
[92] J.J. Engelbrecht, J.A. Engelbrecht, Optimal attitude and flight vector recovery for large transport aircraft using sequential quadratic programming, in: 2016 Pattern Recognition Association of South Africa and Robotics and Mechatronics International Conference (PRASA-RobMech), IEEE, 2016, pp. 1–7, https://doi.org/10.1109/RoboMech.2016.7813153.
[93] Z.I. Butt, I. Ahmad, M. Shoaib, H. Ilyas, M.A.Z. Raja, Electro-magnetohydrodynamic impact on Darrcy-Forchheimer viscous fluid flow over a stretchable surface: Integrated intelligent Neuro-evolutionary computing approach, Int. Commun. Heat Mass Transf.r 137 (2022) 106262, https://doi.org/10.1016/j.icheatmasstransfer.2022.106262.
[94] Z.I. Butt, I. Ahmad, M. Shoaib, H. Ilyas, M.A.Z. Raja, A novel design of inverse multiquadric radial basis neural networks to analyze MHD nanofluid boundary layer flow past a wedge embedded in a porous medium under the influence of radiation and viscous effects, Int. Commun. Heat Mass Transf. 140 (2023) 106516, https://doi.org/10.1016/j.icheatmasstransfer.2022.106516.
[95] Z.I. Butt, I. Ahmad, H. Ilyas, M. Shoaib, M.A.Z. Raja, Design of inverse multiquadric radial basis neural networks for the dynamical analysis of MHD Casson nanofluid flow along a nonlinear stretchable porous surface with multiple slip conditions, Int. J. Hydrog. Energy 48 (42) (2023) 16100–16131, https://doi.org/10.1016/j.ijhydene.2022.12.319.
[96] Z.I. Butt, I. Ahmad, M. Shoaib, Design of inverse multiquadric radial basis neural networks for the dynamical analysis of wire coating problem with Oldroyd 8-constant fluid, AIP Adv. 12 (10) (2022), https://doi.org/10.1063/5.0101601.